Laboratory Experiments of Chemical Reactions on Polar Stratospheric Cloud Particles

by

Keith Donald Beyer

B.S. Chemistry
University of Wisconsin - Stevens Point
(1989)

Submitted to the Department of Chemistry
in Partial Fulfillment of the Requirements for the Degree of

Doctor of Philosophy
in Chemistry

at the

Massachusetts Institute of Technology

February, 1994

Signature of Author _____
Department of Chemistry
November 5, 1993

Certified by _____
Mario J. Molina
Martin Professor of Atmospheric Chemistry
Thesis Supervisor

Accepted by _____
Glenn A. Berchtold
Professor of Chemistry
Chairman, Departmental Committee on Graduate Students

This doctoral thesis has been examined by a Committee of the Department of Chemistry as follows:

Professor Jeffrey I. Steinfeld _ _____
Chairman

Professor Mario J. Molina _____
Thesis Supervisor

Professor Ronald G. Prinn _____
Department of Earth, Atmospheric and Planetary Sciences

Laboratory Experiments of Chemical Reactions on Polar Stratospheric Cloud Particles

by

Keith Donald Beyer

Submitted to the Department of Chemistry on November 5, 1993 in partial fulfillment of

the requirements for the Degree of Doctor of Philosophy in Chemistry

ABSTRACT

Supercooling in solutions representative of aerosols in the stratosphere has been investigated. For the H_2SO_4/H_2O system the critical freezing points for solutions that will form ice has been studied, as well as the length of time needed to nucleate solutions that will form sulfuric acid tetrahydrate (SAT). It was observed that the critical freezing points for solutions that form ice upon freezing are lower than those previously predicted. Also, for solutions that will form SAT, the highest probability of freezing occurs at lower concentrations than has been predicted in the literature. The ternary system $H_2SO_4/HNO_3/H_2O$ has also been studied with respect to time of freezing using a new parameterization of the previous literature data to extrapolate to the conditions of the polar stratosphere. It was found that in the polar regions, where the solubility of nitric acid in stratospheric aerosols is greatly enhanced, the probability of nucleation of ternary solutions is quite high due, most likely, to the formation of NAT in these solutions. Implications of these results to the formation of Polar Stratospheric Clouds (PSCs) is discussed.

The amount of HCl that will incorporate into stratospheric ice particles (PSC type II) is also important. This phenomenon has been investigated using two simple methods, which showed that HCl is not incorporated into the bulk ice matrix; other experiments have shown that it is taken up by the surface layers.

Finally, an experiment has been designed to study chemical reactions on particles that simulate PSCs at polar stratospheric conditions of temperature and reactant partial pressures, using turbulent flow kinetics. The feasibility of the experiment is demonstrated and preliminary results are presented.

Thesis Supervisor: Dr. Mario J. Molina

Title: Martin Professor of Atmospheric Chemistry

Acknowledgments

Thanks be to God, Father, Son and Holy Ghost

Thanks are due to my parents and grandparents, without whom I would not be here. They offered support, encouragement and advice in everything I did.

Thanks to all the great teachers and educators along the way, especially the science teachers who made science interesting and fun.

Thanks to my advisor for his gentle encouragement, teaching and especially for his patience when I thought I knew the answer, but really didn't. Thanks!

Thanks to my officemate, John Seeley, for all the scientific, but mostly political discussions. Thanks for listening to all my complaints, and it helped me to listen to yours, too!

Thanks to all the members of our research group who have helped me, especially: Paul Wooldrige, Jonathan Abbatt, John Jayne, James McMahon, Dana Leard and Tun-Li Shen. A special thanks to the undergraduates who worked with me: Judy Kim, Scott Seago, Mike Schlamp and Chris Feyger.

Thanks to the behind-the-scenes people, without whom, research would move very slowly: Debbie Sykes for the administrative wizardry and Bob DiGiacomo for the great glass blowing work.

And, at the end of the day, thanks be to God for providing all things.

Prologue

Then the LORD answered Job out of the whirlwind and said:

Who is this who darkens council
By words without knowledge?
Now prepare yourself like a man;
I will question you and you shall answer Me.

Where were you when I laid the foundations of the earth?
Tell Me, if you have understanding.
Who determined its measurements?
Surely you know!
Or who stretched the line upon it?
To what were its foundations fastened?
Or who laid its cornerstone,
When the morningstars sang together,
And all the sons of God shouted for joy?

Has the rain a father?
Or who has begotten the drops of dew?
From whose womb comes the ice?
And the frost of heaven, who gives it birth?
The waters harden like stone,
And the surface of the deep is frozen.

Can you lift up your voice to the clouds,
That an abundance of water may cover you?
Can you send out lightnings, that they may go,
And say to you, 'Here we are!'?
Who has put wisdom in the mind?
Or who has given understanding to the heart?
Who can number the clouds by wisdom?
Or who can pour out the bottles of heaven,
When the dust hardens in clumps,
And the clods cling together?

Job 38:1-7, 28-30, 34-38 (NKJV)

Table of Contents

Chapter I

Introduction

In the last 20 years chemical reactions in the stratosphere which destroy ozone have become one of the major global environmental problems. Man-made chemical compounds, chlorofluorocarbons (CFCs), have been shown to cause stratospheric ozone depletion [Molina and Rowland, 1974]. The ozone layer is important because it shields the earth from much harmful ultraviolet radiation. The problem is global in scale because CFCs released from point sources around the world, affect ozone concentrations not only over these areas, but also in areas unrelated and remote from the sources. The foremost example of this that we have today is the annually occurring "ozone hole" over the Antarctic. This region is very remote from the source of most CFCs in the atmosphere. However, due to the nature of tropospheric and stratospheric circulation, the chemical precursors to ozone destruction are present in the region over the Antarctic (see Figure 1.1). Under the appropriate conditions, catalytic cycles are initiated which cause massive depletion of ozone. Part one of this thesis will describe laboratory experiments that were performed in order to investigate these catalytic processes.

It has been established that the following general reactions occur in the stratosphere [Molina and Rowland, 1974]:

$$CFCl_3 + h\nu(UV) \rightarrow CFCl_2 + Cl \qquad (1.i)$$

$$CF_2Cl_2 + h\nu(UV) \rightarrow CF_2Cl + Cl \qquad (1.ii)$$

free radical chlorine then rapidly combines with other stratospheric species:

$$Cl + HO_2 \rightarrow HCl + O_2 \qquad (1.iii)$$

$$Cl + CH_4 \rightarrow HCl + CH_3 \qquad (1.iv)$$

$$Cl + H_2 \rightarrow HCl + H \qquad (1.v)$$

$$Cl + O_3 \rightarrow ClO + O_2 \qquad (1.vi)$$

$$ClO + NO_2 + M \rightarrow ClONO_2 \qquad (1.vii)$$

Reactions (1.iii - 1.v) lead to HCl formation, and reactions (1.vi) and (1.vii) stepwise form chlorine nitrate. Both chlorine nitrate and HCl are reservoir species for chlorine because chlorine in these forms is relatively unreactive in the gas phase to the extent that the reaction of HCl with $ClONO_2$ is negligible in the stratosphere [Molina, et al., 1985].

The mechanism for ozone depletion originally proposed by Molina and Rowland couples reaction (1.vi) with:

$$ClO + O \rightarrow Cl + O_2 \qquad (1.viii)$$

to give a net reaction: $O_3 + O \rightarrow 2O_2$ However, this mechanism would only cause a small amount of ozone depletion, and indeed this was the observed case throughout the decade of the 1970s. The Total Ozone Mapping Spectrometer (TOMS) satellite was launched in 1979 and began providing global observations of ozone column concentrations (total ozone integrated from the ground up.)

In the Antarctic spring of 1984 Farman, et al. [1985] reported an ozone 'hole' over the south pole. Farman used a ground based ozone spectrometer. In fact, low concentrations of ozone were later found in the data from the TOMS satellite back to the beginning of the data (1979). It had been noticed much earlier [Hallet, 1967; McCormick, et al., 1982] that various gasses condense to form Polar Stratospheric Clouds (PSCs). There are two types of PSCs in the Antarctic region. Background aerosols in the polar stratosphere consist of sulfuric acid, nitric acid, and water. When conditions are conducive to these aerosols freezing, they nucleate and form the solids: sulfuric acid tetrahydrate (SAT), nitric acid trihydrate (NAT), and possibly some ice [Molina, et al., 1993]. These aerosols are then termed PSC Type I. These PSCs will then grow rapidly by deposition of nitric acid and water. Type II PSCs occur when the temperature drops below the ice frost point (i.e. the temperature at which the background vapor pressure of water is equal to the vapor pressure of ice.) It has been shown that HCl is readily incorporated into the surface layers of ice [Wofsy, et al., 1988; Molina, et al., 1987;

Hansen and Ravishankara, 1991; Abbatt, et al., 1992a], and NAT [Hansen and Mauersburger, 1988; Hansen and Ravishankara, 1991; Abbatt and Molina, 1992a,b].

Once HCl is incorporated into the surface layers of the PSC particles, the following sequence can occur at the particle surface [Molina, et al., 1987]:

$$HCl_{(g)} + particle \rightarrow HCl_{(abs)} \quad (1.ix)$$

$$ClONO_{2(g)} + particle \rightarrow ClONO_{2(abs)} \quad (1.x)$$

$$HCl_{(abs)} + ClONO_{2(abs)} \rightarrow Cl_{2(g)} + HNO_{3(s)} \quad (1.xi)$$

An alternate route to reaction (1.xi) for the production of Cl_2 is:

$$ClONO_{2(abs)} + H_2O_{(s)} \rightarrow HOCl_{(abs)} + HNO_{3(s)} \quad (1.xii)$$

$$HOCl_{(abs)} + HCl_{(abs)} \rightarrow Cl_{2(g)} + H_2O_{(s)} \quad (1.xiii)$$

Indeed, reactions (1.xii) and (1.xiii) may be the mechanism for reaction (1.xi) [Abbatt and Molina, 1992a] It is postulated that these reactions occur throughout the Antarctic winter when there is no sunlight. The steps that are thought to occur are: stratospheric chlorine at the pole is bound up the reservoir species: HCl and $ClONO_2$. In the polar night which lasts on the order of three months, stratospheric temperatures become very cold (down to 185 K). In these very cold conditions, a polar vortex is created that essentially cuts off the mixing of the air over the Antarctic with other air. This sets up a kind of contained chemical reactor over the pole for the period of the polar night. Under these conditions, it becomes cold enough to form PSCs. These particles act as a catalyst in the reaction of the chlorine reservoir species as illustrated in reactions (1.ix - 1.xiii). This results in a buildup of Cl_2 and HOCl gasses.

If we look specifically at reaction (1.xi), the products are chlorine in the gas phase and nitric acid in the solid phase. As spring arrives in the polar regions, sunlight returns, thereby initiating the reaction:

$$Cl_{2(g)} + h\nu \rightarrow 2Cl_{(g)} \quad (1.xiv)$$

then the following cycle can occur [Molina and Molina, 1987]:

$$2(Cl + O_3 \rightarrow ClO + O_2) \qquad \text{(1.xv)}$$

$$ClO + ClO + M \rightarrow Cl_2O_2 + M \qquad \text{(1.xvi)}$$

$$Cl_2O_2 + h\nu \rightarrow Cl + ClOO \qquad \text{(1.xvii)}$$

$$ClOO + M \rightarrow Cl + O_2 + M \qquad \text{(1.xviii)}$$

$$\text{Net:} \quad 2O_3 + h\nu \rightarrow 3O_2$$

Thus, the result of this cycle of chemical reactions is the depletion of ozone. Anderson, et al. [1991] have calculated that this mechanism accounts for 75% of the observed ozone loss in the springtime Antarctic ozone hole, and that a mechanism put forth by McElroy, et al. [1986] involving ClO and BrO accounts for nearly all the rest of the destruction.

This thesis will address the question of chlorine activation by PSCs. First, it will address the question of the physical nature of PSC particles: their phase, composition, and under what conditions phase changes occur (chapters II and III). Second, it will address the question of performing a chlorine activation experiment on model PSCs Type II (chapters IV and V).

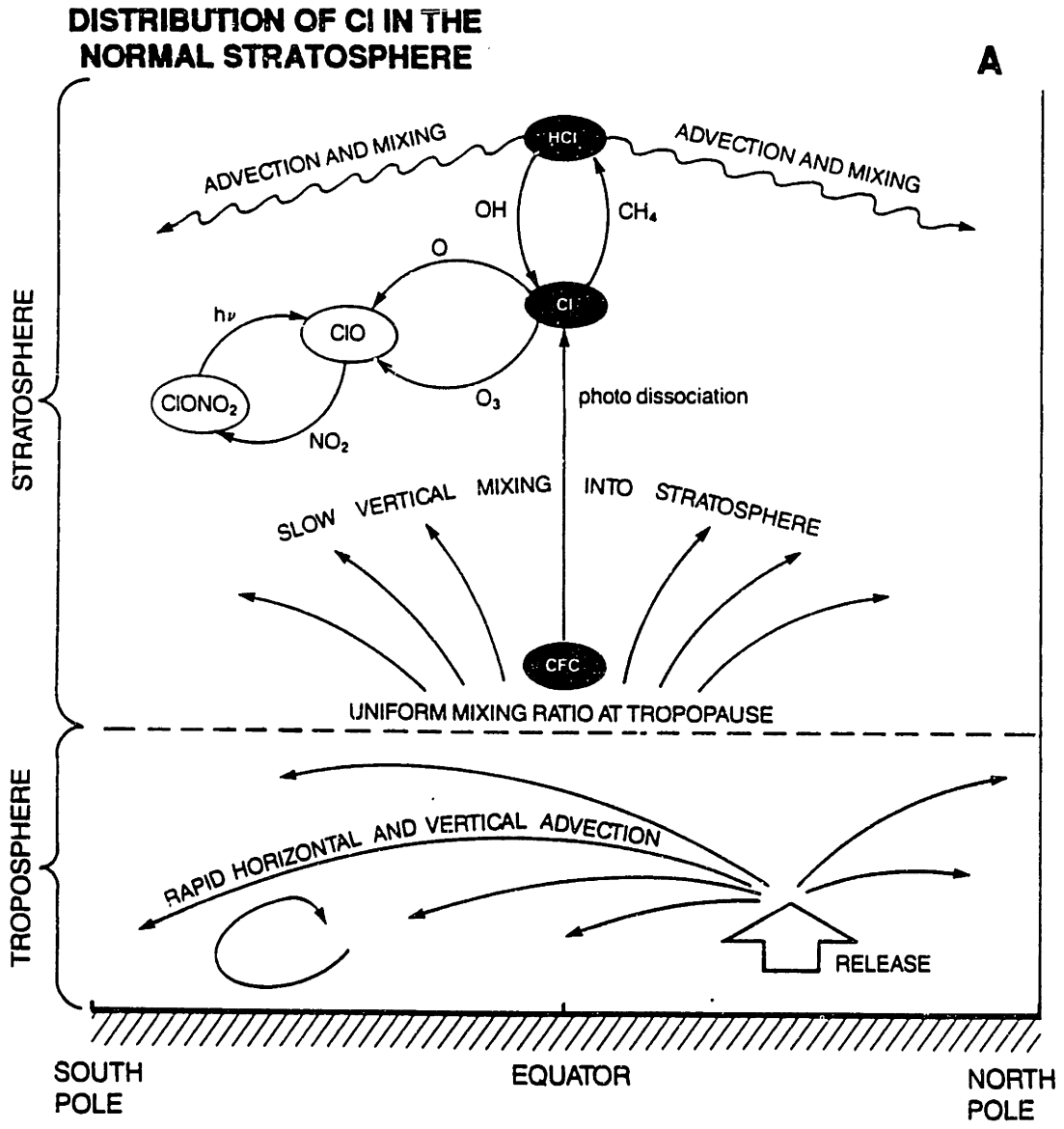

Figure 1.1: Schematic representation of the normal distribution of chlorine compounds in the stratosphere augmented by CFC release. This sequence of slow upward mixing of CFCs, photodissociation, and sequestering, primarily in the form of HCl and $ClONO_2$ results in a uniform mixing ratio of chlorine in any volume element of the stratosphere. Figure from Anderson et al., 1991.

Chapter II

Supercooling / Nucleation Studies

2.1 Introduction

There is always a background layer of aerosols in the lower stratosphere made up mostly of sulfuric acid / water particles [Junge, 1961]. The main source of the sulfuric acid is COS and SO_2, both from natural sources. The conversion of COS to H_2SO_4 will be discussed below. The main sources of COS in the atmosphere are emissions from the oceans, soils and biomass burning, and the conversion of CS_2 to COS. The total emission of COS is about 2 teragrams per year [WMO, 1985] Mixing ratios of COS in the stratosphere are reported by Inn et al. [1979, 1981] as 281-524 ppt for the lower stratosphere (15.2 km) and 14-18 ppt for the upper stratosphere (31 km).

SO_2 from anthropogenic sources does not reach the stratosphere, but rather is scavenged in the troposphere and contributes to the acid rain problem. SO_2 reaches the stratosphere mainly by direct injection from volcanic eruptions (see Warneck [1988] for a compilation of data on volcanic emissions of SO_2). For example, the recent Mount Pinatubo explosion in the Philippines injected approximately 20 million tons of SO_2 directly into the stratosphere [Bluth et al., 1992]. The resulting sulfuric acid aerosol cloud was observed to circulate around the globe by satellite [McCormick et al., 1992].

The reaction sequence for COS conversion to SO_2 is:

$$COS + h\nu \rightarrow S + CO \qquad (2.i)$$

$$S + O_2 \rightarrow SO + O \qquad (2.ii)$$

$$SO + O_2 \rightarrow SO_2 + O \qquad (2.iii)$$

Then, the mechanism for the conversion of SO_2 to H_2SO_4 is as follows [DeMore et al., 1992]:

$$SO_2 + OH \rightarrow HOSO_2 \qquad (2.iv)$$

$$HOSO_2 + O_2 \rightarrow SO_3 + HO_2 \qquad (2.v)$$

$$SO_3 + H_2O \rightarrow H_2SO_4 \qquad (2.vi)$$

Once H_2SO_4 is formed, it clusters with water and other sulfuric acid molecules very rapidly. This process leads to the formation of stratospheric aerosols. Recent studies have been performed on the formation and equilibrium composition of such aerosols [Zhang et al., 1993a]. The formation of these aerosols may have many consequences for stratospheric chemistry. Foremost of these is the catalysis of chemical reactions important to ozone depletion. Sulfuric acid aerosols are thought to be a precursor to the formation of PSCs. The aerosols are about 70% H_2SO_4 by weight at mid latitudes. In colder air (higher latitudes) the aerosols absorb more water to maintain equilibrium with the partial pressure of water in the surrounding air. Other investigators have suggested from theoretical calculations that sulfuric acid aerosols may freeze when they are yet fairly concentrated, ~60 wt. % [Luo et al., 1992]. Our experimental studies on the supercooling of the H_2SO_4/H_2O binary system address these questions as well as others.

We use a simple method to determine the critical freezing points of aqueous sulfuric acid solutions, where possible, and we also performed experiments to determine the length of time it takes for these solutions to freeze. A critical freezing point is the temperature at which the rate of nucleation of the solid phase is one nucleus per cubic centimeter per second (i.e. nucleation occurs instantaneously). This temperature is always below the equilibrium freezing point since liquids have the ability to supercool. The equilibrium freezing points are found by melting frozen samples, since the equilibrium melting point is the same temperature.

Supercooling studies of the ternary system $H_2SO_4/HNO_3/H_2O$ were also carried out and are reported here. Zhang et. al. [1993b] showed that H_2SO_4/H_2O liquid takes up appreciable amounts of HNO_3 at polar stratospheric temperatures and concentrations of HNO_3 and H_2O. This adds a further complication to understanding the function of

H_2SO_4/H_2O aerosols as PSC precursors. Of critical significance is the nucleation in these liquids of a H_2SO_4/H_2O hydrate and NAT.

Seeding studies were performed to determine the ability of crystals of stratospheric species to nucleate solutions of the ternary system. The relevant solids that form when these solutions "freeze" are sulfuric acid tetrahydrate (SAT), nitric acid trihydrate (NAT) and ice. In the studies presented here, the solids mentioned were used as small seeds to see if they would nucleate solutions that are relevant to the stratosphere.

2.2 Theory of Binary Nucleation

2.2.1 Thermodynamics of Nucleation

We are interested in the case of nucleation of a two component solid (NAT and or SAT) from a liquid that may have two or more components. In this case it is necessary to use the theory of binary nucleation (nucleation where two components are involved), rather than applying the traditional case of homomolecular nucleation to nucleation of binary solids, as some have done [Luo et al., 1992].

Binary nucleation was first investigated by Flood [1934], and Reiss [1950] first showed that the free energy change of a nucleation process is correctly represented by a surface: $\Delta G(n_1, n_2)$, where 1 and 2 denote the two components, respectively, and n is the number of moles of each component. However Reiss' work (along with later work in the literature) was developed for the nucleation of liquid drops from the vapor. The applicable theory here is binary nucleation of solids from a solution. Other investigators, most recently Thompson and Spaepen [1983], Trinkaus [1983], and Wu [1993], have applied the theory of binary nucleation to the case of solid nucleation from the liquid. Our goal at the end is to better understand the nucleation of NAT and SAT from binary and ternary solutions.

Classical nucleation theory is based on the capillarity approximation: the free energy of formation of a nucleus is composed of a bulk plus a surface contribution [Zeng

and Oxtoby, 1991]. If we consider a binary solid crystallite forming in a liquid, we have for the differential free energy of the *bulk* of a system at constant temperature and Pressure [Noggle, 1989]:

$$dG^b = \left(\frac{\partial G}{\partial n_1^b}\right)_{T,P,n_2^b} dn_1^b + \left(\frac{\partial G}{\partial n_2^b}\right)_{T,P,n_1^b} dn_2^b \tag{2.1}$$

where the superscript b denotes the bulk portion of the crystallite, n_i denotes the number of moles of component i, T and P are temperature and pressure, respectively. Then the differential free energy for the molecules at the *surface* of the crystallite is:

$$dG^s = \left(\frac{\partial G}{\partial n_1^s}\right)_{T,P,n_2^s} dn_1^s + \left(\frac{\partial G}{\partial n_2^s}\right)_{T,P,n_1^s} dn_2^s + \left(\frac{\partial G}{\partial A}\right)_{T,P} dA \tag{2.2}$$

where the superscript s denotes the surface and A is the surface area. By definition the chemical potential is: $\mu \equiv \left(\frac{\partial G}{\partial n_i}\right)_{T,P,n_{j\neq i}}$, and the surface energy is: $\sigma \equiv \left(\frac{\partial G}{\partial A}\right)_{T,P}$. Then equations 2.1 and 2.2 become:

$$dG^b = \mu_{1c} dn_1^b + \mu_{1c} dn_2^b \tag{2.3}$$

$$dG^s = \mu_{1c} dn_1^s + \mu_{2c} dn_2^s + \sigma dA \tag{2.4}$$

where the subscript c denotes the crystallite. It can be shown [Noggle, 1989] that the free energy expressions for bulk and surface molecules are:

$$G^b = n_1^b \mu_{1c} + n_2^b \mu_{2c} \tag{2.5}$$

$$G^s = n_1^s \mu_{1c} + n_2^s \mu_{2c} + \sigma A \tag{2.6}$$

Then, taking the differential of equation 2.5, we have:

$$dG^b = n_1^b d\mu_{1c} + n_2^b d\mu_{2c} + \mu_{1c} dn_1^b + \mu_{2c} dn_2^b \tag{2.7}$$

Comparison of equation 2.7 with 2.3 immediately shows that:

$$n_1^b d\mu_{1c} + n_2^b d\mu_{2c} = 0 \tag{2.8}$$

Equation 2.8 is the well known Gibbs-Duhem equation. Proceeding in the same manner with equation 2.6 immediately shows:

$$n_1^s d\mu_{1c} + n_2^s d\mu_{2c} + A d\sigma = 0 \tag{2.9}$$

This is the less well known "Gibbs adsorption isotherm" equation [Wilemski, 1984] (so-called among chemical physicists, known simply as the Gibbs equation among physical chemists). These two identities will be used immediately below.

Zeng and Oxtoby [1991] present a brief review of the classical binary nucleation theory for liquids nucleating from the mother vapor phase, and Thompson and Spaepen [1983] have used its analogy for the case of solid nucleation from the liquid. We have the general equation of the free energy change of binary nucleation assuming the nucleus can be described as a sphere:

$$\Delta G = n_1^t(\mu_{1c} - \mu_{1l}) + n_2^t(\mu_{2c} - \mu_{2l}) + A\,\sigma_{lc} \tag{2.10}$$

where l and c denote the liquid and solid phase; σ_{lC} is the surface energy between the crystallite and liquid interface, and n^t is the total number of moles of component i in the crystallite where $n_i^t = n_i^b + n_i^s$. As mentioned above, Reiss showed that the three dimensional surface $\Delta G(n_1, n_2)$ has a saddle point that represents the minimum height of the free energy barrier. This is the critical free energy denoted ΔG^*, and to determine this point we take the derivatives:

$$(d\Delta G)_{T,P,n_1^t} = (d\Delta G)_{T,P,n_2^t} = 0 \tag{2.11}$$

Applying equations 2.11 to equation 2.10 and summing the results (remembering that $d\mu_{il} = 0$ since the liquid molecules have not undergone a free energy change until they convert to the crystal lattice) we have the differential equation [Wilemski, 1984]:

$$\sum_{i=1}^{2}\left[\Delta\mu_i + \sigma\left(\frac{\partial A}{\partial n_i^t}\right)_{n_{j\neq i}}\right]\left(dn_i^t\right)_{n_{j\neq i}} + n_1^b d\mu_{1c} + n_2^b d\mu_{2c} + n_1^s d\mu_{1c} + n_2^s d\mu_{2c} + A d\sigma = 0 \tag{2.12}$$

where $\Delta\mu_i = \mu_{ic} - \mu_{il}$. From the Gibbs-Duhem and Gibbs adsorption isotherm identities, equation 2.12 immediately reduces to the initial sum in the equation. Previously, a number of researchers did not make use of the Gibbs adsorption isotherm identity and thus developed erroneous equations for binary nucleation. See section 2.7 for a discussion of this unfortunate occurrence. Separating the sum of 2.12 back into the initial derivatives of 2.11, we have:

$$\Delta\mu_1 + \sigma\left(\frac{\partial A}{\partial n_1^t}\right)_{n_2^t} = 0 \tag{2.13}$$

$$\Delta\mu_2 + \sigma\left(\frac{\partial A}{\partial n_2^t}\right)_{n_1^t} = 0 \tag{2.15}$$

In order to find the derivative of the surface area with respect to the number of moles in the crystallite, we need to write the expression for the surface area of the crystallite in terms of the number of molecules of each component. Making use of the relation:

$$V = \frac{4}{3}\pi r^3 = n_1^t V_1 + n_2^t V_2 = n^t V_m^t \tag{2.16}$$

where V_i is the partial molar volume of component i, and V_m^t is the molar volume. Then, we have for r:

$$r = \left[\frac{3\left(n_1^t V_1 + n_2^t V_2\right)}{4\pi}\right]^{1/3} \tag{2.17}$$

Now, using $A = 4\pi r^2$, substituting equation 2.17 in for r, and then evaluating the derivative, we have the so-called Gibbs-Thomson (Kelvin) equations:

$$\Delta\mu_1 + \frac{2\sigma_{lc}^* V_1^*}{r^*} = 0 \tag{2.18}$$

$$\Delta\mu_2 + \frac{2\sigma_{lc}^* V_2^*}{r^*} = 0 \tag{2.19}$$

where the superscript * denotes the critical point for the respective variable. We need to proceed now to solve for the critical radius of the crystallite r^*. Following the example of Zeng and Oxtoby [1991], we multiply equation 2.18 by the *bulk* mole fraction of component 1 and equation 2.19 by the *bulk* mole fraction of component 2 and then add the two equations:

$$r^* = -\frac{2\sigma_{lc}^* V_m^*}{x_{1c}^{b*}\Delta\mu_1 + x_{2c}^{b*}\Delta\mu_2} \tag{2.20}$$

where the bulk molar volume is: $V_m^* = x_{1c}^{b*} V_1 + x_{2c}^{b*} V_2$, and the bulk mole fraction is: $x_{ic}^b = n_{ic}^b / n_{ic}^t$. In order to obtain the critical free energy, we substitute equation 2.20 back into equation 2.10, and using equations 2.18 and 2.19 for the change in chemical potential, we have:

$$\Delta G^* = \frac{16\pi\sigma_{lc}^{*3}V_m^{*2}}{3\left(x_{1c}^{b*}\Delta\mu_1 + x_{2c}^{b*}\Delta\mu_2\right)^2} \tag{2.21}$$

Finally we need an expression for the change in chemical potential in terms of measurable quantities. Following the development of Denbigh [1971] the chemical potential for a non-ideal solution is:

$$\mu_i = \mu_i^\theta + RT\ln(\gamma_i x_i) \tag{2.22}$$

where μ_i^θ is the standard state chemical potential of component i in the solution, γ_i is the activity coefficient of component i, and x_i is the mole fraction of component i. We adopt "Convention I" of Denbigh where:

$$\gamma_i \to 1 \text{ as } x_i \to 1 \tag{2.23}$$

(Denbigh also shows that with the constraint of 2.23, Raoult's Law immediately follows from equation 2.22) Then for the change in chemical potential from liquid to crystal we have:

$$\Delta\mu_i = \mu_{ic} - \mu_{il} = \mu_{ic}^\theta - \mu_{il}^\theta + RT\left[\ln(x_{ic}) + \ln(\gamma_{ic}) - \ln(x_{il}) - \ln(\gamma_{il})\right] \tag{2.24}$$

Note that we are considering a supercooled liquid, and hence it is not in equilibrium with the solid state; therefore the chemical potentials of the liquid and solid states upon nucleation are not equivalent. Near the melting point we can write [Oxtoby, 1988]:

$$\mu_{ic}^\theta - \mu_{il}^\theta = -\Delta S_f(T_m - T) \tag{2.25}$$

where T_m is the melting temperature of the solid formed from nucleation, and ΔS_f is the entropy of fusion. Using equation 2.25 in equation 2.24, we have:

$$\Delta\mu_i = -\Delta S_f(T_m - T) + RT\left[\ln\left(\frac{x_{ic}}{x_{il}}\right) + \ln\left(\frac{\gamma_{ic}}{\gamma_{il}}\right)\right] \tag{2.26}$$

Now, at $T = T_m$, $\mu_{ic} = \mu_{il}$, hence $\Delta\mu_i = 0$. We then have:

$$RT_m\ln\left(\frac{\gamma_{ic}}{\gamma_{il}}\right) = -RT_m\ln\left(\frac{x_{ic,eq}}{x_{il}}\right) \tag{2.27}$$

where $x_{ic,eq}$ is the equilibrium mole fraction of component i in the crystal. Substituting equation 2.27 back into equation 2.26, we have the final form for the change in chemical potential:

$$\Delta\mu_i = -\Delta S_f(T_m - T) - RT\ln\left(\frac{x_{il}}{x_{ic}}\right) + RT_m\ln\left(\frac{x_{il}}{x_{ic,eq}}\right) \qquad (2.28)$$

We then use equation 2.28 in the expression for the free energy in equation 2.21 for components 1 and 2. Equation 2.28 is simple to use since the mole fractions of the solid and the liquid can easily be measured for the systems of interest. However, we are left with an entropy of fusion term, and a surface tension term to the third power (equations 2.21). Since there are no measurements of the liquid/crystal surface energy for the liquids/solids we are interested in (SAT in solutions of H_2SO_4/H_2O and SAT and NAT in solutions of $H_2SO_4/HNO_3/H_2O$) the parameter must be guessed at, and there are several papers that attempt to do so [Jensen et al., 1991; Luo et al., 1992; Luo et al., 1993].

Chiang et al. [1988] have attempted to develop a new theory of nucleation specifically for the case of ionic solutions which avoids parameters that are difficult to measure. They state that ionic solids grow from ionic solutions by the incorporation of ions rather than neutral molecules (see the companion paper Chiang and Donohue [1988]). We agree with this position; however, it is unclear that this statement invalidates the 'classical' approach to nucleation in such systems. They compared their results to a number of systems with experimentally determined nucleation rates; however, the comparisons were less than spectacular. It would seem that the greatest benefit of their work is in proposing a viable alternative theory for nucleation in ionic systems which circumvents the need for parameters which are difficult to measure and often even harder to estimate with any degree of accuracy.

2.2.2 Rate of Nucleation

The nucleation rate theory discussed below is outlined by Walton [1969] for homomolecular, single component nucleation of solids from the liquid. We have made minor modifications of this for the analogy to the binary case. Walton [1969] has given the equation for the rate of nucleation of solids from the liquid mother phase as:

$$J = R_i A^* N^* \qquad (2.29)$$

where R_i is the rate of arrival of the post-critical molecule at the crystallite, A^* is the surface area of the crystallite, and N^* is the number of critical clusters per unit volume of the solution. R_i can be said to be equivalent to the rate of transport of molecules across the crystallite/liquid interface:

$$R_i = \frac{k_B T}{h} \exp\left(\frac{-\Delta G_a}{k_B T}\right) \tag{2.30}$$

where ΔG_a is the activation energy barrier for the slowest species in the binary system to diffuse from the bulk solution into the crystallite, and $k_B T/h$ is the frequency of the "jumps" (h is Plank's constant). N^* is given by the equation:

$$N^* = N_1 \exp\left(\frac{-\Delta G^*}{k_B T}\right) \tag{2.31}$$

where N_1 is the number of monomeric species and ΔG^* is as derived in the previous section. Therefore, we have for the rate:

$$J = \frac{k_B T}{h} A^* \exp\left(\frac{-\Delta G_a}{k_B T}\right) N_1 \exp\left(\frac{-\Delta G^*}{k_B T}\right) \tag{2.32}$$

This equation for the nucleation rate is based on the assumption that equilibrium thermodynamics can be validly applied to a kinetic situation. The difficulty of this situation is circumvented by introduction of the so-called Zeldovich factor [Zeldovich, 1943] which takes into account the difference between an equilibrium and a steady-state distribution of crystallite sizes:

$$Z = \frac{V_m^* \Delta G_v^*}{8\pi\sigma_{lc}(\sigma_{lc} k_B T)^{1/2}} \tag{2.33}$$

where $\Delta G_v^* = x_{1c}^{b*}\Delta\mu_1 + x_{2c}^{b*}\Delta\mu_2$. Now, $A^* = 4\pi r^{*2}$, and using equation 2.20 for the critical radius, we have:

$$ZA^* \frac{k_B T}{h} = \frac{2V_m^{*3}(\sigma_{lc} k_B T)^{1/2}}{h} \tag{2.34}$$

Thus, the equation for the rate of nucleation is:

$$J = \frac{2V_m^{*3}(\sigma_{lc} k_B T)^{1/2}}{h} \exp\left(\frac{-\Delta G_a}{k_B T}\right) N_1 \exp\left(\frac{-\Delta G^*}{k_B T}\right) \tag{2.35}$$

One can readily see that we have two difficulties in this equation: determination of the surface free energy and determination of the free energy of activation for diffusion. Discussions of the theoretical aspects of determining ΔG_a are nearly non-existent, and ΔG_a has been determined empirically for only a very few substances such as water/ice [Houghton, 1985].

2.2.3 Crystal growth

An additional factor in the physical chemistry of freezing is the *crystallization velocity*, which is often a controlling factor in determining the time required for a liquid to freeze completely. Mason [1957] has given a generalized theoretical equation for the crystallization velocity based on the analogous case in electrostatics (also, Mason develops the equation for the growth of an ice crystal from the vapor - not exactly our case of interest.) Mason and others [Hallet, 1968; Rogers and Yau, 1989] developed theoretical equations that predicted a linear relationship between the growth rate and the supercooling. Mason's experiments on the growth of ice from vapor were in agreement with this theory; however, Hallet's experiments on ice growth from liquids were not. Hallet's experiments showed that the growth rate is proportional to the square of the supercooling. Pruppacher and Klett [1980] (P&K) reviewed the previous work and showed that the growth rate has a squared dependence on the supercooling in a regime where $\Delta T < 9$ C and a linear dependence for $\Delta T > 12$ C. However, the existing experimental data is reasonably scattered such that a number of conclusions can be drawn. It is reasonable to assume that the results for the growth of binary solids will be similar; however, given the lack of experimental work in this area, no *a priori* conclusions should be drawn.

P & K have developed a quantitative description which is based on the simple theory of reaction rates, i.e.

$$H_2O_{(l)} \rightarrow H_2O_{(ice)} \qquad \text{(2.vii)}$$

In this situation, we are interested in describing the rate of the reaction given by (2.vii). P & K give an equation for the thermodynamic driving force responsible for the advance of the crystal face as:

$$\frac{(\mu_{l,a} - \mu_s)}{a} \tag{2.36}$$

where μ_S and $\mu_{l,a}$ are the chemical potentials for the solid (s) and the liquid (l) one mean molecular jump distance (a) away from the interface, respectively. The mobility of the molecules (water and sulfuric acid) is given by:

$$\frac{D_{H_2SO_4}}{RT_s} \tag{2.37}$$

We use only the diffusivity of sulfuric acid as it is smaller than that for water, and T_S is the temperature at the liquid/solid interface. Then the growth rate is given by the product of 2.36 and 2.37:

$$I = \frac{D_{H_2SO_4}}{RT_s}\frac{(\mu_{l,a} - \mu_s)}{a} \tag{2.38}$$

One should also see Chiang and Donohue [1988] for a discussion of the growth of solids by the addition of ions from solution.

2.2.4 Previous theoretical studies

Luo et al. [1992] have attempted to theoretically determine the nucleation rate for the formation of SAT from H_2SO_4/H_2O supercooled liquid aerosols. Their equation for the free energy change of the system is:

$$\Delta G = -\frac{4}{3}\pi r_s^3\left[N^s_{H_2O}kT\log\left(\frac{P^l_{H_2O}}{P^s_{H_2O}}\right) + N^s_{H_2SO_4}kT\log\left(\frac{P^l_{H_2SO_4}}{P^s_{H_2SO_4}}\right)\right] + 4\pi r_s^2\sigma_{sl} \tag{2.39}$$

where r_S is the radius of the solid particle, and N^S is the number of molecules in the solid of the respective species. In their calculations Luo, et al. postulated that the activation energy to move a sulfuric acid molecule in aqueous solution is larger than that for a water molecule (the case for species 2 above). With this assumption, the process of forming a critical nucleus is limited by the incorporation of sulfuric acid molecules into a SAT germ.

Luo et al. used this assumption to simplify their expression for the free energy change (equation 2.39) by neglecting the energy term due to water, reducing equation 2.39 to:

$$\Delta G \approx -\frac{4}{3}\pi r_s^3\left[N^s_{H_2SO_4} kT \log\left(\frac{P^l_{H_2SO_4}}{P^s_{H_2SO_4}}\right)\right] + 4\pi r_s^2 \sigma_{sl} \qquad (2.40)$$

This is a different method than has been employed in the previous literature, and it does not appear to be valid. As mentioned previously, Reiss [1950] showed that the three dimensional surface, $\Delta G(n_1, n_2)$, has a saddle point that represents the minimum height of the free energy barrier. In general, the saddle point for a surface of $\Delta G(n_1, n_2)$ will not be equivalent to the maxima in $\Delta G(n_2)$. This is clear for the case of sulfuric acid solutions nucleating from the vapor as reported by Heist and Reiss [1974] where they have calculated numerous free energy surfaces demonstrating various positions of the saddle point for different background pressures of water and sulfuric acid. In order for Luo et al.'s assumption to be true, the maxima of $\Delta G(n_1)$ would have to be much greater than the maxima of $\Delta G(n_2)$ where the surface connecting $\Delta G^*(n_1)$ with $\Delta G^*(n_2)$ would have to be all 'down hill' from $\Delta G^*(n_1)$. Luo et al. have not demonstrated this to be the case, but instead merely discard the free energy contribution of the water term based on a kinetic consideration. This is, in itself, incorrect. In addition, they neglect to use the Zeldovich factor discussed above in their nucleation equation. Also, it appears that Luo et al. have not considered the differences between homomolecular and binary nucleation, as their cited references for equation 2.39 are for the nucleation of ice from water or water solutions with impurities. Therefore, we must conclude that their method of calculating the nucleation rate of SAT from solution are not likely to achieve correct results; however, since parameters need to be guessed, equations can not be readily tested.

2.3 Parameterization of $H_2SO_4/HNO_3/H_2O$ Ternary System Experimental Data

2.3.1 Introduction

As has been shown by Zhang et al. [1993b], under the vapor pressure and temperature conditions of the polar stratosphere, nitric acid becomes appreciably soluble in aqueous solutions of sulfuric acid. It is now apparent that as the ice frost point in approached, the equilibrium concentration of nitric acid in polar stratospheric aerosols is comparable to or greater than the equilibrium concentration of sulfuric acid in these same aerosols. A knowledge of the composition of the aerosols at stratospheric temperatures and vapor pressures is critical for our investigation of the supercooling ability of these aerosols.

2.3.2 Previous Parameterization

In their paper, Zhang et al. present a parameterization of their data. We summarize here their results: solutions were made of varying compositions and then the vapor pressures of each solution as a function of temperature measured. The water and nitric acid vapor pressures of each solution were individually parameterized with respect to temperature according to the equation:

$$\log(P) = A - \frac{B}{T} \tag{2.41}$$

The tabulated A and B coefficients for each solution are given in Zhang et al. Then, a parameterization of the vapor pressures is carried out to give a general equation valid over the range of compositions used, and over a general range of temperature . Zhang et al. based their parameterization on Henry's Law; note that they do not use the traditional, physical chemistry definition of Henry's Law, i.e.:

$$P_i = k_x X_i \tag{2.42}$$

where P_i is the vapor pressure of component i over a solution whose mole fraction is X_i, and k_X is the Henry's Law constant (as given by any physical chemistry textbook.) Instead Zhang et al. use a form which is commonly employed in atmospheric sciences:

$$X_i = P_i H \tag{2.43}$$

where H is called the Henry's Law constant. It is simple to convert between the two since $H = 1/k_X$. Zhang et al. derive equations for the vapor pressures based on equation 2.43. For nitric acid, their equation is:

$$\log\left(P_{HNO_3}\right) = a_1 + a_2 y + \log(x) + a_3 x \tag{2.44}$$

(equation 10 of Zhang et al.) where x and y are weight fractions of nitric and sulfuric acids, respectively and P_{HNO_3} is the vapor pressure of nitric acid. Zhang et al. state that the first three terms of equation 2.44 represent ideal behavior, i.e. Henry's Law. Indeed, taking 10 to the power of equation 2.44 (minus the last term on the RHS):

$$P_{HNO_3} = x\ 10^{(a_1 + a_2 y)} \tag{2.45}$$

This is in fact the classical form of Henry's Law, analogous to equation 2.42 with $k_x = 10^{(a_1 + a_2 y)}$. Zhang et al. then state that the fourth term of equation 2.44 accounts for the non-ideality of the ternary system. This introduces the activity coefficient where equation 2.42 becomes:

$$P_i = k_x X_i \gamma_i \tag{2.46}$$

and γ is the activity coefficient which will be discussed in the next section.

The parameterization for the water vapor pressures of Zhang et al. is:

$$\log\left(P_{H_2O}\right) = b_1 + b_2 x + b_3 y + b_4 \log(y) + b_5 \log^2(y) + b_6 \log^3(y) \tag{2.47}$$

Rearranging equation 2.47 to compare it to the Henry's Law form:

$$P_{H_2O} = y^{b_4}\ 10^{\left(b_1 + b_2 x + b_3 y + b_5 \log^2(y) + b_6 \log^3(y)\right)} \tag{2.48}$$

It is apparent that equation 2.48 is not analogous to Henry's Law (either equation 2.42 or 2.43). Thus it appears that equation 2.47 is a straight mathematical parameterization.

The main limitation of the parameterization of Zhang et al. for the partial pressure of water is that it is only valid over the range of their experimental data. This is

unsatisfactory for the range of experiments that we performed. Therefore, we introduced a new parameterization of the data as outlined below.

2.3.3 New Parameterization

We re-analyzed Zhang et al.'s data for the ternary system: sulfuric acid/nitric acid/water for two purposes:

1. to parameterize the water data based on a physical chemical principle - in this case Raoult's Law,

2. to have a parameterization that would extrapolate 'reasonably' beyond the data to higher nitric acid concentrations.

The standard definition of Raoult's Law is:

$$P_i = X_i P_i^0 \tag{2.49}$$

where P_i is the vapor pressure of component i over a solution at a given temperature (T), X_i is the mole fraction of component i, and P_i^0 is the vapor pressure of the pure component i at the same T. This form of Raoult's Law is useful for ideal solutions; however, our system is non-ideal, therefore we need to make a correction due to non-ideality:

$$P_i = X_i P_i^0 \gamma_i \tag{2.50}$$

Since Zhang et al. used the parameter of weight fraction in their experiments rather than mole fraction, we used weight fraction also and define the following symbols: x is the weight fraction of nitric acid, y is the weight fraction of sulfuric acid, and w is the weight fraction of water. We needed to parameterize the data for water vapor pressures using Raoult's Law, since our limiting case is that of ice, where the acids are small impurities, thus the Raoult's Law limit. Zhang et al.'s parameterization of their nitric acid data is based on Henry's Law, and would, in principle, extrapolate reasonably beyond the data. However, we decided to perform a new parameterization.

First, we will focus on the equation for the vapor pressures of nitric acid using a form of Henry's Law:

$$P_{HNO_3} = xH\gamma_{HNO_3} \tag{2.51}$$

We can then rearrange this equation in terms of measured and non-measured parameters and take the logarithm of both sides to ease the data analysis for reasons that are not obvious until after attempting a "first try" parameterization:

$$\log\left(\frac{P_{HNO_3}}{x}\right) = \log\left(H\gamma_{HNO_3}\right) \tag{2.52}$$

All the terms on the left hand side are measured in Zhang et al.'s experiments (or can be calculated from other experiments), the parameters gamma and H on the right hand side are not measured; however, we then calculate the product from the LHS. Now the task is to parameterize gamma in terms of measured quantities: x, y, and T, and H in terms of T only, since it should not change with composition. In choosing a parameter for gamma, it is reasonable to note that the vapor pressures will change as a function of total acid content (HNO_3 + H_2SO_4), not just one of these. Therefore, our first choice of a parameter is: (1-(x+y)). This parameter takes into account both the total acid concentration and the Raoult's Law constraint. We begin with a first order parameterization, moving to higher orders if necessary:

$$\log\left(\gamma_{HNO_3}\right) = a_0 + a_1(1-x-y) \tag{2.53}$$

For H, we chose an equation of the form:

$$\log(H) = b_0 + \frac{b_1}{T+b_2} \tag{2.54}$$

The data was fit to this parameterization for four temperatures: 205, 200, 195 and 190 K. The fit was found to be good, and so the parameters a_0 and a_1 were parameterized with respect to temperature using the data from the four temperatures listed. The equations for the a parameters are as follows:

$$a_0 = 2.64765 - \frac{314.74}{T} \tag{2.55}$$

$$a_1 = -4.46451 - \frac{685.49}{T} \tag{2.56}$$

and the b constants are: $b_0 = 7.616$, $b_1 = -1486$, and $b_2 = -43$. This parameterization was found to be in excellent agreement with the measured data as is shown in Figure 2.1 where the measured and calculated vapor pressures of nitric acid are compared for a temperature of 200 K. The error between the measured and calculated vapor pressures is at most 20% and more typically within 10%.

We then parameterized the equation for water based on Raoult's Law:

$$\log\left(\frac{P_{H_2O}}{wP^0_{H_2O}}\right) = \log\left(\gamma_{H_2O}\right) \tag{2.57}$$

in terms of the parameter $(x+y)$:

$$\log\left(\gamma_{H_2O}\right) = c_0 + c_1(x+y) + c_2(x+y)^2 \tag{2.58}$$

This parameter follows the Raoult's Law constraint, as $w \to 1$, $x \to 0$, $y \to 0$, hence $\gamma_{H_2O} \to 1$, $\log\left(\gamma_{H_2O}\right) \to 0$. This second order equation proved sufficient to parameterize the data. Again the c parameters were parameterized with respect to temperature and their equations are given below:

$$c_0 = 1.99081 - \frac{659.75}{T} \tag{2.59}$$

$$c_1 = -10.17448 + \frac{3465.7}{T} \tag{2.60}$$

$$c_2 = 10.5521 - \frac{4223.5}{T} \tag{2.61}$$

This parameterization was in good agreement with the measured water vapor data also, as is shown in Figure 2.2 for a temperature of 200K.

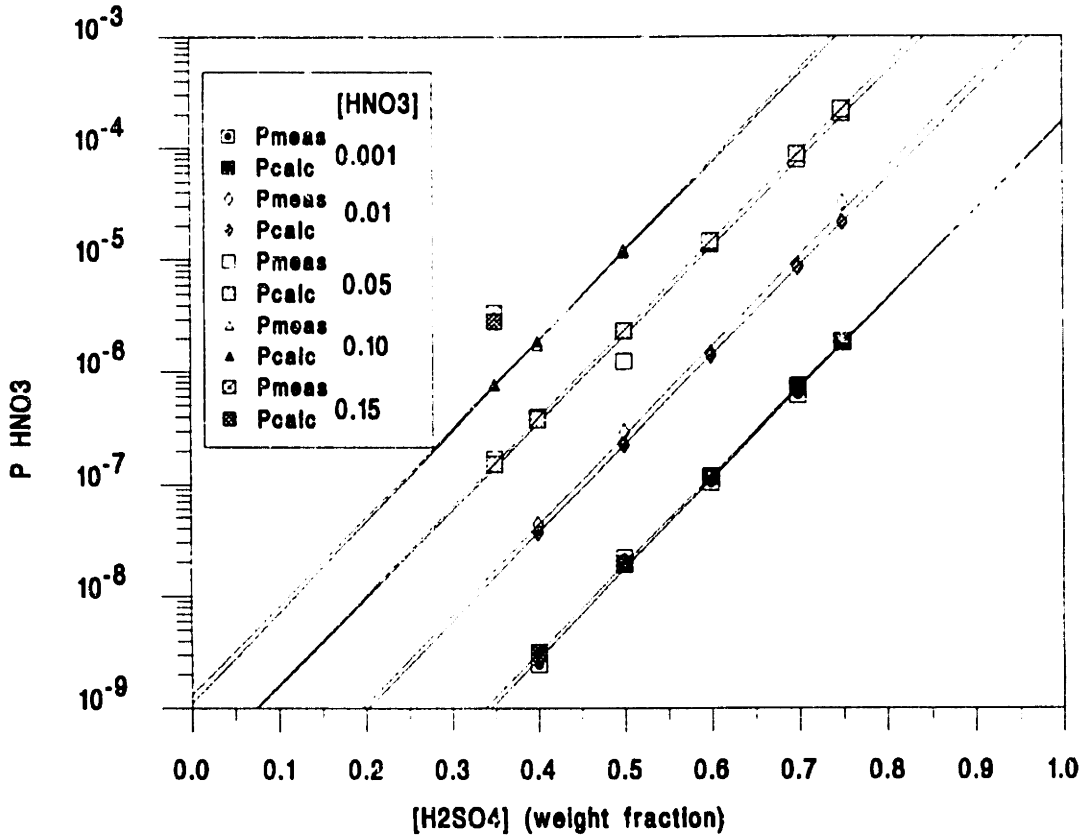

Figure 2.1: Plot of vapor pressure of nitric acid vs. weight fraction of sulfuric acid for the ternary system: $H_2SO_4/HNO_3/H_2O$. Shown are the measured and calculated values as a function of nitric acid weight fraction.

Then, the final equations to calculate the vapor pressures of nitric acid and water over a ternary solution are:

$$P_{HNO_3} = xH10^{(a_0+a_1(1-x-y))} \tag{2.62}$$

$$P_{H_2O} = wP^0_{H_2O}10^{\left(c_0+c_1(x+y)+c_2(x+y)^2\right)} \tag{2.63}$$

Equations 2.62 and 2.63 are of the form of Henry's and Raoult's Law respectively, corrected for non-ideality.

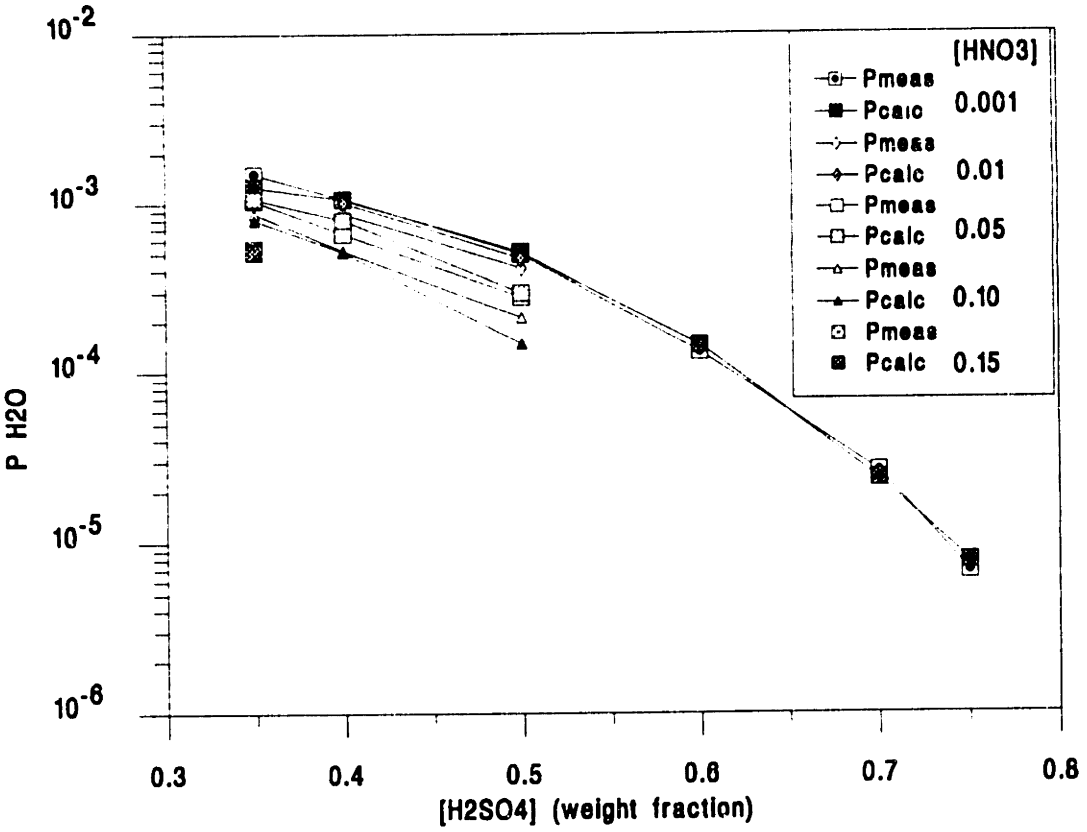

Figure 2.2: Plot of vapor pressure of water vs. weight fraction of sulfuric acid for the ternary system: $H_2SO_4/HNO_3/H_2O$. Shown are the calculated and measured values as a function of nitric acid weight fraction.

Finally, we want to state a vapor pressure of water and nitric acid, and a temperature, and then be able to calculate the equilibrium concentration of the solution with those properties. This requires simultaneously solving equations 2.62 and 2.63. It is easy to solve equation 2.62 for y by first taking the logarithm of both sides and then merely rearranging the terms to give:

$$y = \frac{\log x + \log H - \log P_{HNO_3} + a_0 + a_1(1-x)}{a_1} \tag{2.64}$$

Now we can take the logarithm of both sides of equation 2.63 and substitute (1-x-y) for w:

$$\log\left(P_{H_2O}\right) = \log(1-x-y) + \log\left(P^0_{H_2O}\right) + b_0 + b_1(x+y) + b_2(x+y)^2 \tag{2.65}$$

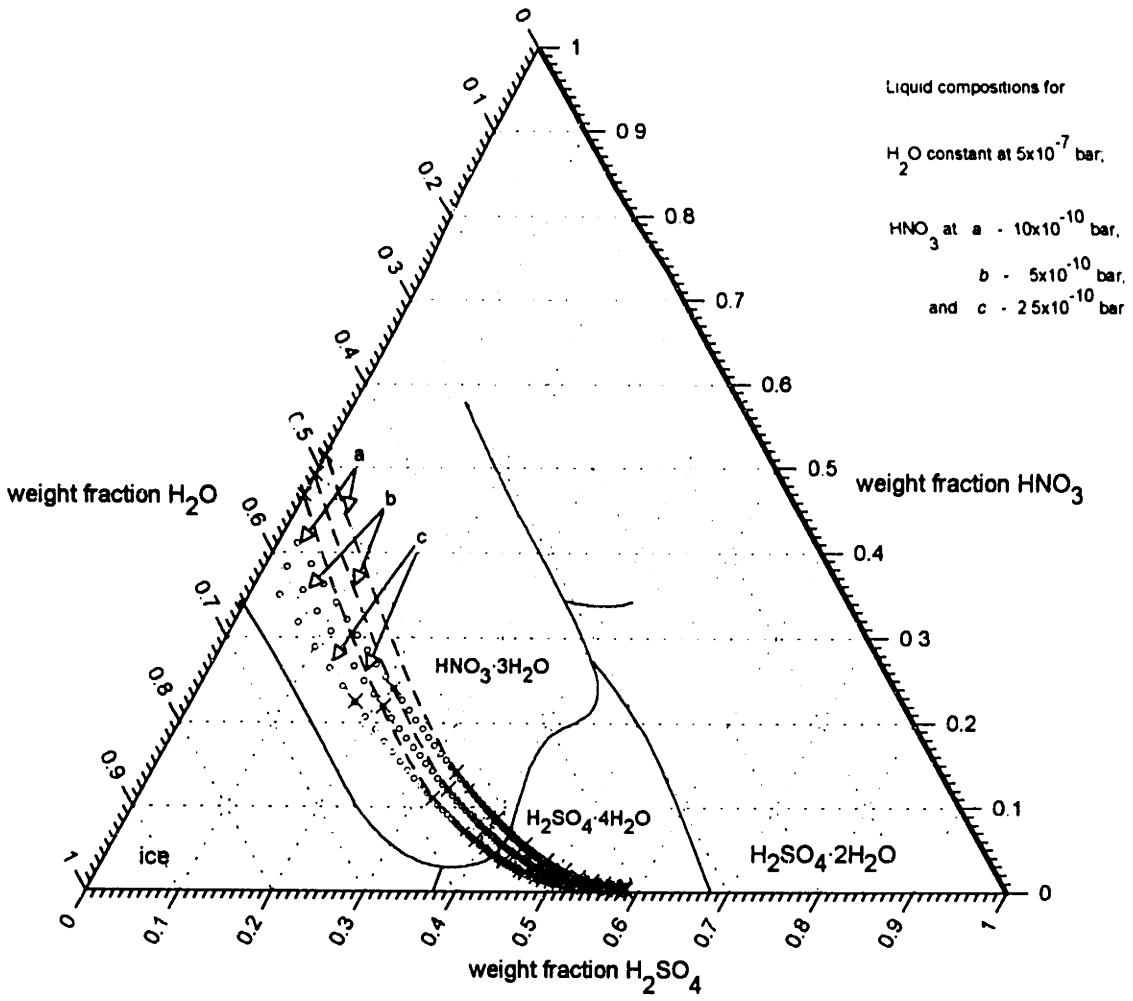

Figure 2.3: Plot of the ternary phase diagram. Solid lines mark out the eutectic lines of Carpenter and Lehrman [1925] (not complete), dashed lines are the extrapolation shown in Molina, et al., [1993], circles are the results of solving equations 2.62 & 2.63, x's mark temperature by integers, the x's on the nitric acid/water axis mark the points calculated from Hanson [1990]. The three different cases are those outlined in the legend.

When we substitute equation 2.64 for y we get an equation in terms of x only. This equation (which will not be repeated here) can be solved by any standard successive approximation technique. We employed Newton's method of first derivatives, using a C program to perform this task for user entered values of P_{HNO3}, P_{H2O}, and T. The results for a water pressure of 5 ppm at 100 mbar and 10 ppb, 5 ppb, 2.5 ppb of nitric acid are shown as circles in Figure 2.3. The x's on the nitric acid/water binary axis represent the calculated vapor pressures of a supercooled liquid based on the parameterization of Hanson [1990]. The limit as the sulfuric acid concentration goes to zero in the ternary system must be these points for the case of the stratosphere. However, the

parameterization presented here does not go to this limit. The extrapolations of Molina et al. [1993] (dashed curves) are simply a smooth connection of the points at the end of the measured data of Zhang et al. with the points of Hanson [1990] on the binary axis. Obviously an empirical correction to the present parameterization must be incorporated.

We wish the present parameterization to be smoothly corrected such that it reaches the nitric acid binary limit. For this purpose we chose a correction factor of the form: $c_1\left(\exp(1-y)^{c_2}-1\right)$, such that the function increases as y decreases, and as $y \to 1$, the function goes to 0 (thus no correction). The exponential c_2 serves to 'initiate' the function at a desired value of y (in this case at the edge of the data ~ $y = 0.3$), therefore, c_2 is set to 8. The pre exponential factor c_1 is a proportionality constant which is a function of temperature for each of the two parameterization equations.

Equation 2.53 for nitric acid then becomes:

$$\log\left(\gamma_{HNO_3}\right) = a_0 + a_1(1-x-y) - a_2\left[\exp(1-y)^8 - 1\right] \tag{2.66}$$

where $a_2 = -0.569 + \frac{189.9}{T}$. Equation 2.58 for water becomes:

$$\log\left(\gamma_{H_2O}\right) = b_0 + b_1(x+y) + b_2(x+y)^2 - b_3\left[\exp(1-y)^8 - 1\right] \tag{2.67}$$

where $c_3 = 0.1187 - \frac{59.74}{T}$. Then the equations for the vapor pressures in log form are, respectively:

$$\log\left(P_{HNO_3}\right) = \log(x) + \log(H) + a_0 + a_1(1-x-y) - a_2\left[\exp(1-y)^8 - 1\right] \tag{2.68}$$

$$\log\left(P_{H_2O}\right) = \log(1-x-y) + \log\left(P^0_{H_2O}\right) + b_0 + b_1(x+y) + b_2(x+y)^2 - b_3\left[\exp(1-y)^8 - 1\right] \tag{2.69}$$

Again, we must simultaneously solve equations 2.68 and 2.69 given T, and vapor pressures of HNO_3 and H_2O. The algorithm used to solve these equations is given in Appendix II. Again Newton's method was employed to solve these equations. The results are plotted in Figure 2.4, and are given for 0.1 K temperature steps between 205 and 190 K in Table 2.1. As can be seen from the plot, the calculated points smoothly reach the binary limit. The C algorithm in Appendix II allows the user to enter the desired

temperature range, background pressures of water and nitric acid, and the desired temperature step. The program will then perform the calculation and place the results in the user-named file. This is useful because aerosol equilibrium compositions can be calculated for any given set of stratospheric conditions.

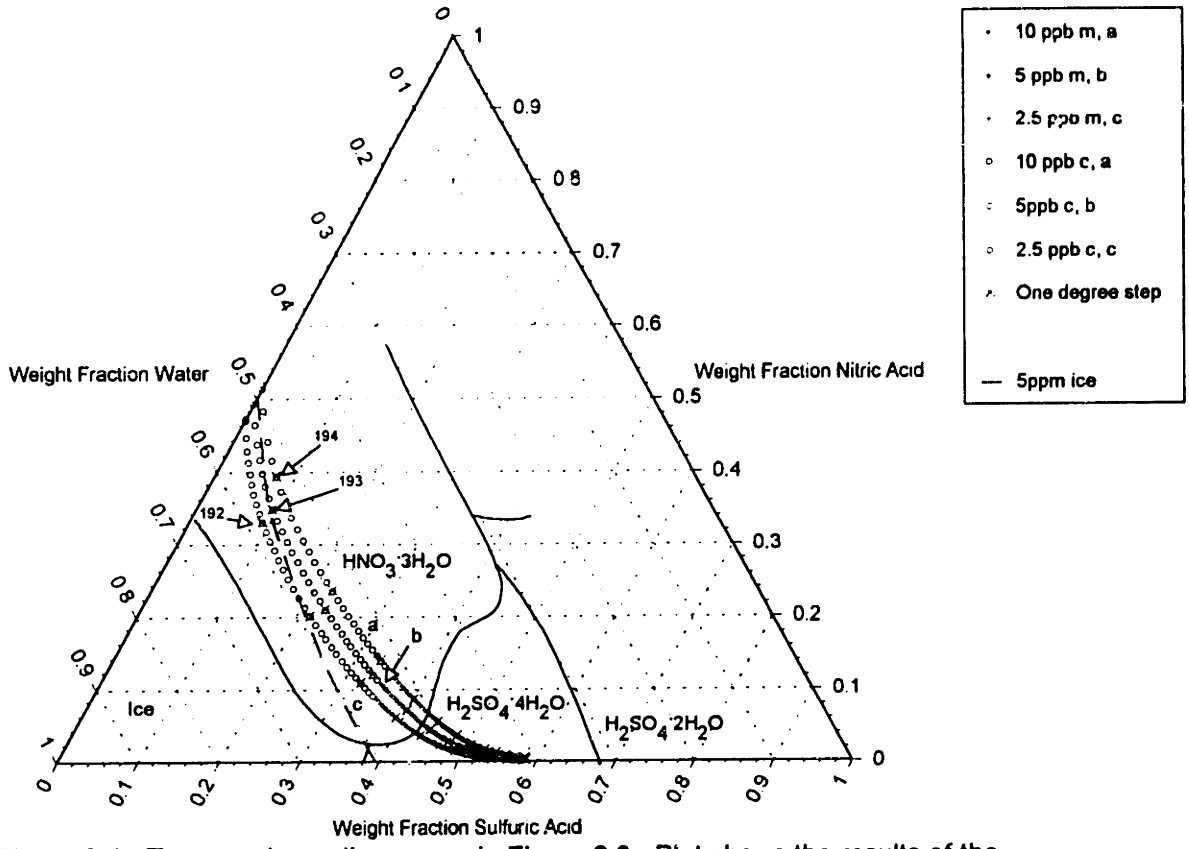

Figure 2.4: Ternary phase diagram as in Figure 2.3. Plot shows the results of the parameterization with empirical correction term (equations 2.69 and 2.70). Plus (+) symbols are for the results of the parameterization over the data range of Zhang, et al., circles are points beyond the measured data. The dashed line is the ice frost point in the ternary solutions (see text for calculation of this line).

It is also of interest to determine the frost point in the ternary system, i.e. the points at which the vapor pressure of the ternary solution is equal to that of ice at stratospheric conditions. In the case we have been studying, we have used a background pressure of water vapor of 5 ppm at 100 mbar. The temperature at which the vapor pressure of ice is equal to 0.0005 bar can be calculated from the equation of Jansco et al. [1970] or determined from tables in the Handbook of Chemistry and Physics [1985], and

Table 2.1

Calculated concentrations of Sulfuric and Nitric Acid and water from equations 2.69 and 2.70

T	P water = 5ppm P HNO3 = 10ppb [H2SO4]	[HNO3]	[H2O]	P water = 5ppm P HNO3 = 5ppb [H2SO4]	[HNO3]	[H2O]	P water = 5ppm P HNO3 = 2.5ppb [H2SO4]	[HNO3]	[H2O]	T
205	58.36073	0.348986	41.29029	58.53514	0.174491	41.29037	58.62234	0.087246	41.29042	205
204.9	58.24667	0.361373	41.39196	58.42727	0.180684	41.39204	58.51757	0.090342	41.39209	204.9
204.8	58.13179	0.374233	41.49398	58.31882	0.187114	41.49407	58.41233	0.093557	41.49412	204.8
204.7	58.01604	0.387586	41.59637	58.20974	0.19379	41.59647	58.30659	0.096895	41.59652	204.7
204.6	57.8994	0.401453	41.69914	58.10003	0.200724	41.69925	58.20034	0.100362	41.6993	204.6
204.5	57.78185	0.415855	41.80229	57.98967	0.207925	41.80241	58.09358	0.103962	41.80246	204.5
204.4	57.66336	0.430814	41.90582	57.87866	0.215404	41.90594	57.9863	0.1077	41.906	204.4
204.3	57.5439	0.446354	42.00975	57.76695	0.223174	42.00988	57.87848	0.111586	42.00994	204.3
204.2	57.42345	0.462493	42.11406	57.65455	0.23125	42.1142	57.77012	0.115624	42.11426	204.2
204.1	57.30194	0.479276	42.21878	57.54144	0.239635	42.21892	57.66119	0.119816	42.21899	204.1
204	57.17939	0.496716	42.32389	57.4276	0.248351	42.32405	57.55171	0.124174	42.32412	204
203.9	57.05575	0.514827	42.42943	57.31301	0.257411	42.42958	57.44163	0.128703	42.42966	203.9
203.8	56.93097	0.533661	42.53537	57.19764	0.266828	42.53554	57.33097	0.133411	42.53562	203.8
203.7	56.80503	0.55324	42.64173	57.08147	0.276613	42.64191	57.2197	0.138306	42.642	203.7
203.6	56.67789	0.573596	42.74851	56.96451	0.286789	42.74871	57.10781	0.143394	42.7488	203.6
203.5	56.5495	0.594764	42.85574	56.84668	0.297372	42.85594	56.99527	0.148685	42.85604	203.5
203.4	56.41984	0.616767	42.9634	56.72801	0.308377	42.96361	56.8821	0.154188	42.96372	203.4
203.3	56.28884	0.639661	43.0715	56.60845	0.319823	43.07173	56.76825	0.159911	43.07184	203.3
203.2	56.15648	0.663476	43.18004	56.48798	0.33173	43.18029	56.65373	0.165864	43.18041	203.2
203.1	56.0227	0.688252	43.28905	56.36657	0.344118	43.28931	56.5385	0.172058	43.28944	203.1
203	55.88746	0.714032	43.39851	56.2442	0.357007	43.39879	56.42257	0.178503	43.39892	203
202.9	55.75069	0.740861	43.50845	56.12083	0.37042	43.50875	56.3059	0.185206	43.50889	202.9
202.8	55.61236	0.768784	43.61886	55.99645	0.38438	43.61917	56.18849	0.192186	43.61933	202.8
202.7	55.47239	0.797853	43.72976	55.87099	0.398913	43.7301	56.0703	0.199452	43.73025	202.7
202.6	55.33077	0.828101	43.84113	55.74447	0.414043	43.84149	55.95133	0.207015	43.84166	202.6
202.5	55.18739	0.859609	43.95301	55.61683	0.429789	43.95339	55.83155	0.214891	43.95356	202.5
202.4	55.0422	0.89242	44.06538	55.48802	0.446193	44.06579	55.71093	0.223093	44.06598	202.4
202.3	54.89514	0.926596	44.17827	55.35802	0.463279	44.1787	55.58946	0.231635	44.1789	202.3
202.2	54.74614	0.962195	44.29167	55.2268	0.481077	44.29213	55.46712	0.240534	44.29234	202.2
202.1	54.59511	0.999288	44.4056	55.09429	0.49962	44.40609	55.34387	0.249805	44.40632	202.1

Table 2.1 continued

T	P water = 5ppm P HNO3 = 10ppb [H2SO4]	[HNO3]	[H2O]	P water = 5ppm P HNO3 = 5ppb [H2SO4]	[HNO3]	[H2O]	P water = 5ppm P HNO3 = 2.5ppb [H2SO4]	[HNO3]	[H2O]	T
202	54.44201	1.037937	44.52005	54.96048	0.518942	44.52058	55.21971	0.259466	44.52082	202
201.9	54.28673	1.078219	44.63505	54.82531	0.53908	44.63561	55.09459	0.269534	44.63587	201.9
201.8	54.1292	1.120207	44.7506	54.68873	0.56007	44.7512	54.96849	0.280029	44.75148	201.8
201.7	53.96934	1.163961	44.8667	54.55071	0.581953	44.86734	54.84139	0.29097	44.86764	201.7
201.6	53.80703	1.209599	44.98337	54.41118	0.60477	44.98405	54.71326	0.302377	44.98437	201.6
201.5	53.64219	1.257196	45.10062	54.27009	0.628566	45.10135	54.58404	0.314274	45.10169	201.5
201.4	53.47473	1.306839	45.21843	54.1274	0.653385	45.21921	54.45374	0.326683	45.21958	201.4
201.3	53.30452	1.35863	45.33685	53.98305	0.679267	45.33769	54.3223	0.339628	45.33808	201.3
201.2	53.13147	1.41267	45.45586	53.83696	0.70628	45.45676	54.18969	0.353129	45.45718	201.2
201.1	52.95544	1.469066	45.57549	53.68908	0.734471	45.57646	54.05588	0.367223	45.5769	201.1
201	52.77636	1.527906	45.69574	53.53934	0.763897	45.69677	53.92082	0.381934	45.69724	201
200.9	52.59403	1.589357	45.81661	53.38767	0.794615	45.81772	53.78448	0.397292	45.81823	200.9
200.8	52.40836	1.653518	45.93812	53.234	0.826689	45.93931	53.64682	0.413327	45.93985	200.8
200.7	52.21918	1.720528	46.06029	53.07825	0.860188	46.06157	53.50778	0.430074	46.06215	200.7
200.6	52.02637	1.790524	46.18311	52.92034	0.895177	46.18448	53.36734	0.447566	46.1851	200.6
200.5	51.82974	1.863655	46.30661	52.76019	0.931734	46.30808	53.22542	0.465842	46.30874	200.5
200.4	51.62917	1.940048	46.43078	52.59771	0.96992	46.43237	53.08198	0.48494	46.43308	200.4
200.3	51.42443	2.019916	46.55566	52.4328	1.009843	46.55736	52.93698	0.5049	46.55812	200.3
200.2	51.21537	2.103407	46.68123	52.26536	1.051577	46.68306	52.79036	0.525765	46.68387	200.2
200.1	51.00176	2.190715	46.80752	52.09529	1.095217	46.8095	52.64205	0.547583	46.81037	200.1
200	50.78344	2.282023	46.93453	51.92248	1.140853	46.93666	52.492	0.5704	46.9376	200
199.9	50.56021	2.377506	47.06229	51.74682	1.188595	47.06459	52.34014	0.594257	47.0656	199.9
199.8	50.33176	2.47744	47.1908	51.56817	1.238547	47.19329	52.18641	0.619228	47.19437	199.8
199.7	50.0979	2.582024	47.32008	51.38642	1.290822	47.32276	52.03072	0.645359	47.32392	199.7
199.6	49.85837	2.691503	47.45013	51.20146	1.345519	47.45302	51.87301	0.672713	47.45428	199.6
199.5	49.61294	2.806095	47.58097	51.01309	1.402807	47.5841	51.71319	0.701353	47.58546	199.5
199.4	49.36126	2.926136	47.7126	50.8212	1.462802	47.716	51.5512	0.731344	47.71746	199.4
199.3	49.10305	3.051888	47.84507	50.6256	1.52565	47.84875	51.38692	0.762763	47.85032	199.3
199.2	48.838	3.183647	47.97835	50.42616	1.591497	47.98235	51.22028	0.79568	47.98404	199.2
199.1	48.56582	3.321699	48.11248	50.22267	1.660511	48.11682	51.05118	0.83018	48.11864	199.1
199	48.28607	3.466462	48.24747	50.01498	1.732831	48.25219	50.87951	0.866333	48.25415	199
198.9	47.99841	3.618265	48.38332	49.80286	1.808689	48.38846	50.70517	0.904253	48.39058	198.9
198.8	47.70251	3.777443	48.52005	49.5861	1.888251	48.52565	50.52803	0.944024	48.52794	198.8

Table 2.1 continued

T	P water = 5ppm P HNO3 = 10ppb [H2SO4]	[HNO3]	[H2O]	P water = 5ppm P HNO3 = 5ppb [H2SO4]	[HNO3]	[H2O]	P water = 5ppm P HNO3 = 2.5ppb [H2SO4]	[HNO3]	[H2O]	T
198.7	47.39782	3.944493	48.65769	49.36448	1.971728	48.66379	50.34798	0.985752	48.66627	198.7
198.6	47.08397	4.119809	48.79623	49.13778	2.059332	48.80289	50.16488	1.029541	48.80558	198.6
198.5	46.76051	4.303809	48.93569	48.90577	2.151265	48.94296	49.97861	1.07551	48.94588	198.5
198.4	46.42686	4.497068	49.07608	48.66813	2.247826	49.08404	49.78902	1.123779	49.0872	198.4
198.3	46.08252	4.70007	49.21741	48.42461	2.349252	49.22614	49.59595	1.174481	49.22957	198.3
198.2	45.72699	4.913313	49.3597	48.17491	2.455819	49.36927	49.39927	1.227731	49.373	198.2
198.1	45.35954	5.137502	49.50296	47.91873	2.567797	49.51348	49.19876	1.283717	49.51753	198.1
198	44.97966	5.373164	49.64718	47.6557	2.685552	49.65875	48.99426	1.342578	49.66316	198
197.9	44.58654	5.621067	49.79239	47.38546	2.809401	49.80514	48.78557	1.404484	49.80995	197.9
197.8	44.17954	5.88188	49.93858	47.10766	2.939695	49.95264	48.57251	1.469611	49.95788	197.8
197.7	43.75793	6.156316	50.08575	46.82192	3.076782	50.1013	48.35483	1.538155	50.10702	197.7
197.6	43.32077	6.445314	50.23391	46.52773	3.221146	50.25112	48.13233	1.610294	50.25738	197.6
197.5	42.86732	6.74962	50.38306	46.22468	3.37319	50.40214	47.90473	1.68629	50.40898	197.5
197.4	42.39655	7.070287	50.53317	45.9123	3.533336	50.55437	47.67177	1.766358	50.56187	197.4
197.3	41.90755	7.408207	50.68425	45.58999	3.702168	50.70784	47.43318	1.850752	50.71607	197.3
197.2	41.39921	7.764547	50.83625	45.25726	3.88018	50.86256	47.18866	1.939736	50.87161	197.2
197.1	40.87049	8.140349	50.98917	44.91352	4.067907	51.01857	46.93791	2.033572	51.02852	197.1
197	40.32016	8.536889	51.14295	44.55808	4.266047	51.17588	46.68054	2.132619	51.18684	197
196.9	39.74692	8.955529	51.29755	44.19031	4.47518	51.33451	46.4162	2.237188	51.34661	196.9
196.8	39.14955	9.397545	51.45291	43.80943	4.696088	51.49448	46.14451	2.347634	51.50785	196.8
196.7	38.52649	9.864577	51.60893	43.41467	4.929515	51.65582	45.86507	2.464308	51.67062	196.7
196.6	37.87642	10.35807	51.76551	43.00528	5.176204	51.81852	45.57739	2.587679	51.83493	196.6
196.5	37.19759	10.87989	51.92252	42.58023	5.437156	51.98262	45.28098	2.718173	52.00085	196.5
196.4	36.48852	11.4317	52.07979	42.13871	5.713197	52.14809	44.97539	2.856222	52.16839	196.4
196.3	35.74731	12.01558	52.23711	41.67957	6.005464	52.31497	44.65998	3.002411	52.33761	196.3
196.2	34.97221	12.63355	52.39424	41.2018	6.314954	52.48325	44.33418	3.157278	52.50854	196.2
196.1	34.16134	13.28782	52.55083	40.70415	6.642949	52.6529	43.99739	3.321379	52.68124	196.1
196	33.31288	13.98062	52.7065	40.18549	6.990602	52.82391	43.64885	3.495429	52.85572	196
195.9	32.42526	14.71395	52.86079	39.64436	7.359374	52.99627	43.28782	3.680123	53.03205	195.9
195.8	31.49565	15.49132	53.01304	39.07934	7.750763	53.16989	42.91357	3.876161	53.21027	195.8
195.7	30.52261	16.31486	53.16253	38.48897	8.166289	53.34474	42.52512	4.084474	53.3904	195.7
195.6	29.5045	17.18716	53.30834	37.87152	8.607754	53.52072	42.12163	4.30587	53.5725	195.6
195.5	28.43961	18.11106	53.44933	37.2254	9.076879	53.69772	41.70199	4.541409	53.7566	195.5

Table 2.1 continued

T	P water = 5ppm P HNO3 = 10ppb [H2SO4]	[HNO3]	[H2O]	P water = 5ppm P HNO3 = 5ppb [H2SO4]	[HNO3]	[H2O]	P water = 5ppm P HNO3 = 2.5ppb [H2SO4]	[HNO3]	[H2O]	T
195.4	27.32693	19.08896	53.58411	36.54874	9.5757	53.87556	41.26515	4.792121	53.94273	195.4
195.3	26.1655	20.1235	53.711	35.8395	10.10642	54.05408	40.80996	5.059115	54.13093	195.3
195.2	24.95525	21.21685	53.82791	35.09589	10.67112	54.23299	40.33511	5.343696	54.32119	195.2
195.1	23.69666	22.37096	53.93238	34.31573	11.27228	54.412	39.83914	5.647288	54.51357	195.1
195	22.39121	23.58735	54.02144	33.49688	11.91245	54.59067	39.32068	5.971288	54.70804	195
194.9	21.04164	24.86679	54.09158	32.63736	12.59413	54.76851	38.77799	6.317423	54.90459	194.9
194.8	19.65161	26.20968	54.13871	31.73501	13.32014	54.94485	38.20945	6.687362	55.10319	194.8
194.7	18.22594	27.61594	54.15812	30.78796	14.09316	55.11889	37.61307	7.083155	55.30378	194.7
194.6	16.7704	29.08516	54.14444	29.79461	14.91578	55.28961	36.98699	7.506754	55.50626	194.6
194.5	15.29085	30.61764	54.09151	28.75341	15.7908	55.45579	36.32894	7.960536	55.71053	194.5
194.4	13.79327	32.21439	53.99234	27.66435	16.71975	55.6159	35.63675	8.446898	55.91636	194.4
194.3	12.28133	33.88013	53.83854	26.52621	17.70574	55.76805	34.90792	8.968577	56.1235	194.3
194.2	10.75575	35.62464	53.61961	25.34064	18.74931	55.91005	34.14013	9.528237	56.33163	194.2
194.1	9.210822	37.46827	53.32091	24.10958	19.85116	56.03926	33.33081	10.12893	56.54027	194.1
194	7.629407	39.45122	52.91937	22.83685	21.01047	56.15268	32.47747	10.77372	56.74881	194
193.9	5.968465	41.66027	52.37126	21.52751	22.2256	56.24689	31.5776	11.46591	56.95649	193.9
193.8	4.106755	44.327	51.56625	20.18858	23.49325	56.31817	30.62933	12.20839	57.16229	193.8
193.7	1.047163	49.29681	49.65602	18.82821	24.80918	56.36261	29.63069	13.00438	57.36494	193.7
193.6	0	51.21539	48.85903	17.45559	26.16824	56.37617	28.58082	13.85633	57.56285	193.6
193.5				16.08052	27.56455	56.35493	27.47954	14.76642	57.75404	193.5
193.4				14.71207	28.99286	56.29508	26.32805	15.73583	57.93612	193.4
193.3				13.3582	30.44885	56.19295	25.12921	16.76451	58.10628	193.3
193.2				12.02486	31.93023	56.04491	23.88849	17.85019	58.26132	193.2
193.1				10.71521	33.43777	55.84702	22.61183	18.99056	58.39761	193.1
193				9.429751	34.9756	55.59465	21.30887	20.17969	58.51145	193
192.9				8.164738	36.55396	55.2813	19.99032	21.41055	58.59913	192.9
192.8				6.912207	38.19037	54.89743	18.66826	22.67449	58.65725	192.8
192.7				5.657374	39.91531	54.42732	17.35456	23.96255	58.68289	192.7
192.6				4.372963	41.78478	53.84226	16.06043	25.26581	58.67376	192.6
192.5				3.001527	43.91814	53.08034	14.79522	26.57642	58.62836	192.5
192.4				1.365077	46.68803	51.9469	13.5659	27.88843	58.54566	192.4
192.3				0	49.21009	50.81859	12.37708	29.19767	58.42525	192.3
192.2							11.23073	30.50247	58.2668	192.2

Table 2.1 continued

T	P water = 5ppm P HNO3 = 10ppb [H2SO4]	[HNO3]	[H2O]	P water = 5ppm P HNO3 = 5ppb [H2SO4]	[HNO3]	[H2O]	P water = 5ppm P HNO3 = 2.5ppb [H2SO4]	[HNO3]	[H2O]	T
192.1							10.12664	31.8034	58.06996	192.1
192							9.063092	33.10275	57.83415	192
191.9							8.036397	34.40555	57.55805	191.9
191.8							7.041901	35.7186	57.2395	191.8
191.7							6.073397	37.05173	56.87487	191.7
191.6							5.123208	38.41842	56.45837	191.6
191.5							4.181346	39.83778	55.98087	191.5
191.4							3.233699	41.33917	55.42714	191.4
191.3							2.257893	42.97212	54.76999	191.3
191.2							1.21144	44.8349	53.95366	191.2
191.1							0	47.15943	52.8426	191.1

is found to be 192.75 K. Then, we for this fixed temperature and partial pressure of water, we allow the pressure of nitric acid to float. We find the concentrations of interest by fixing the nitric acid concentration at convenient intervals and then solving equation 2.70 for the sulfuric acid concentration. The result is the dashed line in Figure 2.4. One can see that the concentrations remain above the frost point until the concentration reaches about 0.22 and 0.20 weight fraction sulfuric and nitric acid respectively, for a partial pressure of nitric acid equivalent to 2.5 ppb at 100 mbar. The implications of this will be discussed in the results section of the supercooling studies.

2.3.4 Conclusions

A new parameterization of the experimental data of Zhang, Wooldridge and Molina [1993b] has been performed based on Raoult's and Henry's Law. The parameterization is in excellent agreement with the data reported by Zhang et al. Furthermore it has the advantage of smoothly extrapolating beyond the experimental data to the nitric acid binary limit which is of crucial import and interest in the Polar Stratosphere. This parameterization is used to calculate concentrations of the ternary system for our supercooling studies.

2.4 Experimental

Figure 2.5 shows a schematic of the experimental setup for the capillary studies. In this experiment crystallization of the sample was detected by observing a corresponding decrease in light transmitted through the sample with crystallization. Sample meltings were determined by an increase in the transmitted light through the sample. The sample cooling block and the capillary sample holder are made of copper. A capillary tube made of glass was used to hold the sulfuric acid sample. Samples were typically five microliters in volume. The liquid sample was normally kept from touching the ends of the glass tube so as not to enhance nucleation. A HeNe laser beam was passed through the sample via a tube with a window glued onto the end which was used to keep moisture from condensing

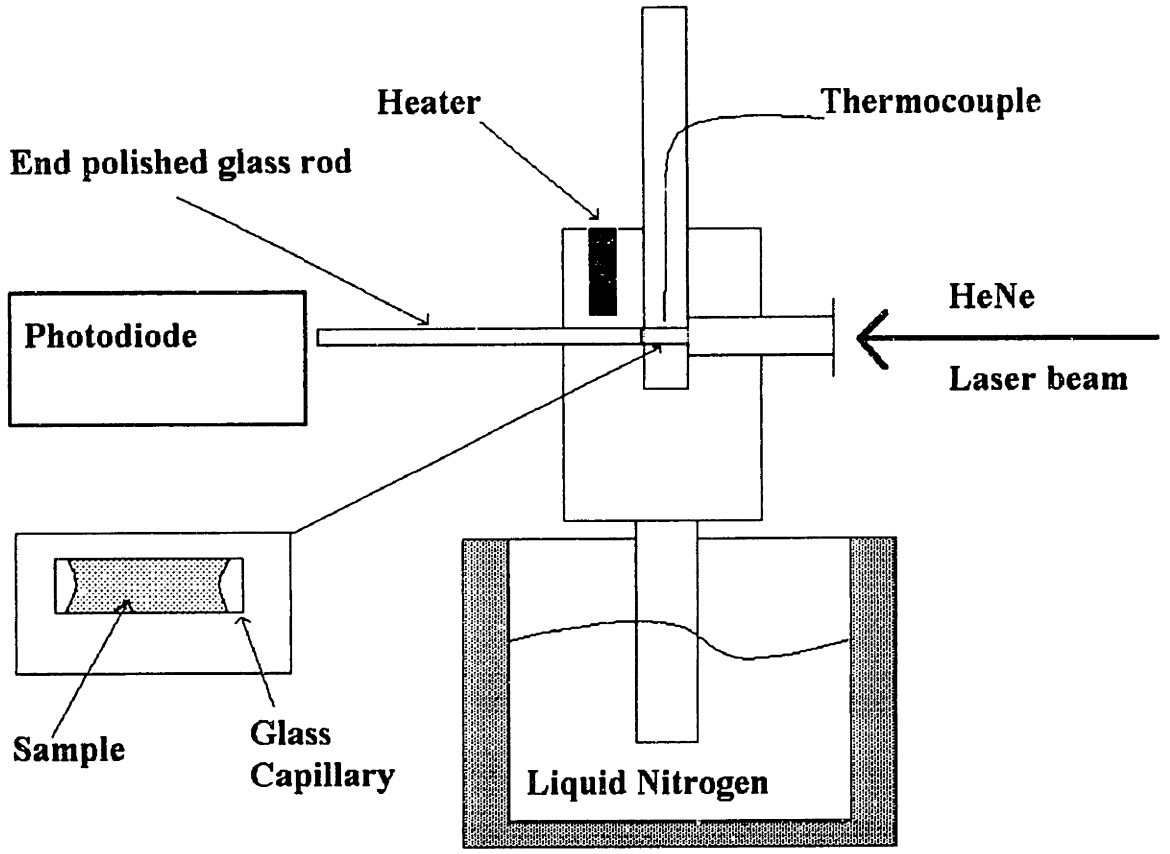

Figure 2.5: Schematic of apparatus used in the capillary sample supercooling experiments. An Omega temperature controller was used to regulate the temperature of the system. The cooling block is a solid copper cylinder with holes drilled as shown in the cross section view.

on the cold sample or sample block. The laser light passing out of the sample at the rear was "guided" to a photo diode detector via an end-polished glass rod. The voltage output as a function of temperature (or time) was recorded via a National Instruments AT-MIO-16 data acquisition board and an IBM AT. When measuring temperature vs. transmitted light, the temperature was ramped down using an Omega temperature controller and a ramp of two degrees Kelvin per minute.

Figure 2.6 shows the apparatus for experiments where time vs. temperature was monitored. Sample volumes were 3, 0.3 and 0.03 milliliters. In these experiments we were interested in holding the samples at a given temperature and then determining the time at which the sample fi ,zes. A phase transition can be seen by a rapid rise and then

drop in the temperature of the sample. This temperature change corresponds to the heat release upon crystallization.

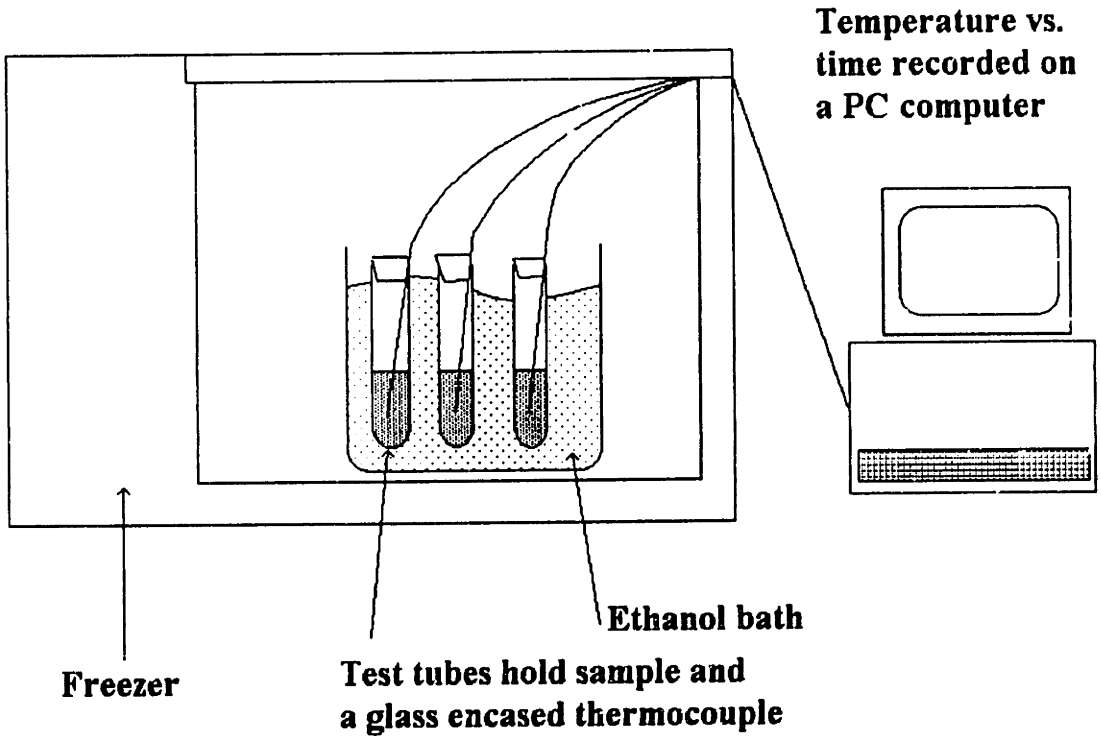

Figure 2.6: Schematic of apparatus used in supercooling solutions of 3, 0.3 and 0.03 milliliters. In the case of the smallest samples (0.03 ml) the ethanol bath was not used. In each case 32 test tubes of samples were used.

'Seed' crystals of SAT, NAT, ice and mixed NAT and SAT were made by placing a small amount (~0.5 ml) of the mother solution in a test tube, and cooling it down in liquid nitrogen. The seed solution either crystallized on cooling or warming. After the solid seed was formed it was allowed to equilibrate to 195K by placing the test tube holding it into a dry ice/acetone bath (195 K). The sample solution to be nucleated had a volume of ~3 ml and was placed in the dry ice/acetone bath also. After the seed had equilibrated for about a minute, the seed was placed in the supercooled solution to be nucleated and the result observed. In order to observe the sample solution, a special dewar that was

partially unsilvered was used. A light source was directed at the sample to aid in the observation. A schematic of the apparatus is given in Figure 2.7.

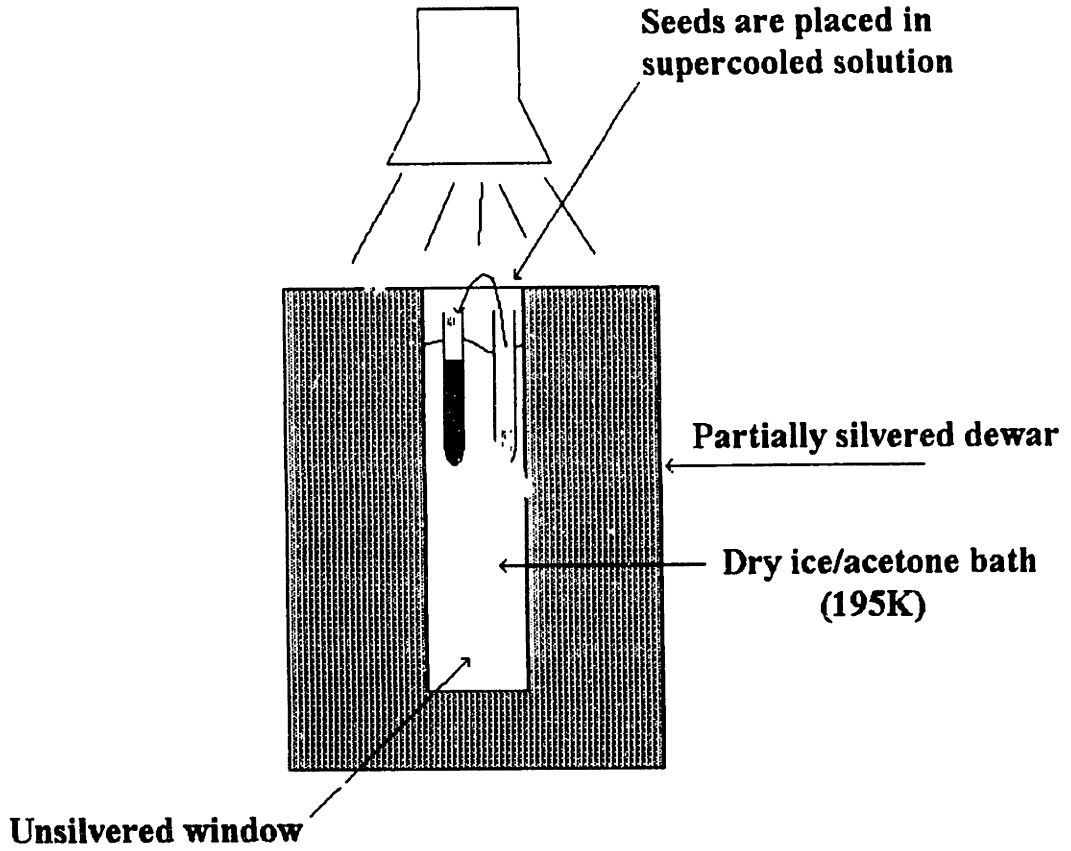

Figure 2.7: Schematic of apparatus used in seeding experiments.

2.5 Results and Discussion

2.5.1 *H_2SO_4 - H_2O Binary System: Nucleation on cooling.*

Figure 2.8 shows the critical freezing points determined in the capillary studies (apparatus as shown in Fig. 2.5) with the equilibrium freezing/melting points as given by Gable et al. [1950]. Samples of deionized, filtered water were also run in the capillary apparatus for comparison. It is seen that water crystallized at about 251 K. This result can be compared with other experimental results regarding the supercooling of water. Bigg [1953] has given the most consistent and reliable data for nucleation of ice from liquid water. Bigg took drops of distilled water and placed them between two immiscible liquids which were also immiscible with water. He used various cooling rates and droplet

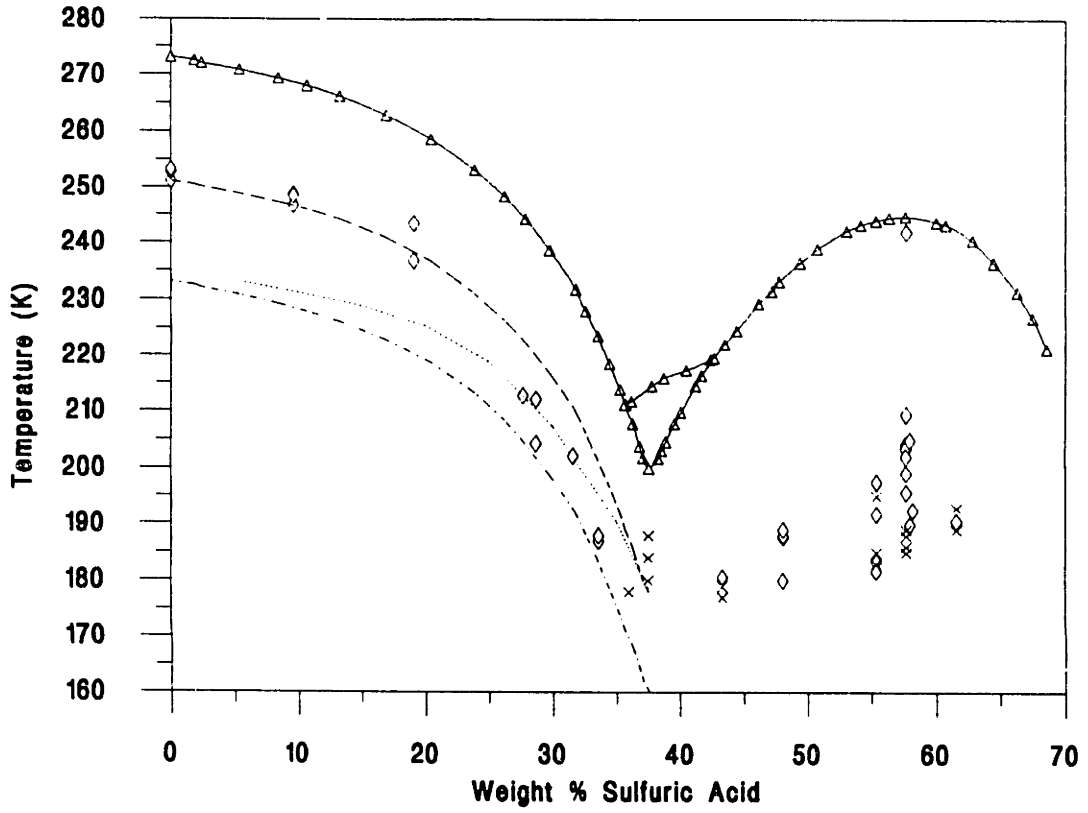

Figure 2.8: Phase diagram of sulfuric acid - water binary system. Solid line with triangles represents the equilibrium freezing/melting points from Gable, et al. [1950]; upper dashed line represents supercooling of 21 K from equilibrium freezing points; lower dashed line represents supercooling of 40 K from equilibrium freezing points; the middle, dotted line is the theoretical work of Jensen, et al. [1991]; diamonds represent spontaneous freezing of a sample on cooling; X's represent freezing on warming (from ~150 K).

sizes in his experiments where he recorded the freezing temperature. Based on his studies he deduced an empirical relationship:

$$\ln\left(\frac{-a\ln(1-P)}{3.193x10^{-8}V}\right)=T_s \qquad (2.70)$$

where a is the cooling rate in degrees per minute, P is the probability of freezing, V is the volume and T_S is the supercooling. Using this equation for a sample volume of 5 μl, a cooling rate of 2 degrees per minute and a probability of freezing of 0.5, the result is a supercooling of 25.2 degrees. The average supercooling in our capillary experiments was 22 degrees. This is probably well within the error of this calculation: Bigg based his equation on 100 trials for each drop size; in contrast, we have only a few data points for

water. Another possibility is enhanced nucleation from the glass surface. Because of this possibility which we can not rule out, our results are used as upper limits (although there is evidence from the freezing of bulk solutions of pure water that a glass surface does not enhance nucleation [Wang and Vonnegut, 1984]).

Hallet and Lewis [1967] have previously suggested that aqueous solutions which form ice upon freezing will have the ability to supercool to the same degree that water supercools. In our case, we see a supercooling of water by an average of 22 K from its equilibrium freezing point. The upper dashed line in Figure 2.8 is for a supercooling of 22 K from the equilibrium freezing points. Pure water drops of ~1μm have been shown to supercool ~40 K below the equilibrium freezing point [Schaeffer, 1952]. The lower dashed line in Figure 2.8 is for a supercooling of 40 K from the equilibrium freezing point of the respective solutions (equivalent to that postulated by Hallet and Lewis). The dotted line is the theoretical critical freezing temperature for 1μm solution drops calculated by Jensen et al. [1991]. Interestingly, the two lines are not the same. As previously mentioned, Hallet and Lewis' line represents a constant supercooling of 40 K from the equilibrium freezing points. The line of Jensen et al. was calculated using theoretical values for the solid/solution surface energy, the phase change activation energy, and the activity of the solution.

Observing the data for solutions of 0 - 36% sulfuric acid (solutions that will produce ice upon freezing), it is seen that for dilute sulfuric acid solutions (<~20%), the supercooling is ~21 K, independent of concentration, and agrees with the freezing temperature predicted from the hypothesis of Hallet and Lewis based on pure water (upper dashed line). It is worth noting that the surface energies of dilute solutions for the solid/liquid interface, σ_{sl}, approximates the surface energy of the pure ice/liquid water interface, σ_{iw}. The difference between σ_{sl} and σ_{iw} becomes increasingly larger as the solution becomes more concentrated in sulfuric acid, since the solution becomes less and less like pure water. As a result, the observed critical freezing points for the capillary

samples correspond to increasingly larger supercoolings for more concentrated solutions (30 - 36% H_2SO_4), and thus the deviations from the predicted critical freezing points of capillary solutions become larger (upper dashed line). In fact, the observed freezing points of the capillary samples between 30 - 36% H_2SO_4 are lower than those predicted by Jensen et al. [1991] for 1μm solution drops (dotted line), and they approach that predicted by Hallet and Lewis for 1μm solution drops (lower dashed line). It would seem that the prediction of Hallet and Lewis is valid (with respect to sulfuric acid) only for very dilute solutions (0 - 20% H_2SO_4). As such, 1μm drops of 30 - 36% H_2SO_4 should freeze at temperatures lower than that predicted by Hallet and Lewis. It is also clear that for these concentrated solutions, the predictions of critical freezing points for 1μm drops of Jensen et al. are also too high, although in their paper they admit that they are only predicting upper limits because of the uncertainties in their calculations. However, even for dilute solutions our data do not follow their predictions. From our data, we show new upper limits to the freezing of 1μm sulfuric acid drops with concentrations of 30-36% H_2SO_4 which are lower than those predicted by Jensen, et al. We also postulate that the predictions of Hallet and Lewis are also too high for these solutions, since our capillary samples froze near the temperatures predicted for 1μm drops by Hallet and Lewis. We expect our experimental results to be upper limits for the freezing of drops in the stratosphere, since our samples are about two orders of magnitude larger in volume than 1μm drops, and our samples are in contact with a glass surface.

2.5.2 *H_2SO_4 - H_2O Binary system: Nucleation only on warming.*

Solutions of 36 to 44% sulfuric acid did not nucleate when cooled down to very low temperatures (~ 150 K). However, when these solutions were warmed, the solutions crystallized in the range 180 to 190 K (see Figure 2.8), and often melted at a temperature corresponding to the hemihexahydrate. It is quite possible that the cooling rate used was too fast for these solutions to nucleate. However, two experiments were run using a

solution of 37.5% sulfuric acid where the sample was held in one experiment at 177 K, and in the other at 192 K for ~17 hours. In neither case did the sample crystallize.

The glass transition temperature for sulfuric acid solutions of the above concentrations has been observed to be ~152 K [Vuillard, 1957; Kanno, 1990]. In the cooling experiments these solutions were cooled below the glass transition (to 143-150 K). Passing through the glass transition, the solution becomes more ordered, thus possibly facilitating the genesis of nuclei for the respective solid that forms on warming. Though nuclei form at this low temperature, crystallization does not occur because the crystallization velocity is extremely low. Crystallization velocity is dominated at these low temperatures by the corresponding very high viscosity. Thus, as the sample warms, with nuclei present, when the viscosity decreases sufficiently such that the crystallization velocity becomes appreciable, the sample "freezes". Much of this theory is given by Hallet [1968], and is well known in the field of materials science [Levy and Herley, 1969].

2.5.3 *H_2SO_4 - H_2O Binary system: Time studies.*

A number of experiments were done where a solution of a given composition of sulfuric acid was held at a constant temperature to determine the time at which freezing would occur. Two different types of experiments were performed: one using 5 μl samples in the capillary apparatus (Fig. 2.5), and the other using 3 ml samples in the freezer apparatus (Fig. 2.6). The results of the capillary experiments are given in Table 2.2, and the results of the freezer experiments are given in Table 2.3.

The capillary studies summarized in Table 2.2 show significant results only for the 48.1 % sample. In this case the time required to nucleate the sample decreased with a decrease in temperature. However, many more experiments need to be run in order to draw conclusions for these samples. There were more experiments for the 60 % samples; however, half of them did not freeze, therefore we can not draw quantitative conclusions based on these results.

Table 2.2

Supercooling time experiments of the H_2SO_4 binary system using capillary samples.

[H2SO4] (wt. fraction)	Equilibrium T (K) (at 5ppm H2O)	Experimental T (K)	Nucleation Time (hours)	Experiment Time (hours)
0.375	192	192	n	16.9
		176.8	n	16.7
0.481	197.5	200	n	3
		198	2.3	NA
		193	0.19	NA
		193	0.47	NA
0.577	204.8	200	21.9	NA
0.58	205	204.7	n	15.3
		204.1	n	20
		203.5	3	NA
0.6	207	208.8	n	18.1
		206.7	n	17.5
		205.7	n	16.7
		204.4	0.38	NA
		202.2	0.15	NA
		197.7	0.42	NA

Notes: NA: Experiment was stopped after nucleation occurred.
n: sample did not freeze.

Figure 2.9 shows the results of the time experiments using 3 ml solutions along with the equilibrium freezing lines of Gable et al. [1950], and theoretical predictions of Luo et al. [1992] (see figure caption). Shown on the plot are the freezing ratios (i.e. the number of samples that froze divided by the total number of samples in the experiment) and average freezing times (the average time it took for the samples to freeze, for those samples that did freeze) of the experiments. The results show that the freezing ratio reaches a peak for the solution that corresponds to an equilibrium temperature of 198 K (48.9 wt. % H_2SO_4). The average freezing time is a minimum for the solution corresponding to an equilibrium temperature of 200 K (51.8 wt. % H_2SO_4). For higher and lower points than these the freezing fractions are smaller and the average freezing times are longer, respectively.

Table 2.3

Results of binary sulfuric acid supercooling experiments using 3 ml samples corresponding to a pressure of water of 5 ppm @100 mbar.

Experiment #	1	2	3	4	5	6
Equilibrium T	212	210	208	206	204	202
Experimental T	214.8	214.8	209.4	209.4	200.5	200.5
[H2SO4]	0.6491	0.6304	0.6107	0.59	0.5678	0.544
	Time to		Time to	Time to	Time to	Time to
Thermocouple #	Freeze	Freeze	Freeze	Freeze	Freeze	Freeze
0						
1					0.68	
2						
3			3.38			16.62
4						3.13
5			1.59			2.89
6						
7						
8						
9				1.45		0.24
10						
11						14.94
12						
13					23.88	
14						
15			4.65		1.48	
16						
17						
18						
19						
20						
21						
22						
23						
24						
25						
26						
27						
28						
29						
30						
31						
Freezing Ratio	0/16	0/16	3/16	1/16	3/16	5/16
Exper. time (h)	24	24	24	24	24	24
Ave Freeze. Tim.			3.206667	1.45	8.68	7.564

Notes:
Blank areas indicate no nucleation.
Shaded areas indicate no samples were run.
Two freezing times are given when two separate phase transitions were seen.
nt: No freezing signal was seen, however the sample was observed to be frozen when it was removed from the freezer.

Table 2.3 continued

Experiment #	7		8		9	10
Equilibrium T	200		198		197	196.35
Experimental T	196.5		196.5		196.1	195.4
[H2SO4]	0.518		0.4892		0.4736	0.4628
	Time to Freeze		Time to Freeze		Time to	Time to
Thermocouple #	time #1	time #2	time #1	time #2	Freeze	Freeze
0	2.25		6.12		4.56	5.4
1					2.04	1.68
2	1.64		2.5			3.24
3	0.2		1.89			
4	0.52	1.68	1.87	2.01		
5	0.76	1.51	3.27			
6			2.26			
7	1.52		2.6			
8	4.32		7.42			
9			1.46			
10	6.33		10.36			
11						
12	3.76		18.42			
13						
14			7.71			
15	0.36					
16						
17						
18						
19						
20						
21						
22						
23						
24						
25						
26						
27						
28						
29						
30						
31						
Freezing Ratio	10/16		12/16		2/4	3/4
Exper. time (h)	24		24		24	24
Ave Freeze. Tim.	2.166		5.49		3.3	3.44

Table 2.3 continued

Experiment #	11	12	13		14	15
Equilibrium T	196	195.5	195		195	195
Experimental T	197.4	196.4	204.8		190.9	198.3
[H2SO4]	0.4567	0.4478	0.4383		0.4383	0.4383
	Time to	Time to	Time to Freeze		Time to	Time to
Thermocouple #	Freeze	Freeze	time #1	time #2	Freeze	Freeze
0	6.36		20.51		1.51	
1			4.48		1.9	
2					1.33	
3			15.59	15.73	0.69	
4			4.66		0.88	
5					0.41	
6					2.43	
7						
8			1.71		2.32	
9			12.5	12.62	1.34	
10					2.79	
11					1.81	
12			0.23		1.87	
13					1.34	
14			7.9	8.02	1.35	
15			17.9	18.05	0.64	
16			6.76		2.18	
17			4.34		2.81	
18			nt		0.23	
19			9.61	9.74	1.73	
20			2.3	2.47	0.88	
21			0.78		0.66	
22			8.63	8.83	0.94	
23					0.05	
24			2.4	2.53	1.48	
25			3.08		1.08	
26			7.49		1.29	
27					0.39	
28			2.3		2.19	
29			3.1	3.22	1.49	
30			1.6		3.54	
31			4.54	4.7		
Freezing Ratio	1/4	0/4	23/32		30/31	0/4
Exper. time (h)	24	24	24		24	24
Ave Freeze. Tim.	6.36		6.473182	8.591	1.451667	

Table 2.3 continued

Experiment #	16	17	18	19	20	21
Equilibrium T	194.5	194	194	193.5	193	192
Experimental T	197.2	193.6	197.2	195.7	192.6	191.4
[H2SO4]	0.4288	0.4186	0.4186	0.4079	0.3966	0.3717
Thermocouple #	Time to Freeze	Time to Freeze	Time to Freeze	Time to Freeze	Time to Freeze	Time to Freeze
0		5.01				8.05
1					3.94	
2		3.69				
3		7.14				13.05
4		5.37				8.8
5		2.69				
6						
7		5.54				4.41
8		10.83			8.47	
9		2.39			20.87	
10		2.01				2.13
11						
12						
13		22.95				
14		5.4			11.62	
15		20.08				
16						
17					9.27	
18		3				
19						
20						
21		1.25				3.79
22						
23						
24						2.52
25					1.51	8.47
26		2.35			6.9	
27						
28						
29						10.43
30		4.42				
31						12.43
Freezing Ratio	0/4	16/32	0/4	0/4	7/32	10/32
Exper. time (h)	24	24	24	24	24	24
Ave Freeze. Tim.		6.5075			8.94	7.408

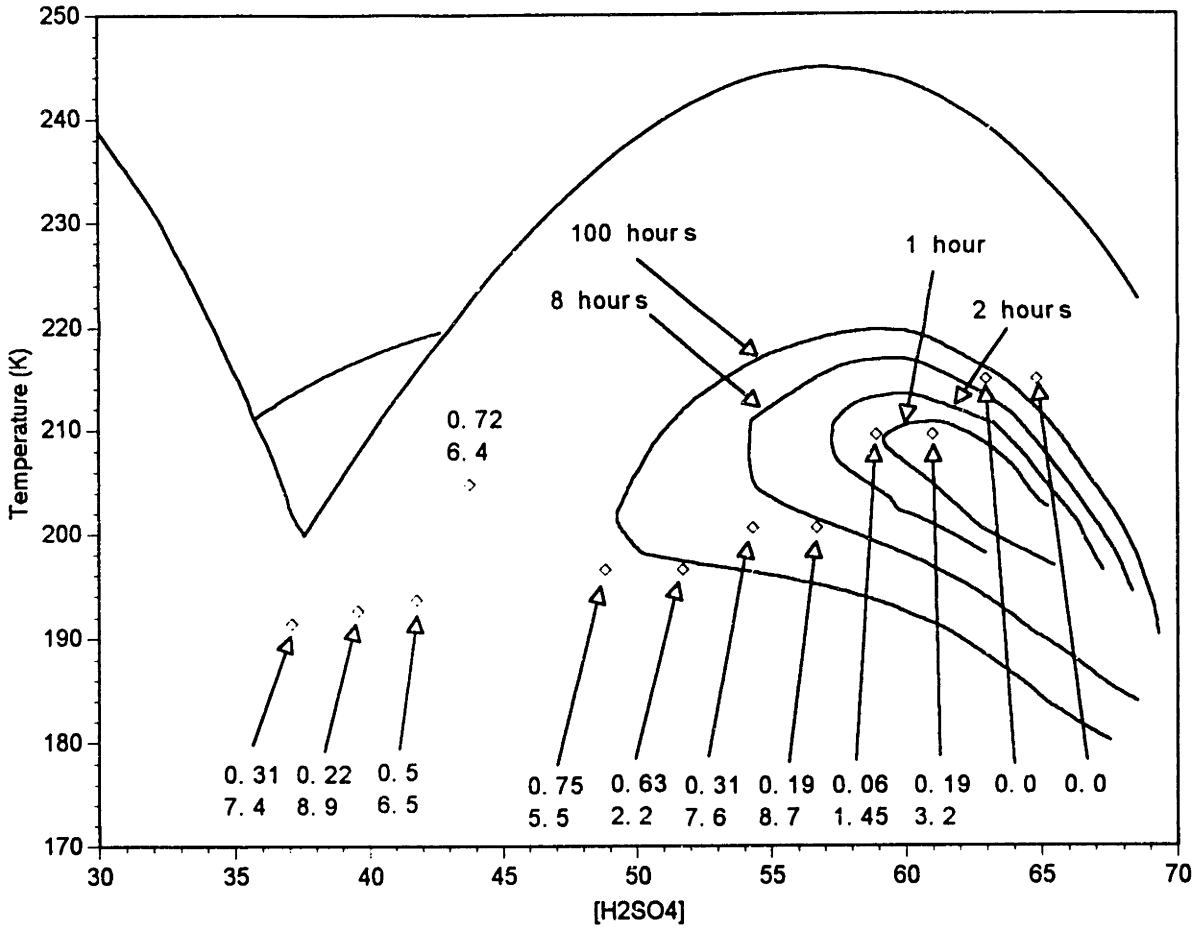

Figure 2.9: Comparison of sulfuric acid time studies with the theoretical calculations of Luo, et al. [1992]. The upper solid curve marks the equilibrium melting points of Gable, et al. [1950], the curved line across the center of the plot is the equilibrium temperature/ concentration line for 5 ppm water calculated from Zhang, et al. [1993a], time contours are those of Luo, et al. [1992], diamonds are the results of the supercooling experiments as given in Table 2.3 for experiments where at least 16 samples were run. Numbers referenced to each point are the freezing ratio on top and the average freezing time on the bottom.

Luo et al. [1992] recently performed theoretical calculations on the critical freezing temperatures for solutions that will form sulfuric acid tetrahydrate (SAT) on freezing. Their time to freeze contours are reproduced in Figure 2.9. They predict a maximum in nucleation rate for stratospheric equilibrium solutions of concentration roughly 60 to 66 wt. % corresponding to temperatures of ~206 to ~210 K (where the equilibrium line is inside the 1 hour contour.) Their predictions are for approximately 1 micron drops. Our results are for solutions of much larger volume, thus they should freeze much more readily. However, we find a maximum in nucleation rate that is not

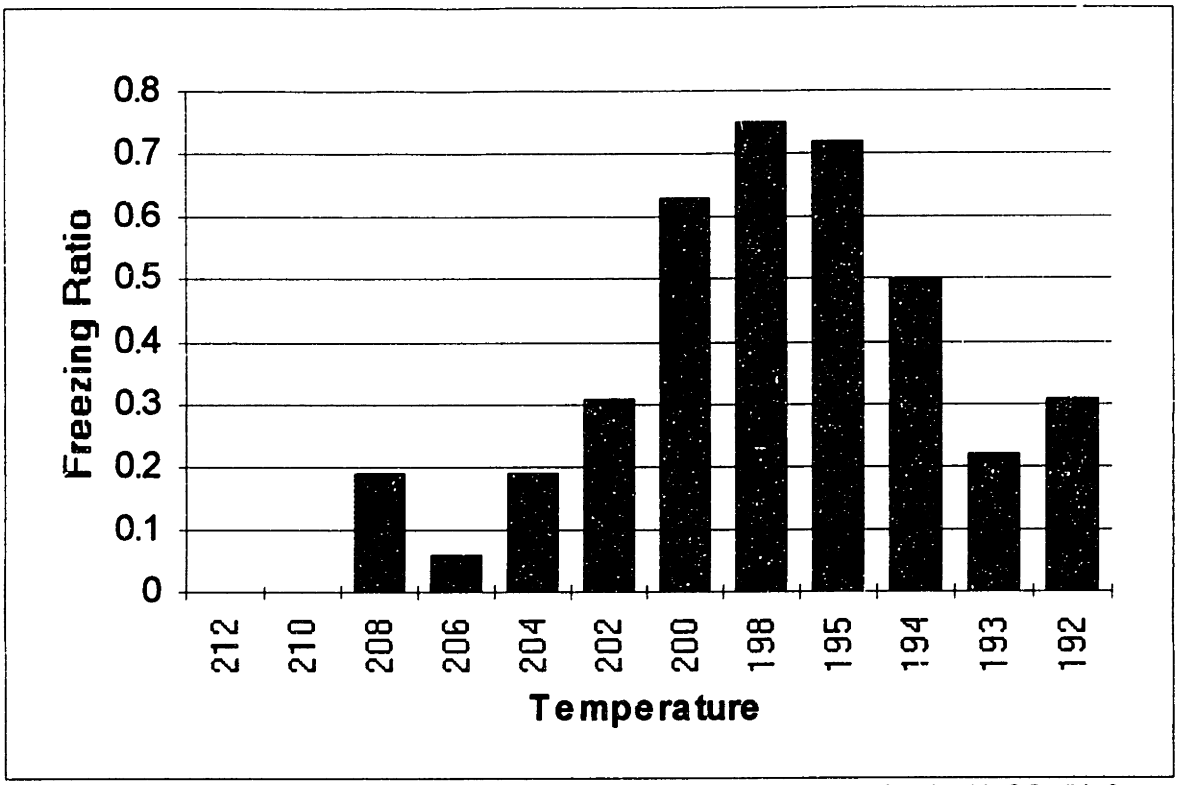

Figure 2.10: Plot of freezing ratio vs. equilibrium sample temperatures for the H_2SO_4/H_20 results given in Table 2.3.

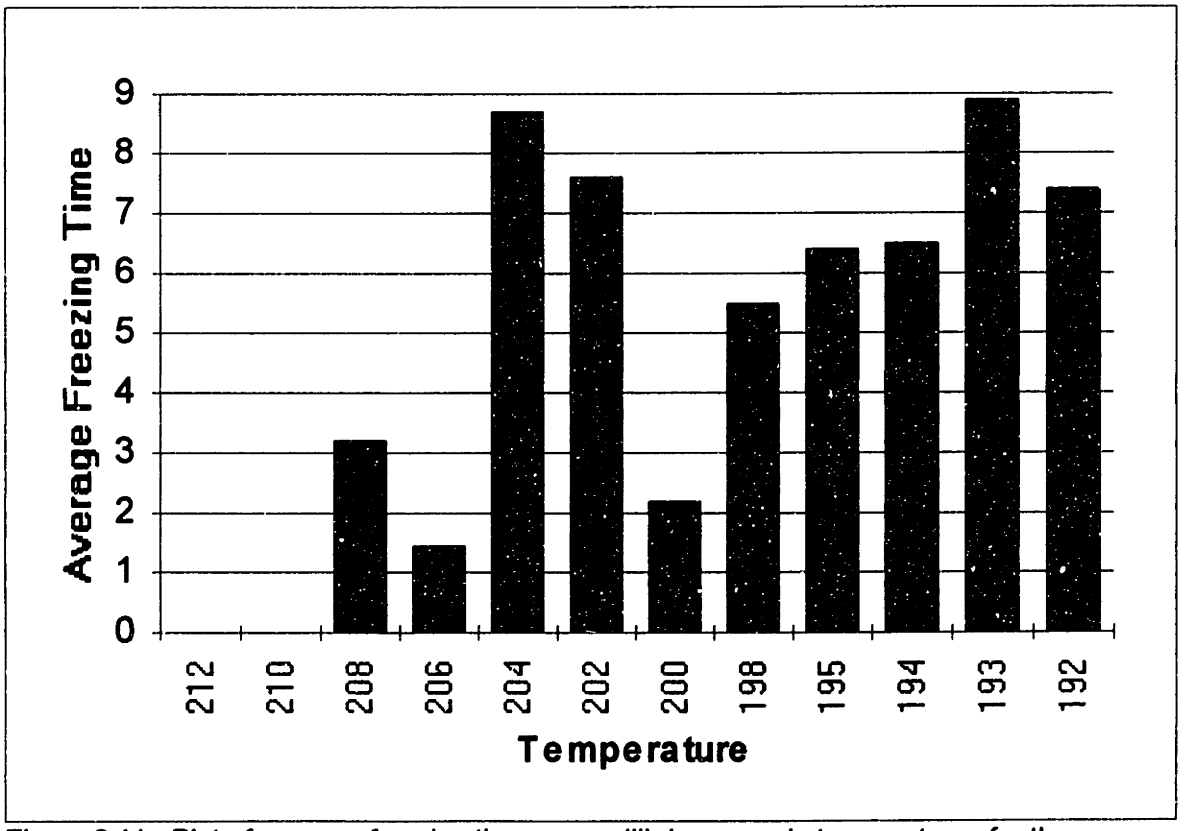

Figure 2.11: Plot of average freezing time vs. equilibrium sample temperatures for the H_2SO_4/H_20 results given in Table 2.3.

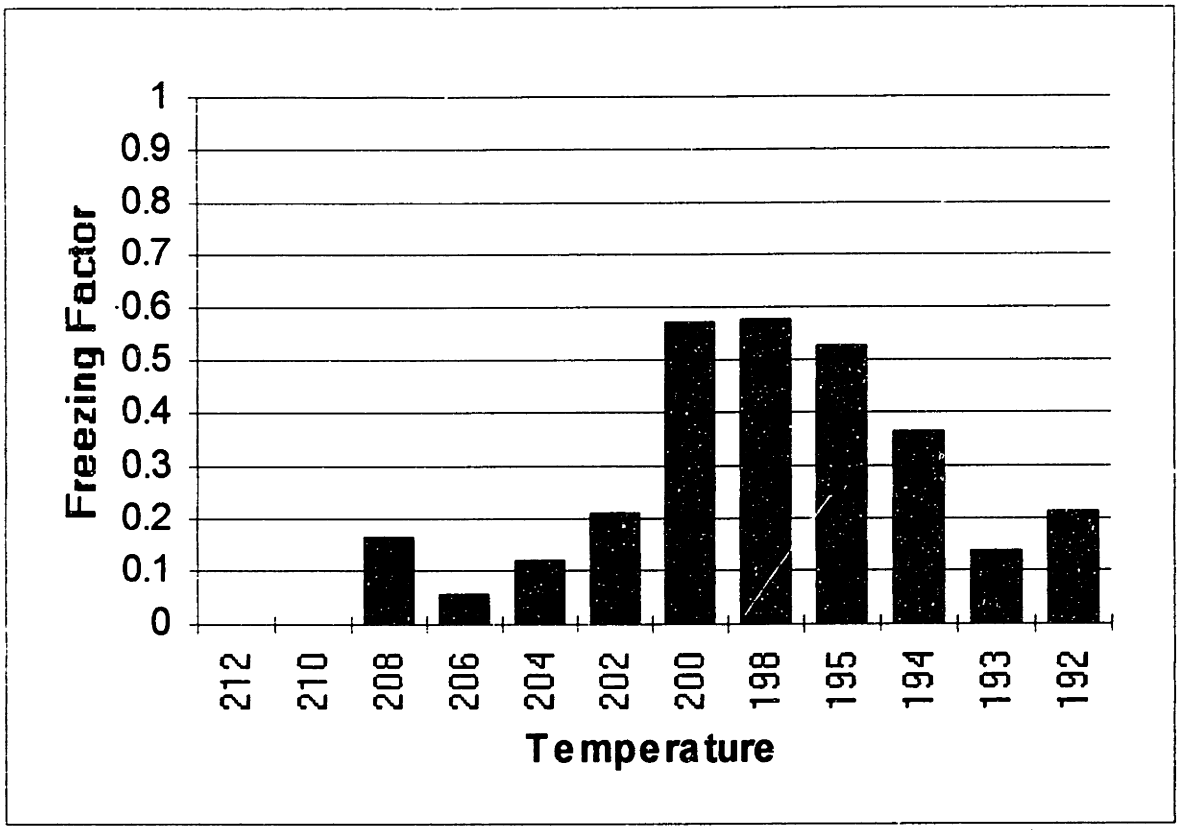

Figure 2.12: Plot of the freezing factor (see text for definition) vs. equilibrium sample temperatures for the H_2SO_4/H_20 results given in Table 2.3.

within their 1 hour contour, but in fact outside their 100 hour contour! One micron drops will take much longer to freeze than our 3 ml samples, thus the fraction of stratospheric aerosols that will freeze in the regions predicted by Luo et al., we conclude will be insignificant. The only area we see for possible significant nucleation rates is the 40 to 50 wt. % region. Figure 2.10 shows a plot of the freezing ratio vs. the sample equilibrium temperatures. In this figure it is easy to see that there is a definite peak in the freezing ratio between 200 and 195 K. Figure 2.11 shows the trend in the average time to freeze, with the minimum being at 200. In Figure 2.12 I introduce a new parameter to combine the variables of freezing ratio and average time to freeze. The "Freezing Factor", FF, is defined as: $FF = 1 - \frac{(FR)(AFT) + (1-FR)(ET)}{ET}$, where FR is the freezing ratio, AFT is the average freezing time of the samples that froze and ET is the experimental time (in most cases 24 hours). This effectively combines the two variables into one to show overall trends in the results. The more likely a solution is to nucleate the higher the

freezing ratio and the lower the average freezing time. The freezing factor ranges between zero and one with higher numbers indicating a greater probability to freeze in a relatively short time (short compared to the total time of the experiment.) The trend in the combined variables is quite obvious. We see a peak in the freezing factor in the range 200 to 195 K (also clearly seen in the freezing ratio, but not so obvious in the average freezing time). Can we now make predictions about the freezing probability of H_2SO_4/H_2O aerosols in the stratosphere? Since our samples are much larger than those in the atmosphere, we can make few statements about the probability of sulfuric acid aerosols to freeze. What we can conclude is that these survey results are promising and further work should be done in this area.

Luo et al. [1993] have recently reported a revision of their earlier work. They report an error in their previous calculation of the surface energy, and in light of recent laboratory studies of the nucleation of sulfuric acid solutions [Ohtake, 1992] their new calculations have much lower freezing probabilities .

2.5.4 *H_2SO_4 - H_2O Binary system: Filtering studies / bulk solution studies.*

Experiments were performed in the capillary studies with filtered solutions of sulfuric acid, and the data are shown in Figure 2.13. A 10% sulfuric acid solution was drawn through a 4.5 - 5.5 μm glass frit filter to remove particulates greater than that size range. As shown in Figure 2.13, no real difference in freezing temperature was seen. A 57.7% solution (~4:1 H_2O:H_2SO_4), was drawn through a 0.9 - 1.4 μm glass frit filter, and again, no appreciable change in the freezing temperature was seen.

The freezing of bulk solutions (~20 ml) of sulfuric acid was also studied with respect to filtered and unfiltered samples. The filtered samples were drawn through the 0.9 - 1.4 μm filter. This data is also given in Figure 2.13. In all cases the difference between the freezing temperature of the filtered versus unfiltered bulk solutions was minimal (at most 10 K). However, the freezing temperatures of the bulk solutions departed from the freezing temperatures of the capillary samples most markedly for

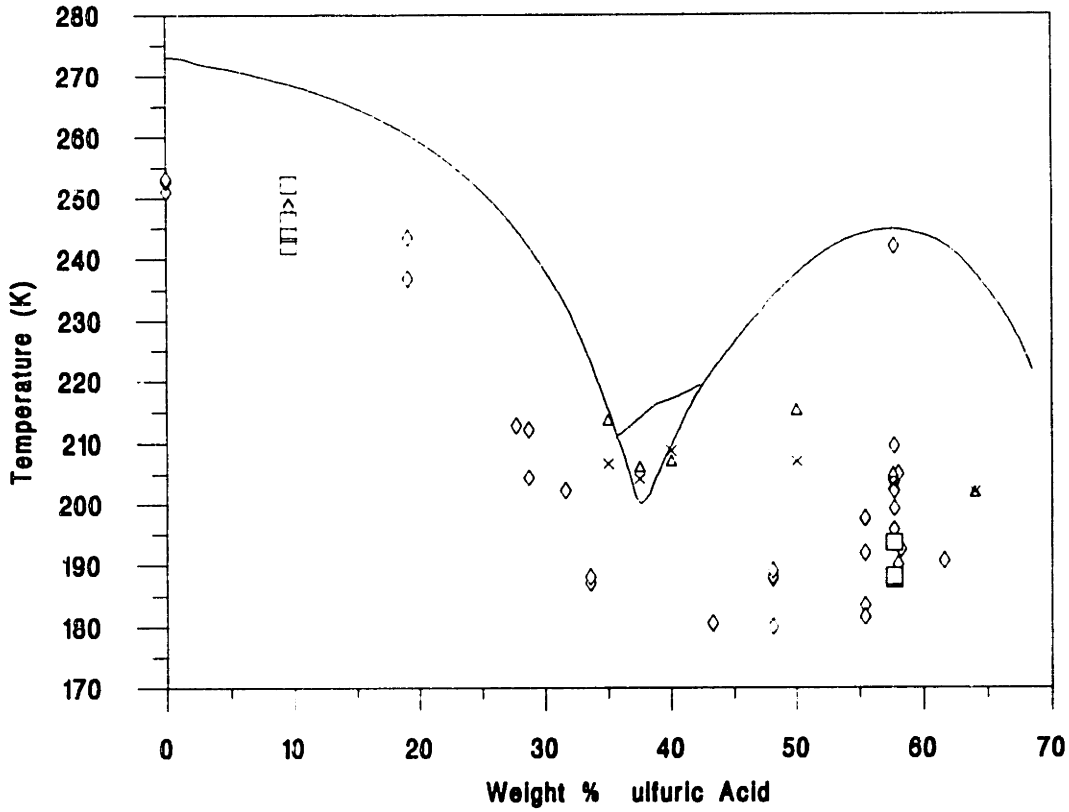

Figure 2.13: Phase diagram of sulfuric acid/water binary system. Solid line represents the equilibrium freezing/melting points from Gable, et al. [1950]. Capillary samples (see text for details): boxes represent freezing on cooling for unfiltered samples; diamonds represent freezing on cooling for filtered samples. Bulk samples (see text for details): triangles represent the onset of nucleation for unfiltered samples; X's represent the onset of nucleation for filtered samples.

concentrations of 35 to 40% sulfuric acid. Higher freezing temperatures are seen for the bulk samples than for the capillary samples in the mentioned concentration range. We expect to see a higher freezing temperature for solutions of larger volume than used in the capillary studies, since nucleation rate is a function of volume. Thus, the larger the volume, the higher the probability of a nucleation event. The size dependence on the freezing temperature of pure water drops has been shown by a number of researchers [Hobbs, 1974; Mason, 1960]. The observation that was unexpected was that seen for the 57.6% solution. It had a freezing temperature similar to that observed in the capillary studies. We are somewhat at a loss to explain this except for the possibility that foreign

substances (smaller than those filtered out) enhanced the nucleation of the 57.6% capillary samples.

Table 2.4

Cooling and warming capillary experiments for line 'a' concentrations.

[H2SO4] wt. fractio	[HNO3] wt. fractio	m T (K)	Trial #	(K) n	(K)	(K)
0.3865	0.0858	196.8	1	n	185-196	221-227
			2	n	188-195	227-229
			3	n	191-199	220-230
0.3600	0.1059	196.4	1	n	n	n
			2	n	n	n
			3	n	n	n
0.3546	0.1210	196.3	1	n	n	n
			2	n	n	n
			3	n	n	n
0.3090	0.1620	195.7	1	n	n	n
			2	n	n	n
			3	n	n	n
0.2210	0.2510	195	1	n	191-195	243-245
			2	n	192-196	242-246
			3	n	188-195	241-244.5
0.0763	0.3945	194	1	n	n	n
			2	n	180-190	249-251
			3	n	n	n
Cooling and warming capillary experiments for line 'c' concentrations.						
0.4665	0.0214	197	1	n	n	n
			2	n	n	n
			3	n	n	n
0.4360	0.0349	196	1	n	176-183	233-235
			2	n	179-186	229-234
			3	n	n	n
0.3920	0.0598	195	1	n	186-195	221-228
			2	n	179-190	225-227
			3	n	184-189	224-227
0.3258	0.1070	194	1	n	n	n
			2	n	n	n
			3	n	n	n
0.2147	0.2004	193	1	n	n	n
			2	n	n	n
			3	n	n	n
0.0919	0.3296	192	1	n	n	n
			2	n	173-179	243-244
			3	n	n	n

Notes: n: No crystallization observed.

2.5.5 *$H_2SO_4/HNO_3/H_2O$ Ternary system: Capillary cooling and warming experiments.*

Supercooling and melting of the sulfuric acid/nitric acid/water ternary system has been studied using the capillary method described above. From the parameterization of the data of Zhang et al. [1993b] (given in section 2.3) samples containing stratospheric equilibrium compositions of sulfuric acid, nitric acid and water were used. Table 2.4 lists the composition of each component in the samples and gives the results of the experiments. None of the samples actually froze during cooling, and some of them froze when the sample was warmed as indicated in the table. No real information can be drawn from these experiments regarding nucleation of ternary samples, except that at our cooling rate (2 K per minute) and sample size, these solutions do not appear to readily freeze. As a result, the main focus of nucleation studies for the ternary system was on the time studies discussed below. For the samples that did freeze, the melting temperatures were checked against those reported by Carpenter and Lehrman [1925] and found to be in agreement within experimental error.

2.5.6 *$H_2SO_4/HNO_3/H_20$ Ternary system: Time studies*

Figure 2.14 shows the parameterization of the data of Zhang et al. [1993b] as given in section 2.3. Lines a, b and c correspond to the equilibrium state of stratospheric aerosols at a given temperature and with an equilibrium composition of H_2SO_4, HNO_3 and H_2O corresponding to background partial pressures of HNO_3 and water given in the figure. Samples of $H_2SO_4/HNO_3/H_2O$ were prepared and held at the equilibrium temperature corresponding to their respective compositions using the apparatus shown in Figure 2.6. Theses are shown by various symbols in Figure 2.14 as given in the caption. Table 2.1 gives the equilibrium compositions for cases a, b and c over the temperature range 205 to 190 K. The results of the time experiments are given in: Table 2.5 for samples of 3 ml for conditions corresponding to line 'a', Table 2.6 for samples of 3 ml for conditions corresponding to line 'c', Table 2.7 for samples of 0.3 and 0.03 ml for

Table 2.5

Results of ternary supercooling experiments using 3 ml samples corresponding to conditions of line 'a'.

Experiment #	1	2*	3**	4		5
Equilibrium T	196.8	196.8	196.8	196.4		196.4
Experimental T	197.3	195.1	188.3	195.9		195.5
[H2SO4]	0.3865	0.3865	0.3865	0.36		0.36
[HNO3]	0.0858	0.0858	0.0858	0.1059		0.1059
	Time to	Time to	Time to	Time to Freeze (h)		Time to
Thermocouple #	Freeze	Freeze	Freeze	time #1	time #2	Freeze
0			0.6	13.78	13.97	
1			1.6			
2			1.56			
3			0.84	14.67		
4			0.84	23.28		
5						13.13
6						1.61
7						
8				nt		0.27
9				8.1		
10				15.85		
11				7.44		11.83
12				5.76		
13				11.87		
14				6.51	6.62	
15				23.05		
16				18.52		
17	2.5			2.92	3.09	
18				9.9		
19				19.1		
20				<slush>		
21				3.2		
22				<slush>		
23				9.44		
24				4.4		
25				6.46		
26				20.19		
27				23.15		
28				3.6	3.81	
29				<slush>		
30				10.21		
31				<slush>		
Freezing Ratio	1/32	0/8	5/5	22/32	(4 slush)	4/32
Exper. time (h)	25.4	27	27	24		24
time (hours)	2.5		1.09	11.9		6.71

Notes: Blank areas indicate no nucleation. Shaded areas indicate that no samples were run.
Two freezing times are given when two separate phase transitions were seen.

Table 2.5 continued

Experiment #	4&5	6*	7**	8		9*
Equilibrium T	summary	196.4	196.4	196.3		196.3
Experimental T		195.5	189	196		196.4
[H2SO4]		0.36	0.36	0.3546		0.3546
[HNO3]		0.1059	0.1059	0.121		0.121
		Time to	Time to	Time to Freeze (h)		Time to
Thermocouple #		Freeze	Freeze	time #1	time #2	Freeze
0		<40	2.44			<48
1		9.6	2.28	<slush>		5.52
2			18.72			20.52
3			18.72			<40
4			1.8			4.35
5			3.12			<48
6			0.36	<slush>		31.68
7			0.6			20.5
8			0.48	11.87		
9				<slush>		
10				14.77		
11				<slush>		
12				10.98		
13				4.67	11.01	
14						
15						
16						
17				3.02		
18						
19						
20						
21						
22						
23				<slush>		
24						
25				<slush>		
26						
27				<slush>		
28						
29				<slush>		
30				<slush>		
31						
Freezing Ratio	26/64	2/10	9/14	5/32	(9 slush)	8/14
Exper. time (h)	24	40	24	24		48
time (hours)	11.1		5.39	9.06		16.51

Notes continued: *: These experiments were performed with a different apparatus (see text for details.)

**: These are the same as the * experiments, except the samples were placed in a dry ice/acetone bath.

Table 2.5 continued

Experiment #	10**	11*	12**	13	14*	15*
Equilibrium T	196.3	196	196	195.7	195.7	195.45
Experimental T	188.3	194.7	188.3	195	195.3	196.5
[H2SO4]	0.3546	0.3319	0.3319	0.309	0.309	0.2795
[HNO3]	0.121	0.1396	0.1396	0.162	0.162	0.184
Thermocouple #	Time to Freeze	Time to Freeze	Time to Freeze	Time to Freeze	Time to Freeze	Time to Freeze
0	<24	18.7	16		5.88	1.93
1	<25	18.64	<24	2.8-4.0?	17.76	22.15
2	<26		10.94		17.88	6.66
3	<27		<24		6	
4					13.2	
5				6.27	2.4	
6				nt	17.64	
7					5.04	
8					2.76	
9				3.46	19.44	
10				14.05	0.72	
11				3.48	0.36	
12					0.6	
13				0.4	0.6	
14					2.76	
15						
16						
17						
18						
19				8.63		
20				nt		
21						
22						
23						
24						
25						
26						
27						
28						
29						
30				18.06		
31						
Freezing Ratio	4/5	2/3	4/4	10/32	14/14	3/4
Exper. time (h)	27	43		24	24	43
time (hours)		18.67		7.76	7.54	10.25

Notes continued: #: In these experiments the samples were purposely kept several detrees below the equilibrium temperature to determine the effects of much lower temperatures.

Table 2.5 continued

Experiment #	16*	17*	18*	19		20*
Equilibrium T	195.45	195.2	195.2	195		195
Experimental T	196.5	194.5	194.5	194		194.3
[H2SO4]	0.2795	0.2482	0.2482	0.221		0.221
[HNO3]	0.184	0.211	0.211	0.251		0.251
	Time to	Time to	Time to	Time to Freeze (h)		Time to
Thermocouple #	Freeze	Freeze	Freeze	time #1	time #2	Freeze
0	1.08	6.66	15.3	<some crystals>		0.11
1	30.6	2.58	0.18	.06-.81?		0.21
2	29.7	2.58	<35	0.12		3.57
3	29.16		12.6	0.31		0.21
4	9.18		0.36	0.28	9.25	1.16
5			<35	0.23		1.26
6				4.65		0.21
7				1.36		
8				0.51		
9				0.06		
10				0.05		
11				0.1		
12				0.37	6.1	
13				0.1	1.7	
14				0.16		
15				0.11		
16				0.11		
17				0.13	8.12	
18				0.35		
19				2.08	15.22	
20				0.12		
21				0.1		
22				1.93		
23				1		
24				1.85		
25				0.46		
26				1.43		
27				.08-.20?		
28				nt		
29				nt		
30				0.13		
31				1.45		
Freezing Ratio	5/7	3/4	6/7	31/32		7/7
Exper. time (h)	35	43	35	24		20
time (hours)	19.94	3.94	7.11	0.72		0.96

Notes continued: <slush>: The sample only partially froze, as determined by visual observation.

Table 2.5 continued

Experiment #	21#		22#		23
Equilibrium T	195		195		194
Experimental T	191.8		186.6		194.2
[H2SO4]	0.221		0.221		0.0763
[HNO3]	0.251		0.251		0.3945
	Time to Freeze (h)		Time to Freeze (h)		Time to
Thermocouple #	time #1	time #2	time #1	time #2	Freeze
0	2.47		1.02		0.05
1	6.05	11.37	1.27		0.46
2	7.28		0.65		2.62
3	2.16		0.14		0.09
4	0.44	8.8	0.85		1
5	1.4	12.13	0.13		0.39
6	2.93		3.59		0.04
7	1.14		0.44	0.95	0.07
8	0.17	2.42	3.35		0.03
9	0.83		0.16		1.15
10	0.1		0.15		0.06
11	1.4		0.66		0.16
12	0.48		0.1		0.07
13	1.58	5.98	1.42		0.02
14	2.92	9.66	1.31		0.07
15	6.92	9.18	4.13		0.09
16	0.13	3.16	0.4		0.04
17	0.24		0.16		0.04
18	4.66		nt		nt
19	1.94		0.12		0.06
20	0.83		nt		0.03
21	1.66		nt		0.04
22	23.01		2.38		0.18
23	5.36		1.22		0.04
24	0.06	0.88	0.8		0.9
25	0.89	5.6	0.83		0.05
26	1.4		0.9		0.74
27	2.94		0.12		1.09
28	0.32		0.27		0.03
29	0.87		0.12		0.04
30	0.72		0.69		0.02
31	0.11		1.78		0.78
Freezing Ratio	32/32		32/32		32/32
Exper. time (h)	24		23		24.16
time (hours)	2.61		1.01		0.34

Notes continued: nt: No freezing signal was seen, however the sample was observed to be frozen when it was removed from the freezer.

Table 2.6

Results of ternary supercooling experiments usint 3 ml samples corresponding to conditions of line 'c'.

Experiment #	1		2		3	4
Equilibrium T	197		196		195	194
Experimental T	196		194.8		195.41	195.1
[H2SO4]	0.4665		0.436		0.392	0.3258
[HNO3]	0.0214		0.0349		0.0598	0.107
	Time to Freeze (h)		Time to Freeze (h)		Time to	Time to
Thermocouple #	time #1	time #2	time #1	time #2	Freeze (h)	Freeze (h)
0						nt
1						
2	15.83					nt
3	2.54					
4						
5	12.43					
6	0.09		0.07		0.17	0.21
7						13.94
8	0.06		11.56		0.18	0.21
9			0.33	0.62		
10						8.37
11			2.25			nt
12						
13	1.32	1.43				
14	12.22	12.38				
15	5.07	5.37				
16						
17			12.27			
18						
19						
20	6.03					23.31
21	0.3					
22						
23			4.95			
24	1.88					
25						
26	8.71					
27			3.46			
28	17.76		2.42	2.52		
29	3.33		11.65			
30						
31						
Freezing Ratio	14/32		9/32		2/32	8/32
Exper. time (h)	24		26.5		24	24.7
time(h)	6.255		5.44		0.175	9.208

Notes: Blank areas indicate no nucleation.
Two freezing times are given when two separate phase transitions were seen.

Table 2.6 continued

Experiment #	5		6#		7
Equilibrium T	193		193		192
Experimental T	193.7		188.3		192.5
[H2SO4]	0.2147		0.2147		0.0919
[HNO3]	0.2004		0.2004		0.3296
	Time to Freeze (h)		Time to Freeze (h)		Time to
Thermocouple #	time #1	time #2	time #1	time #2	Freeze (h)
0	0.63		2.51		0.43
1	0.66		1.03		.11-.21
2	0.61		1.87		1.59
3	0.71		1.2		0.09
4	1.02		0.4		0.13
5	0.5		0.95		0.35
6	0.41		1.68		0.4
7	0.33		0.56		0.1
8	0.19	2.21	0.87		0.05
9	3.88		0.88		1.39
10	2.25		0.08		0.09
11	1.56		1.38		1.36
12	3.05		0.45		0.12
13	2.69		0.16		0.07
14	18.08		1.94		0.08
15	0.73		2.33		1.32
16	3.38		0.36		1.22
17	0.42		0.38		1.75
18	2.61		0.1		0.08
19	0.55		1.63		0.92
20	1.4		4.8	5.12	2.54
21	1.41		3.73		1.1
22	nt		2.27		1.07
23	1.55		2.5		1.3
24	8.38		0.29		0.53
25	0.29		7.3		0.38
26	0.44		3.01		1.05
27	3.31		0.4		0.88
28	nt		1.73		1.94-4.7
29	0.66		1.73		1.39
30	1.09		1.59		0.22
31	0.23		1.18		2.99
Freezing Ratio	32/32		32/32		32/32
Exper. time (h)	24		24		24.5
time(h)	2.100667		1.602813		0.833

#: In this experiment, the temperature was specifically set several degrees below the equilibrium temperature in order to determine a temperature effect on nucleation.

nt: No freezing signal was seen, however the sample was observed to be frozen when it was removed from the freezer.

Table 2.7

Results of supercooling time studies for the ternary system using 0.3 and 0.03 ml of sample corresponding to conditions of line 'a'.

Experiment #	1	2		3		4
Equilibrium T	195	194		195		194
Experimental T	195.3	193.9		196.15		194.21
[H2SO4]	0.221	0.0763		0.221		0.0763
[HNO3]	0.251	0.3945		0.251		0.3945
Sample Vol. (ml)	0.3	0.3		0.03		0.03
	Time to	Time to Freeze (h)		Time to Freeze (h)		Time to
Thermocouple #	Freeze (h)	time #1	time #2	time #1	time #2	Freeze (h)
0		0.36				0.17
1	0.16	nt				0.46
2	3.76	0.67		2.81		2.63
3	4.24	0.02				0.09
4	0.46	0.03				1
5	0.76	0.03		0.6		0.39
6	0.15	0.05	0.32			0.04
7	0.16	nt		11.08		0.07
8	0.05	nt				2.63
9	0.19	0.03				1.15
10	0.16	0.03		0.95	14.22	0.06
11	1.02	0.19				0.16
12	0.09	0.03	0.62			0.07
13	0.12	0.03		0.52		0.01
14	23.05	0.04	0.32			0.07
15	0.18	nt				0.09
16	2.18	0.05				0.03
17	1.2	0.11				0.04
18	0.96	0.18				nt
19		0.2	0.62	0.52		0.06
20	0.43	0.2	0.61	nt		0.05
21	0.08	nt				0.03
22		0.85	1.07	13.3		0.19
23	0.07	0.85	1.07			0.04
24	0.16	0.03				0.9
25	0.12	0.2				0.04
26	0.29	0.02				0.73
27	0.56	0.44				1.09
28	0.22	0.02	0.62			0.03
29	0.44	0.2		3.47		0.04
30	0.07	0.65				0.03
31	5.28	0.13				0.78
Freezing Ratio	29/32	32/32		9/32		32/32
Exper. time (h)	24	24		24		24
Ave. Freeze Tim.	1.607241	0.208889		4.15625		0.424839

Blank areas indicate no nucleation.
Two freezing times are given when two separate phase transitions were seen.
nt: No freezing signal was seen, however the sample was observed to be frozen when it was removed from the freezer.

Table 2.8

Results of supercooling time studies for the ternary system using 0.3 and 0.03 ml of sample corresponding to conditions of line 'c'.

Experiment #	1	2		3	4
Equilibrium T	193	192		193	192
Experimental T	194.1	191.9		193.62	193
[H2SO4]	0.2131	0.0906		0.2131	0.0906
[HNO3]	0.2018	0.331		0.2018	0.331
Sample Vol. (ml)	0.3	0.3		0.03	0.03
	Time to	Time to Freeze (h)		Time to	Time to
Thermocouple #	Freeze (h)	time #1	time #2	Freeze (h)	Freeze (h)
0	23.24	8.53		10.94	0.17
1		nt		11.84	0.49
2		2.05			0.19
3	13.98	0.02			12.33
4	3.24	0.05			0.15
5		4.87			0.96
6	0.59	0.4		21.93	0.13
7		5.04		nt	0.43
8	0.44	0.08		nt	4.61
9	4.54	0.11		2.55	11
10	1.23	0.07	3.72	nt	4.31
11		1.49		0.97	0.43
12		0.99			6.37
13	2.94	0.91	4.88		0.19
14		0.9		1.65	0.12
15	2.85	0.04	5.05	nt	0.48
16	0.55	0.14		10.03	
17		2.95			0.19
18	2.2	3.71			3.08
19		3.72		nt	2.51
20	7.6	0.1	0.37		17.95
21		0.09	0.38	16.11	nt
22	0.87	9.99		1.42	0.22
23		9.99		9.12	0.14
24		0.04	0.13	7.55	3.21
25	16.06	1.27		1.87	6
26		0.88			0.38
27		4.68		0.97	0.25
28		2.12		1.65	
29		0.03			0.22
30		0.66		6.84	0.58
31		1.63			2.15
Freezing Ratio	15/32	32/32		20/32	30/32
Exper. time (h)	24	24		24	24
Ave. Freeze Tim.	5.737857	2.179032		7.029333	2.732414

Blank areas indicate no nucleation.

Two freezing times are given when two separate phase transitions were seen.

nt: No freezing signal was seen, however the sample was observed to be frozen when it was removed from the freezer.

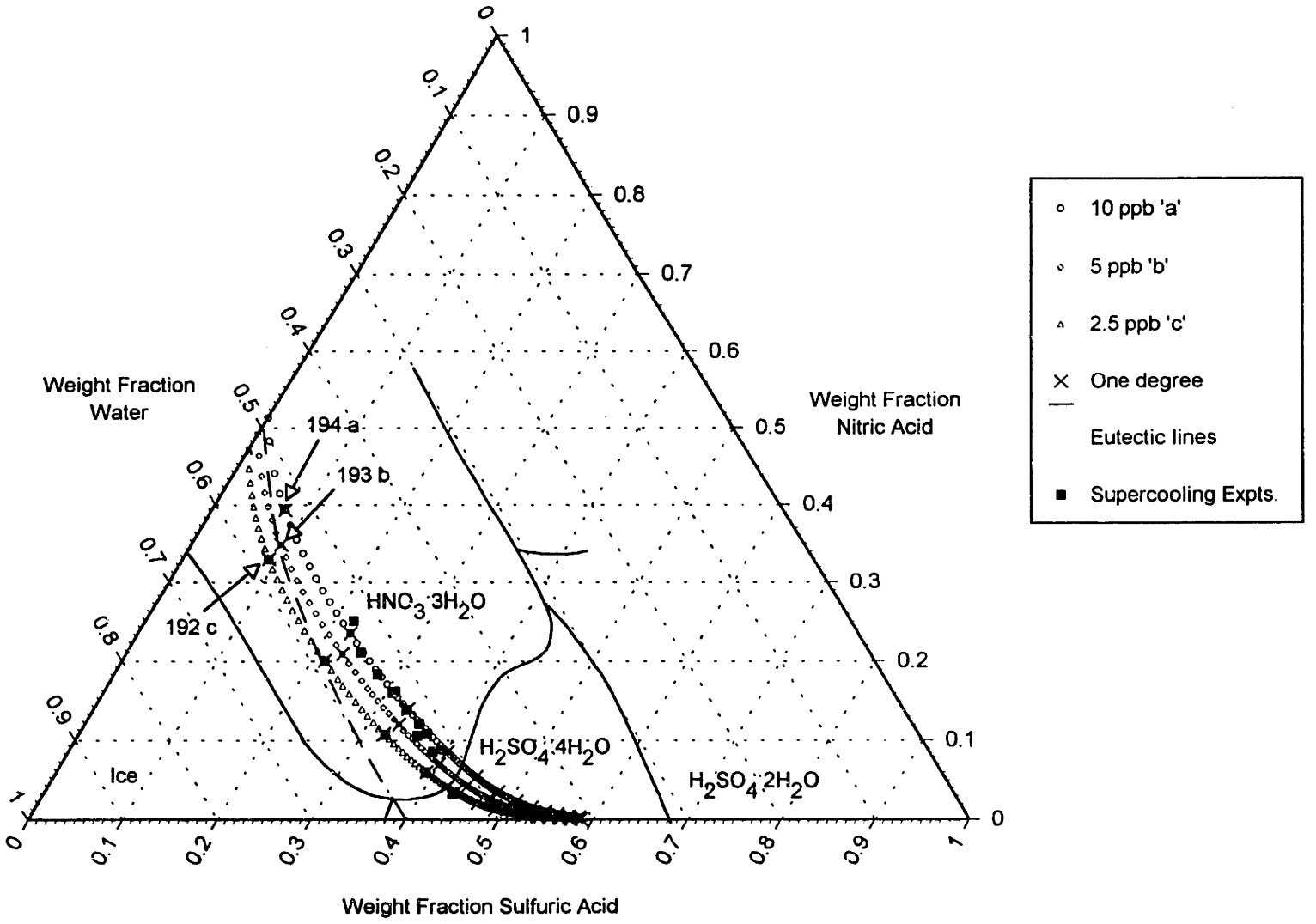

Figure 2.14: $H_2SO_4/HNO_3/H_2O$ ternary system freezing/melting data. Solution concentrations are given in Table 2.1.

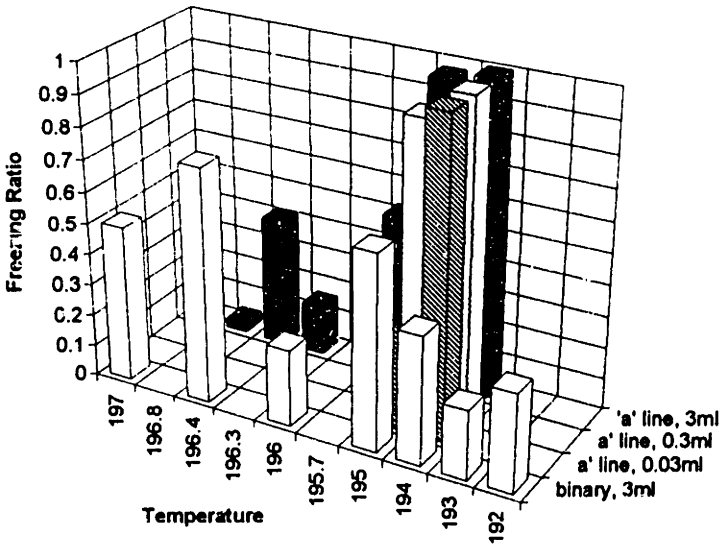

Figure 2.15: Summary of freezing ratios for ternary and binary experiments as given in Tables 2.3 and 2.5. Front data is for binary sulfuric acid/water solutions using samples of 3 ml. Back data is for ternary samples corresponding to line 'a' using 3 ml samples. Middle data, as labeled, is for 0.3 and 0.03 ml samples of ternary solutions corresponding to line 'a'.

conditions corresponding to line 'a', and Table 2.8 for samples of 0.3 and 0.03 ml for conditions corresponding to line 'c'.

Since nucleation is a stochastic process, we are interested in finding trends in the results. The first parameter of interest is the freezing ratio as a function of equilibrium temperature (which in turn determines the solution composition). The freezing ratio is the number of samples that nucleated during the experiment divided by the total number of samples run in the experiment. Line 'a' and line 'c' freezing ratios are plotted in Figures 2.15 and 2.16, respectively with the raw data given in Tables 2.3, 2.5 and 2.6. In these figures we show the results for the 3, 0.3 and 0.03 ml ternary samples. Also shown are the results for binary solutions of H_2SO_4/H_2O which correspond to a background pressure of 5 ppm of water (at 100 mbar). We are interested in this comparison in order to determine the effect that nitric acid has on nucleation of the ternary solution. In Figure 2.15, one can see that the trend for the 3 ml ternary samples is that the freezing ratio

increased rapidly as temperature decreased. For the 0.3 and 0.03 ml ternary samples we are interested in the

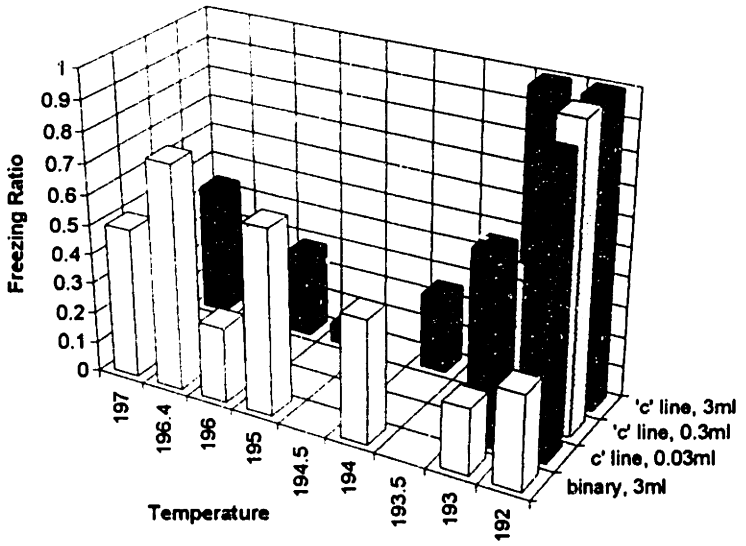

Figure 2.16: Summary of freezing ratios for ternary and binary experiments as given in Tables 2.3 and 2.5. Front data is for binary sulfuric acid/water solutions using samples of 3 ml. Back data is for ternary samples corresponding to line 'c' using 3 ml samples. Middle data, as labeled, is for 0.3 and 0.03 ml samples of ternary solutions corresponding to line 'c'.

volume effect (smaller samples should take longer to nucleate, thus less samples will nucleate in a fixed amount of time). However, there was little change in the freezing ratio from 3 ml to 0.3 ml. A more dramatic drop in the freezing ratio is seen for the 0.03 ml sample at 195 K. This is as expected because of the much smaller volume; however, the 194 K case for 0.03 ml samples showed no significant decrease in the freezing ratio. For the binary solution, the general trend is the opposite of that for the ternary samples: the freezing ratio decreases as temperature decreases. Clearly the addition of the nitric acid is having an effect upon the nucleation of the ternary solutions for the same temperatures. We believe this is because the nucleation of NAT out of the ternary solution is driving the crystallization of the entire solution. The same general trends are seen in Figure 2.16 for the conditions of line 'c', except for the volume comparison of the ternary solutions. In this case, the freezing ratio decreases for the 0.3 ml sample, but then is increases slightly

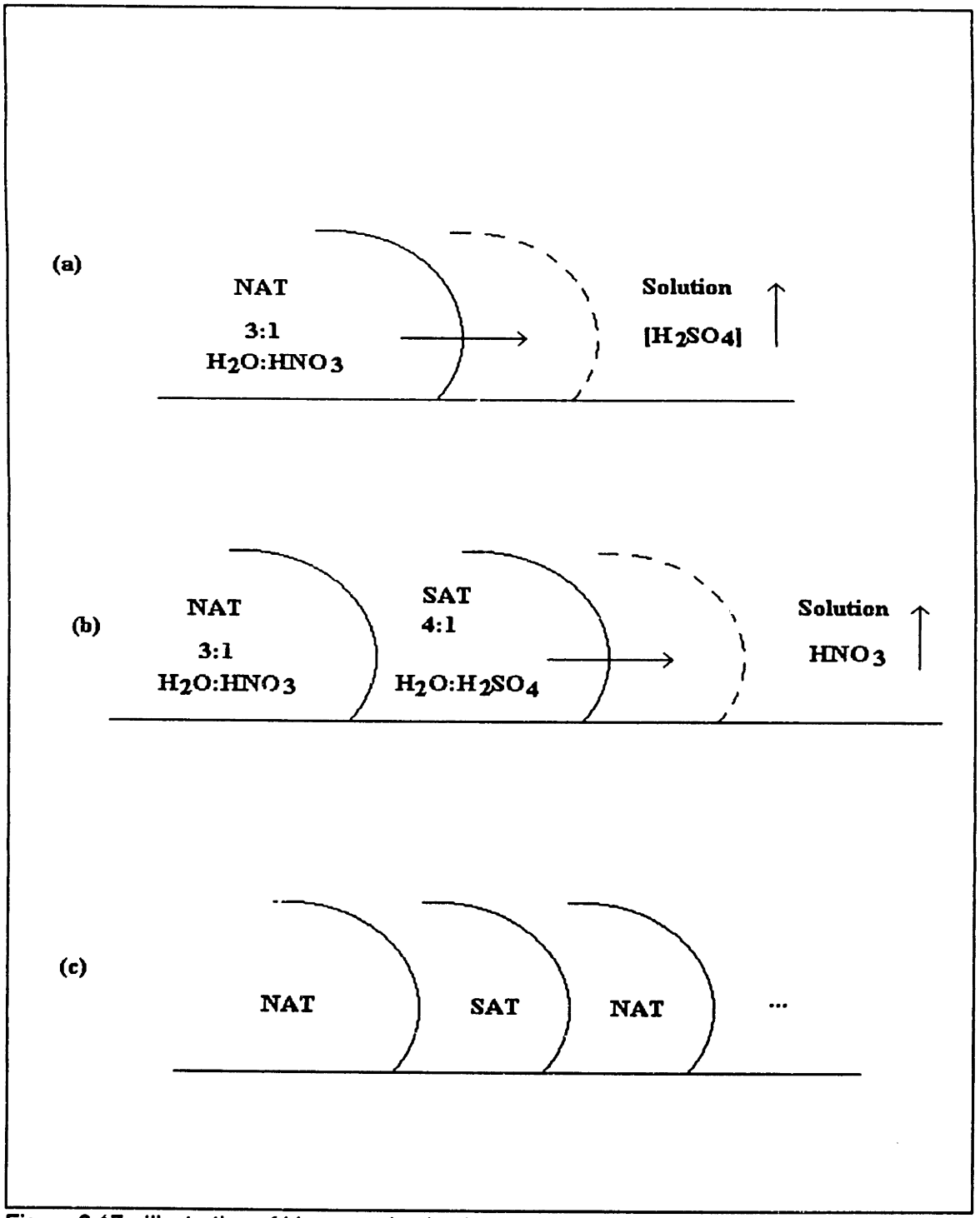

Figure 2.17: Illustration of binary nucleation in a ternary solution. One solid nucleates first, and from the evidence presented here and in Molina, et al. [1993], most likely this is NAT as frame (a) shows. As the front advances, the remaining solution becomes more concentrated in sulfuric acid as nitric acid and water are removed from the solution. When the liquid becomes close to a ratio of 1:4 sulfuric acid/water, SAT nucleates as shown in frame (b). Then SAT grows and the remaining liquid becomes more concentrated in nitric acid until NAT again nucleates. This process continues as shown in frame (c), until all the liquid has either crystallized or evaporated.

for the 0.03 ml samples. This is opposite of the trend we expect: the freezing ratio should decrease with decreasing volume. If we did more experiments with 0.03 ml samples we would expect the overall trend to be a decrease in the freezing ratio for the 0.03 ml samples from the 0.3 and 3 ml cases.

It is interesting at this point to consider nucleation in a multicomponent solution from a conceptual standpoint. Figure 2.17 illustrates the case of a NAT crystal growing in a ternary solution. The crystallization front advances, building nitric acid and water molecules (or ions) into the crystal lattice. As nitric acid and water are removed from the solution, it becomes more concentrated in sulfuric acid until the ratio of water to sulfuric acid becomes near 4:1. At this point conditions become favorable for the nucleation of SAT, not because the SAT nucleates on NAT (a topic that will be discussed in the next section), but rather because the crystallization front acts like a stirrer on the solution, inducing motions that enhance the probability of forming a critical nucleus. (In some of our experiments, the solution turned to slush, indicating that only one of the solids nucleated.) Then the SAT crystal grows concentrating the remaining solution in nitric acid until NAT again nucleates (see Figure 2.17). This process continues until essentially all the liquid has crystallized into NAT and SAT (and possibly ice and sulfuric acid hemihexahydrate.) If any acid is remaining in liquid form it will either evaporate or deliquesce more water until it freezes. Since NAT will only nucleate from the solution when it is supersaturated with respect to the gas phase, after the ternary droplet freezes, there will be a nucleation site for NAT condensation from the gas phase, thus the particles will grow until the partial pressure of nitric acid has dropped to equilibrium with NAT.

The second parameter of interest in the supercooling experiments is the average time of freezing. One can calculate the average time it took for the solutions that did freeze, to freeze. Figures 2.18 and 2.19 show the average freezing times in the supercooling experiments analogous to Figures 2.15 and 2.16. Figure 2.18 shows the results for line 'a' along with the binary results for comparison, and Figure 2.19 shows the

results for line 'c' also with the binary results for comparison. For the 3 ml solutions in Figure 2.18 there is a trend of decreasing average freezing times with a decrease in equilibrium temperature. Again for the binary the trend is the opposite that of the ternary

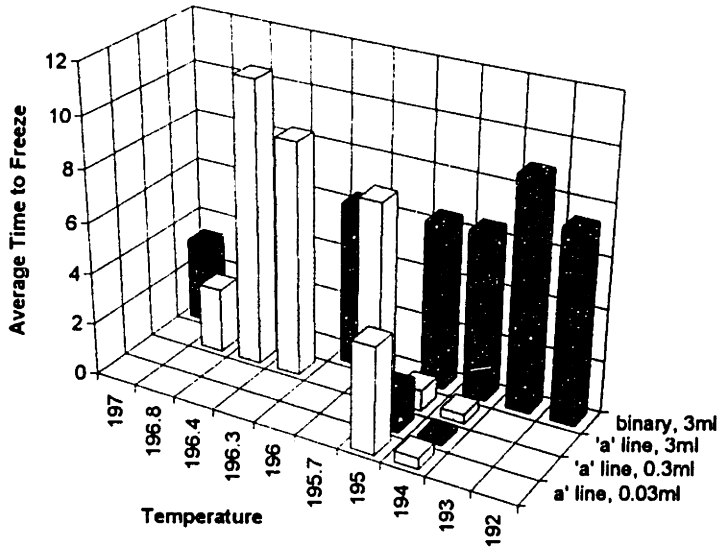

Figure 2.18: Summary of the average time to freeze for ternary and binary experiments as given in Tables 2.3 and 2.5. Back data is for binary sulfuric acid/water solutions using samples of 3 ml. Front data is for ternary samples corresponding to line 'a' using 0.3 ml of sample. Middle data, as labeled, is for 0.03 and 3 ml samples of ternary solutions corresponding to line 'a'.

with freezing times increasing with decreasing equilibrium temperatures, indicating the centrality to nucleation of nitric acid in the ternary solutions. The 0.3 ml solutions show a slightly longer average freezing time at 195 and the 0.03 ml solutions even longer, as expected, and essentially no difference at 194 K. In Figure 2.19 we see a similar case. The trend for the 197 to 194 K range is a bit ambiguous, possibly indicating the reality of no actual trend for solutions of these compositions. However, there is then the clear trend for the 193 and 192 cases of clear decreases in average freezing time with decreasing temperature. The 0.3 and 0.03 ml ternary samples exhibited a more dramatic volume effect than the line 'a' results, and still in line with our expectations. The binary data is the same as in Figure 2.18. Note that in some cases the range of sample freezing times is

large, and the number of samples that froze is small, thus an "average freezing time" does not convey significant information.

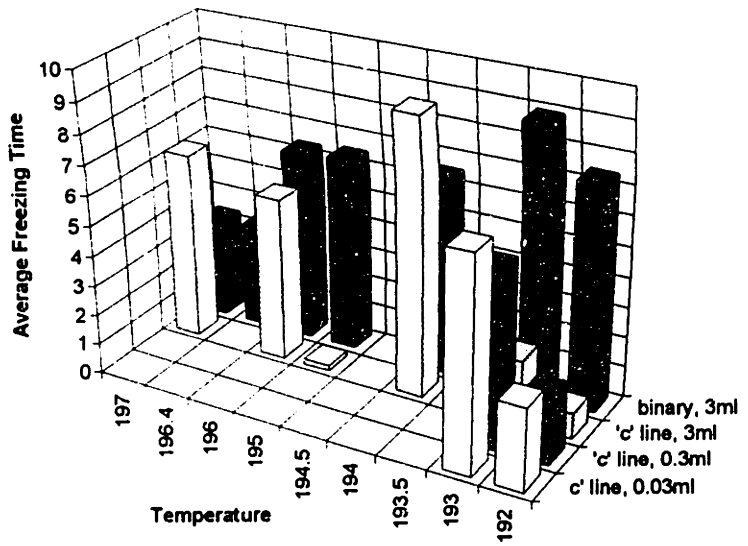

Figure 2.19: Summary of the average time to freeze for ternary and binary experiments as given in Tables 2.3 and 2.5. Back data is for binary sulfuric acid/water solutions using samples of 3 ml. Front data is for ternary samples corresponding to line 'c' using 0.3 ml of sample. Middle data, as labeled, is for 0.03 and 3 ml samples of ternary solutions corresponding to line 'c'.

In Figures 2.20 and 2.21 we have plotted the data vs. the "Freezing Factor" which was introduced earlier; the definition is repeated here for clarity:
$FF = 1 - \frac{(FR)(AFT) + (1 - FR)(ET)}{ET}$, where FF is the freezing factor, FR is the freezing ratio, AFT is the average freezing time of the samples that froze and ET is the experimental time (in most cases 24 hours). Again, the freezing factor ranges between zero and one with higher numbers indicating a greater probability to freeze in a relatively short time (short compared to the total time of the experiment.) Clear trends of the

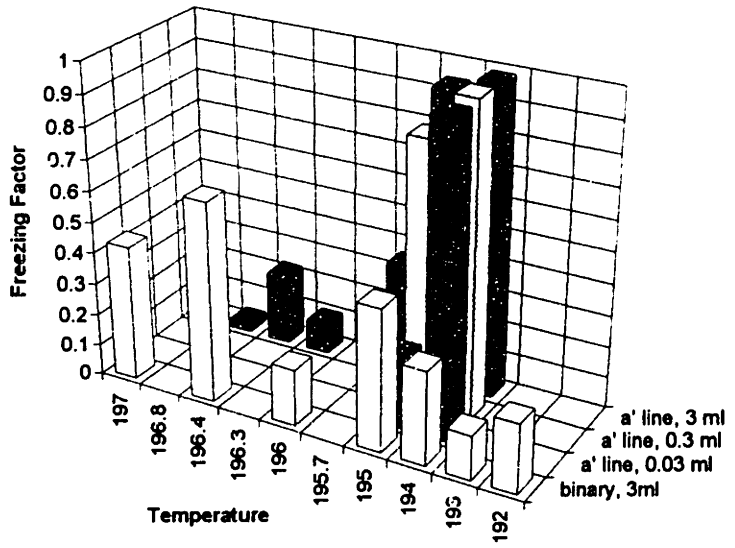

Figure 2.20: Combined summary of the data using the parameter: Freezing Factor whose equation is given in the plot. Results are for conditions of line 'a' and sulfuric acid binary for comparison.

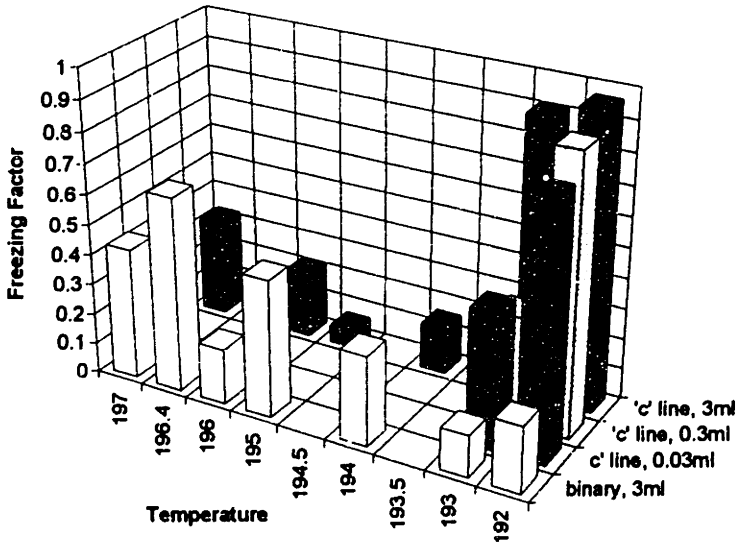

Figure 2.21: Combined summary of the data using the parameter: Freezing Factor whose definition is given in the plot. Results are for conditions of line 'c' and sulfuric acid binary for comparison.

combined variables can now be seen in Figures 2.20 and 2.21. The freezing factor for the 3 ml ternary samples increases from low values to very high values for the last two temperatures of lines a and c. The opposite trend is clearly seen in the binary case. The volume effect is minimal for the lowest ternary temperature, but significant for the second

lowest in each of the two cases. As mentioned in the freezing ratio discussion, the 193 K experiment of 0.03 ml in Figure 2.21 shows a slight increase in the freezing factor over that of the 0.3 ml experiment. This is not as predicted; however, more experiments are expected to decrease the freezing factor for these samples.

In the atmosphere we see 'threshold' effects for the formation of Polar Stratospheric Clouds (PSCs), that is, the volume of the background aerosols suddenly and rapidly increases when the temperature drops to a certain level. Our experiments are in line with these observations. Rather than nucleation being dependent on a critical temperature, we find that it depends on a critical composition which is controlled by the temperature and the background vapor pressures of nitric acid and water. When the solution concentration of nitric and sulfuric acids becomes approximately equivalent (in our cases ~20% by weight of each acid), nucleation begins to occur rapidly both in the fraction of samples that freeze and in the average time it takes for the samples to freeze. Before the state of equivalent acid concentrations is reached, the results are somewhat random, with slight trends being seen, but barely. When the nitric acid weight fraction is larger than the sulfuric acid weight fraction, we see even more rapid nucleation than the case for equivalent concentrations. This leads us to again conclude that the nucleation of nitric acid is driving the overall freezing of these solutions. Thus, the 'threshold' temperature in the atmosphere for PSC formation will depend on the background vapor pressure of nitric acid and water, but will most likely correspond to the aerosols having concentrations of nitric and sulfuric acid of ~20% by weight. The atmospheric implications of these results will be discussed in more detail in Chapter 3.

We were also interested in discerning between temperature and composition effects. Three experiments were done where the samples were purposely held at a temperature significantly below their equilibrium temperature. They are listed in Table 2.5 as experiments 21 and 22, and in Table 2.6 as experiment 6. In experiment 21 the sample was held 3.2 degrees below its equilibrium temperature of 195 K. Its freezing ratio is

essentially the same as that for experiment 19 (were the samples were held at 194 K), and the average freezing time is longer by nearly 2 hours. In experiment 22, the samples were placed 8.4 degrees below 195 K and the freezing ratio is again the same with the average freezing time being slightly longer than in experiment 19. Thus no temperature effects were seen here. In experiment 6 of Table 2.6, the samples were held 4.7 degrees below their equilibrium value of 193 K. Freezing ratio was the same as that of experiment 5, and the average freezing time was only slightly shorter. Thus, we conclude that colder temperatures do not significantly enhance the freezing of these solutions.

Finally, we would like to attempt to apply our results to the conditions of the stratosphere. The obvious difference between these experiments is that we have samples held in glass containers; in the atmosphere they are spherical drops. Also, there is always the question of impurities in the samples (or in the stratospheric aerosols, for that matter) which might enhance (or deter) nucleation. Along with this comes the questions of whether the nucleation process is heterogeneous or homogeneous. We could alleviate the first problem of having the sample in contact with a glass surface by levitating drops and observing their nucleation. However, this type of experiment is difficult and not necessarily definitive. The second problem is even more difficult since there is yet no conclusive evidence regarding insoluble impurities in stratospheric aerosols. To make "nuclei free" concentrated acid samples in the laboratory is essentially impossible. Studies where nuclei free water has been made used elaborate ion exchange filtering systems, a process which obviously would not work here. If we place these matters aside, there is at least one outstanding difference which we can address: volume. The volume of the samples we studied is several orders of magnitude larger than that of stratospheric aerosols. One method we could employ is to empirically determine the nucleation rate of the samples. For example, for the 192 K data for samples of line 'c', the average freezing times are given in Table 2.9. If we assume that only one nucleus initiated the freezing, we

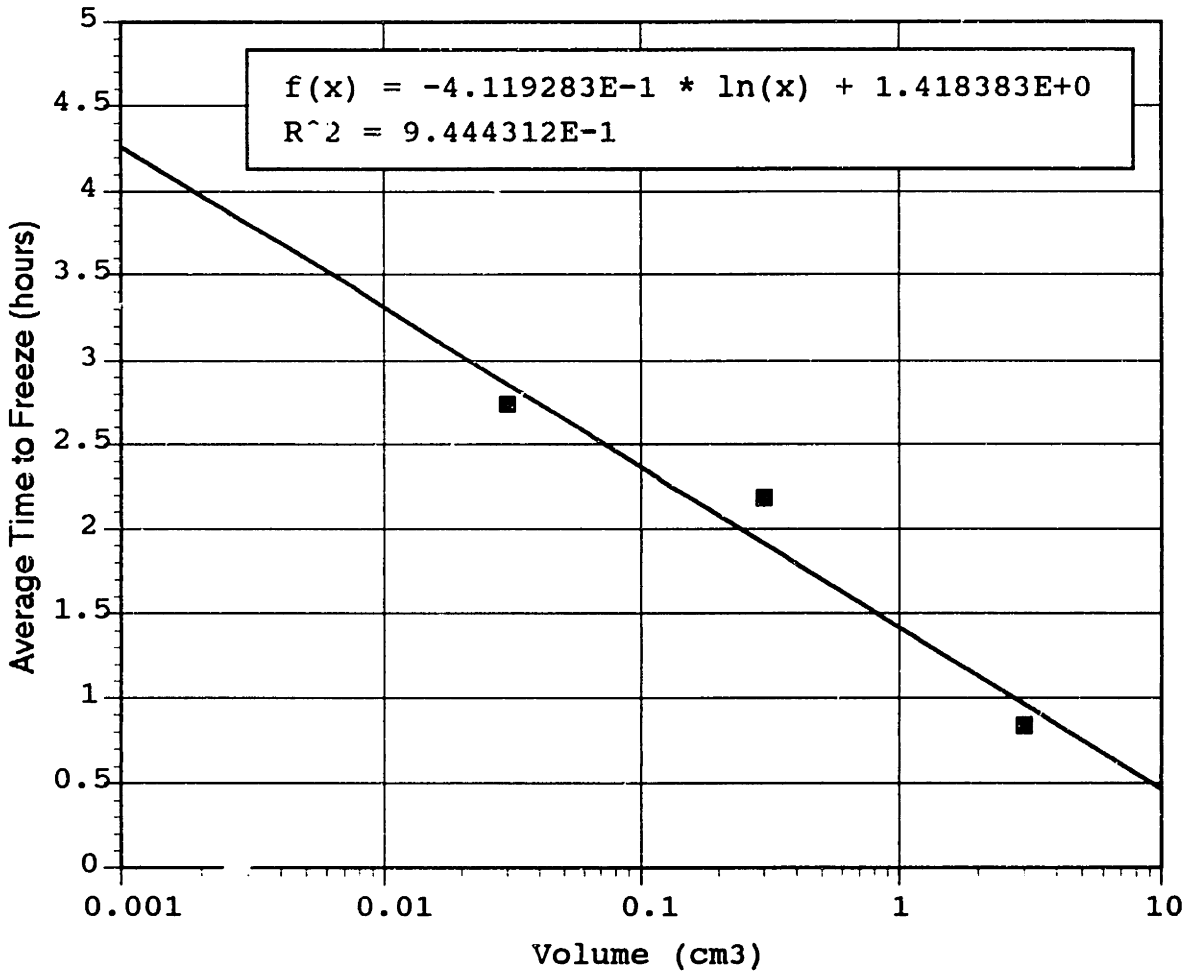

Figure 2.22: Plot of volume vs. average freezing time for the experiment of ternary solutions corresponding to an equilibrium temperature of 192 K under the conditions of line 'c'. The solid line is the fit to the data with the equation given in the figure.

Table 2.9

Comparison of experimental nucleation times to stratospheric aerosols.

Sample Volume	Average Freezing Time (hours)	Nucleation Rate (nuclei/cm^3 s)	Freezing Time for 1 μm drops (hours)
0.03 ml	2.73	0.00339	1.56×10^{10}
0.3 ml	2.18	0.000425	5.97×10^{10}
3 ml	0.833	0.000111	5.3×10^{12}

can write the rate as one nucleus per volume per average freezing time. Typically nucleation rates are given as nuclei/cm^3 second. This is the form used in Table 2.9. To

obtain the predicted time for nucleation of a 1 μm (radius) drop, we multiply the calculated rate times the droplet volume and then invert to get time per nuclei. The result for 1 μm drops is shown in Table 2.9. As can be seen, there is no consistency in the predicted nucleation time for 1 μm drops using this method. Alternatively, we can parameterize the average freezing time vs. volume data, and use that to calculate the freezing time for 1 μm drops. Figure 2.22 shows the plot of the data, with the equation of the fit to the data given on the figure. Using this equation, the average freezing time for a 1 μm drop will be ~12 hours. Why does the first method break down? The assumption that freezing is initiated by only one nucleus may be invalid. Beyond this, it is not clear. The trend in the data would suggest that the second method is a better predictor since the average freezing time did not change much when the volume decreased an order of magnitude. Only one data set of four is shown in Table 2.9 where volume effect information was available. In the other cases either the freezing ratio was not one or the average freezing time did not show a clear trend. Thus, the only useful information we have is for this one case.

2.5.7 *Freezing Observations*

We have observed the nature of the freezing of these ternary samples. When solutions of 40, 45, 50 and 57.6% H_2SO_4 (with their respective concentrations of HNO_3 as given in Table 2.1) freeze, in the bulk samples, it was observed that they always freeze from the top of the solution downward. An initial 'white' solid formed at the top surface of the sample and grew downward at a slow pace. Another more cloudy/clear solid crystallized from the white solid and grew at a faster rate dependent on solution concentration. The more concentrated the solution was in sulfuric acid (hence less concentrated in nitric acid) the larger the crystallization velocity of this cloudy solid. The cloudy solid also grew downward and was the first to engulf the entire sample. However, the white solid continued to grow downward as well (although slower) and eventually engulfed the entire sample. From freezing samples of pure H_2SO_4 tetrahydrate (SAT) the

cloudy solid in the ternary solutions visually looked identical to SAT. When freezing SAT the white solid does not appear. From our observations we have tentatively concluded that the cloudy solid is SAT and the white solid is NAT. Carpenter and Lehrman [1925] have shown conclusively (along with new evidence from Molina et al. [1993]) that no mixed hydrates are formed in the ternary system. The cloudy solid appears to have 'strains' in it parallel to the direction of crystallization. An explanation for this could be that SAT grows in needle shapes. This would allow for tubes of liquid to exist between the needles, hence the growth of the white solid may be the nucleation of these tubes to form NAT. The observation of two distinct crystallization fronts is further evidence that two different solids are being formed.

2.5.8 *Seeding experiments*

A number of 'seeding' experiments were carried out and the results are summarized in Table 2.10. In each case the 'seed' was made and equilibrated to the same temperature as the supercooled liquid being seeded. The apparatus is shown in Figure 2.7.

SAT as seed: Crystals of SAT were found to nucleate supercooled solutions of the ternary system with concentrations higher than 40% H_2SO_4 (hereafter "SNW2"). Thus giving further evidence that H_2SO_4 tetrahydrate is being formed in the ternary solution. Crystals of SAT did not nucleate a ternary solution of 30% H_2SO_4 (13% HNO_3) (hereafter "SNW1"), nor does SAT nucleate NAT.

NAT as seed: NAT, however did not nucleate solutions of SAT or SNW2. No changes to the NAT crystal or the solutions were observed when a NAT crystal was placed in the supercooled solutions. However, it is possible that with the small amount of nitric acid present in the SNW2 samples, a change in the size of the NAT crystal was not discernible. It is possible to say, however, that NAT does not nucleate a non-NAT solid that forms from SNW2 solution on nucleation. In the case of SNW1, NAT did nucleate the solution. When this solution nucleates it turns slushy and does not from a complete solid. This happens because the temperature of the sample (205K) is above the ice/SAT

eutectic point. Nucleation of SNW1 by NAT was slower than the other nucleations observed (taking ~15 minutes to change the whole solution, within observational error).

SNW2 as seed: We were also interested to see if the frozen ternary sample would nucleate NAT. Small samples of the 45 and 50% H_2SO_4 SNW2 solutions were frozen. Liquid HNO_3 (with the correct stoichiometric composition for NAT) was supercooled to ~205 K (in some of the trials the nitric acid solution spontaneously froze at this temperature). As soon as the ternary crystal touched the surface of the supercooled nitric acid liquid, the solution immediately and rapidly froze. Complete crystallization in a sample volume of ~2 ml took less than a second. SNW2 seeds also nucleated SAT and SNW1 solutions.

Table 2.10

	SAT	*SNW2*	*SNW1*	*NAT*
SAT nucleates	yes	yes	no	no
SNW2 nucleates	yes	yes	yes, slowly	yes
SNW1 nucleates	yes	no	yes	yes
NAT nucleates	no	no	yes	yes
Ice nucleates	no	no	yes, slowly	no

SNW1 as seed: SNW1 seeds nucleated SAT and NAT.

Ice as seed: In our seeding studies we found that ice did not nucleate NAT, SAT or SNW2, but this is as expected since none of these solutions is expected to form ice on nucleation. Ice did nucleate solutions of SNW1. Again the crystal growth was slow.

2.6 Conclusions

Debates have recently developed about the role of stratospheric aerosols in the formation of Polar Stratospheric Clouds (PSCs) [Hamill and Toon, 1991; Jensen et al., 1991; Hofmann et al., 1992; Dye et al., 1992; Luo et al., 1992; Zhang et al., 1993a,b]. Background stratospheric aerosols are largely made up of sulfuric acid and water. The sulfuric acid content ranges from about 75% by weight at tropical latitudes to as low as possibly 20 - 30% at the poles. However, as shown by Zhang et al. [1993b], sulfuric acid takes up significant amounts of nitric acid at low temperatures and moderate to low compositions.

2.6.1 *Proposed Theory of PSC Formation*

Based on the nucleation experiments presented here, we postulate that PSC type I is in fact a solid made by the following mechanism: $H_2SO_4/HNO_3/H_2O$ liquid drops nucleate and crystallize in the stratosphere when their compositions reach the ranges of ~20% H_2SO_4 and ~20% HNO_3. The solid particle consists of H_2SO_4 tetrahydrate and NAT as confirmed by FTIR, DSC and vapor pressure measurements in our lab [Molina et al., 1993], and in harmony with the results of Carpenter and Lehrman [1925]. These frozen aerosols grow by deposition of nitric acid and water to form an outer surface of NAT. Obviously, this deposition of NAT does not occur until the ternary liquid aerosols nucleate to form a solid, hence there is a threshold temperature (and time) when this occurs. We agree with Dye et al. [1992] who suggest that only a fraction of the aerosol cloud nucleates to form frozen particles (leading to type I PSCs). This is apparent from purely statistical reasoning with respect to the probability of aerosols nucleating. Dye et al. suggest that the larger aerosols preferentially nucleate first. Indeed, by volume considerations they have the greatest probability of nucleating. Observations by Dye et al. for the Arctic and by Fua et al. [1992] for the Antarctic are consistent with our laboratory observations of the freezing nature of the ternary stratospheric aerosols. We point out

that time spent by an aerosol at a given temperature is a major factor in whether it will nucleate or not.

2.6.2 *Mechanism involving NAD*

Also of note are reports by Ji and Petit [1991], and Worsnop et al. [1993] that nitric acid dihydrate (NAD) is important in the stratosphere. Comparing Worsnop et al.'s diagram of the vapor pressures of NAM, NAD, NAT and ice with measured polar stratospheric vapor pressures of water and nitric acid, it appears that NAD is not stable unless the pressure of nitric acid corresponds to a supersaturation of 10 or greater. Given that the water vapor pressure is relatively constant around 5 ppmv, one would need ~5 ppmv of nitric acid at ~205K to be in the NAD stability region. This situation is never seen in the polar stratosphere. Another answer would be to have ~0.5 ppmv of water and ~25 ppbv nitric acid at ~190K. Again this is ruled out for obvious reasons. Also of note, the calorimetery work of Ji and Petit showed that NAD exists at a much higher temperature than that reported by Worsnop, et al. They show, in fact, that NAD has a melting point, whereas Worsnop, et al. show that NAD does not melt, but always converts to either NAT or NAM. This discrepancy needs to be resolved in order to correctly define the NAD stability region.

From discussions with Doug Worsnop, he experimentally shows that NAD is stable (once formed) at stratospheric conditions, but will decay to NAT. The point that is missed here, however, is that he did not make NAD at stratospheric conditions, but rather at conditions where NAD or NAM are stable. He then changed the pressure of water and nitric acid to stratospheric conditions. We see no evidence (experimental or theoretical) that NAD will form (nucleate from gas to liquid to solid) at stratospheric conditions. In order for the hypothesis of Worsnop et al. to be viable, it must be demonstrated that NAD is more likely to nucleate out of the polar stratosphere than NAT. In private discussions D. Worsnop clarified that they believe NAD has a lower barrier to nucleation than NAT has (in the NAT stability region) even though NAD is less stable thermodynamically.

However, even with this claim, they have yet to demonstrate that NAD can be nucleated preferentially in the NAT stability region. Given the existing evidence, we conclude that NAD is not likely be a component of PSCs given stratospheric conditions.

If we consider the possibility of NAD vs. NAT nucleation and consider which one has a lower nucleation barrier, we need to look at the nucleation equation and evaluate the parameters that are involved. Equation 2.35 for the rate of nucleation is:

$$J = \frac{2V_m^{*3}(\sigma_{lc}k_BT)^{1/2}}{h}\exp\left(\frac{-\Delta G_a}{k_BT}\right)N_1\exp\left(\frac{-\Delta G^*}{k_BT}\right) \qquad (2.35)$$

Obviously NAD is not more *thermodynamically* stable than NAT in the NAT stability region (corresponding to the range of possible stratospheric conditions). It is, in fact, metastable there which means it has a higher free energy. Therefore ΔG^* is smaller for NAT nucleation than for NAD nucleation in the NAT stability region. We don't expect the Zeldovich factor (see section 2.2.2) to be significantly different for the two solids. This leaves us with the activation energy for diffusion across the solid/liquid interface as the only remaining variable. Now, if we consider which solid will more readily nucleate, NAT, or NAD from a single solution, then the activation energy for diffusion of a nitric acid molecule (nitrate ion) through the solution to the solid/liquid interface will be the same whether the crystallite nucleus is NAT or NAD. Furthermore, if we consider the diffusion of nitric acid (nitrate ions) to be the limiting step (i.e. water diffuses much faster), then, being that more nitric acid (nitrate ion) molecules are needed per water molecule (0.5) to build the NAD lattice than that for NAT (0.33 nitric acid per water), the total diffusional free energy change will be greater for a NAD crystallite than for a NAT crystallite. This is true because less NAT aggregates are needed to form a crystallite than NAD aggregates are needed to form a crystallite of the critical size. And this follows from the fact that ΔG^* is lower for NAT than NAD in the NAT stability region, thus the critical nucleus size is lower.

2.6.3 *Mechanism involving SAT*

Another hypothesis that our work has shown to be incorrect is the nucleation of SAT from H_2SO_4/H_2O aerosols. The PSC mechanism that has been proposed [Luo et al., 1992] is that stratospheric H_2SO_4/H_2O aerosols freeze forming solid SAT particles. Then nitric acid and water condense on these aerosols to form an outer layer of NAT. Our experiments have shown that H_2SO_4/H_2O solutions of much larger volume do not freeze where Luo, et al. have predicted them to, and that the only possibility for freezing is for lower concentrations: ~40 to 50 wt. % H_2SO_4. However, as Zhang et al. [1993b] have shown, in this concentration range and at stratospheric temperatures H_2SO_4/H_2O aerosols take up significant amounts of HNO_3. We have shown that ternary solutions in this concentration range have a low probability to freeze. Our second conclusion is from our seeding studies (section 2.5.8) where we show that SAT crystals do not seed supercooled solutions of 1:3 HNO_3/H_2O. For these reasons we do not agree with the PSC mechanism of Luo et al.

2.7 Appendix I

Doyle [1961] expanded on Reiss's theory for binary nucleation and applied it to nucleation of liquid drops in the sulfuric acid/water system. Doyle considered the surface tension to be a function of composition, thus when taking the derivatives of 2.11 he came up with the equation:

$$\Delta\mu_1 + \frac{2\sigma V_1}{r} + 4\pi r^2 \frac{d\sigma}{dn_1^l} = 0 \qquad (2.71)$$

Equation 2.72 has been called the generalized Kelvin equation by Doyle. For two components, the resulting two equations must be solved simultaneously, and Yue [1979] reviewed various methods of solving these equations. However, Renninger et al. [1981] showed that Doyle's method was incorrect, and thus the work of binary nucleation for 20 years had been incorrect! This is a crucial point since there have been researchers after the publication of Renninger et al. who have used the work of Doyle [1961] (see Seinfeld [1986], for example!)

Wilemski [1984] reconciled the difference between Renninger et al. and Doyle's reply (Doyle, [1981]) by distinguishing between bulk and surface molecules in the droplet, as if it were a large droplet (macroscopic approximation). Wilemski [1988] has since pointed out the thermodynamic consistency or inconsistency of four different theoretical approaches to binary nucleation.

2.8 Appendix II

```
/* program to calculate the weight percents of nitric and sulfuric acid
   based on Keith's parameterization of Renyi's data of the ternary
   system: sulfuric acid/nitric acid/water.

   July 27, 1993

   Revised August 9, 1993
   */

#include "stdio.h"
#include "math.h"

main()
   {
   float a0, a1, b0, b1, b2, T, Pn, Pw, P0n, P0w, x, fy, w, dfy, fx, dfx, x1,
     Tend, step, y1, a2, b3, y, xold, Tbegin, xprev, yprev;
   int i, flag=0;
   FILE *ptr, *f1;
   char file1[15];

   clrscr();
   gotoxy(5,2);
   printf("Enter beginning temperature in Kelvin: ");
   scanf("%f", &T);
   gotoxy(5,4);
   printf("Enter ending temperature in Kelvin: ");
   scanf("%f", &Tend);
   gotoxy(5,6);
   printf("Enter the temperature step: ");
   scanf("%f", &step);
   gotoxy(5,8);
   printf("Enter the Pressure of water in ppm: ");
   scanf("%f", &Pw);
   gotoxy(5,10);
   printf("Enter the Pressure of nitric acid in ppb: ");
   scanf("%f", &Pn);
   gotoxy(5,12);
   printf("Enter the file name: ");
   scanf("%s", file1);

   clrscr();

   gotoxy(1,1);
```

```
printf("Temp");
gotoxy(10,1);
printf("[H2SO4]");
gotoxy(20,1);
printf("[HNO3]");
gotoxy(30,1);
printf("[H2O]");

fl=fopen(file1, "w");

Pw=Pw*0.750246792E-4; /* conversion from ppm to torr at 100mb */
Pn=Pn*0.750246792E-7;
Tbegin=T;

for(i=3; i<200; i++)
  {
  if (T<Tend)
       break;
  if (i>22)
       i=3;
  P0n=pow(10, 7.61628-(1486.238/(T-43)));
  P0w=0.750246792*pow(10, 8.42926609-(1827.17843/T)-(71208.271/T/T));

  a0=-0.54477+0.00809*T;
  a1=-11.41355+0.0176*T;
  a2=-0.5696+189.9/T;
  b0=-4.69823+0.01694*T;
  b1=24.96014-0.08897*T;
  b2=-32.26236+0.10842*T;
  b3=0.1187-59.74/T;

  /* First, want to take a guess at y, then solve the nitric acid
       vapor pressure equation for x, with y as a constant.
       Then, take that x value and plug it into the water vapor
       equation and solve for a new value of y & repeat the process until
       x and y converge on a single value.
       */

  y= yprev = 0.60-3*(Tbegin-T)/100; /* first guess at y */
  x= xprev = 0.001; /* first guess at x */
  gotoxy(1,i);
  printf("%4.1f", T);

  while (1)
       {
```

```
/* y a constant here */
if (x<0)
  x=0.001;
fx=-log10(Pn)+log10(x)+log10(P0n)+a0+a1*(1-x-y)-a2*(exp(pow(1-y, 8))-1);
dfx=(1/(x*log(10)))-a1;
x1=x-(fx/dfx);

if ( (x-x1>-.000001 && x-x1<0.000001) )
  {
  x=x1;
  yprev = y;
  if( flag == 1 )
    {
    flag = 0;
    }
  while (1)
    {
    /* x a constant here */
    fy=log10(1-x-y)+log10(P0w)-log10(Pw)+b0+(b1*(x+y))+
            b2*(x+y)*(x+y)-b3*(exp(pow(1-y, 8))-1);
    dfy=-(1/((1-x-y)*log(10)))+b1+2*b2*(x+y)+8*b3*pow(1-y, 7)*
            exp(pow(1-y, 8));
    y1=y-(fy/dfy);

    if ( y<0 )
        {
        flag = 2;
        break;
        }
    if( ( y-y1<0.000001) && ( y-y1>-.000001) )
        {
        flag = 1;
        xprev = x;
        }
    y = y1;
    gotoxy(10,i);
    printf("%f", y);
    if( flag == 1)
        break;
  }
}
if (kbhit())
  {
  fprintf(f1,"%4.1f %f %f %f\n", T, y*100, x1*100, (1-y-x1)*100);
  fclose(f1);
```

```
            gotoxy(5,i+1);
            printf("Press a key to continue...");
            getch();
            exit();
          }
          if (flag == 2)
            {
            fprintf(fl,"%4.1f %f %f %f\n", T, y*100, x1*100, (1-y-x1)*100);
            fclose(fl);
            gotoxy(5,i+1);
            printf("Press a key to continue...");
            getch();
            exit();
          }
          x=x1;
          gotoxy(20,i);
          printf("%f", x1);
          if( ( (xprev - x) > -.000001 ) && ( (xprev - x) < .000001 ) &&
              ( (yprev - y) > -.000001 ) && ( (yprev - y) < .000001 ) )
            break;
      }
      flag = 0;
      x=x1;
      gotoxy(30,i);
      printf("%f", 1-y-x1);
      fprintf(fl,"%4.1f %f %f %f\n", T, y*100, x1*100, (1-y-x1)*100);
      T=T-step;
    }
    fclose(fl);
    gotoxy(5,i+1);
    printf("Press a key to continue...");
    getch();
}
```

Chapter III

Study of the Sorption of HCl onto the Surfaces of Ice

3.1 HCl Solution Freezing Experiments

3.1.1 Introduction:

The purpose of this experiment was to quantitatively determine the amount of HCl incorporated into the bulk of small particles of ice. These experiments were intended to be a refinement of those carried out previously [Wofsy et al., 1988] where it had been determined that HCl did incorporate into the bulk of ice, and that the amount of HCl that could be incorporated into ice is on the order of 30 % of the ice volume. However, the experiments described here showed that HCl is not taken up into the bulk of ice, but rather is restricted to sorption into the surface layers of ice. The experimental method is similar to that given in the reference and will be presented in the next section with deviations from the previous method.

3.1.2 *Experimental:*

Partitioning of HCl between liquid and solid was studied by freezing solutions with HCl concentrations corresponding to mole fractions between 0.03 and 0.13. The solutions were placed in an ethanol bath which was cooled by a liquid nitrogen reservoir conducting heat away from the bath (see Figure 3.1). In experiments 1-8, the temperature of the bath was placed at 10 degrees C below the determined freezing point of the solution. This was done because a "rolling effect" is observed upon freezing of these solutions according to Figure 3.2. Since HCl is not wholly incorporated into ice (as we conclude later), as ice begins to form, only a small amount of the HCl in the liquid is incorporated into the ice when the liquid freezes (on order of 1%). Therefore as ice forms, the remaining liquid becomes more concentrated in HCl, hence the solution concentration moves to the right in Figure 3.2. The solution is thereby "rolling" down the

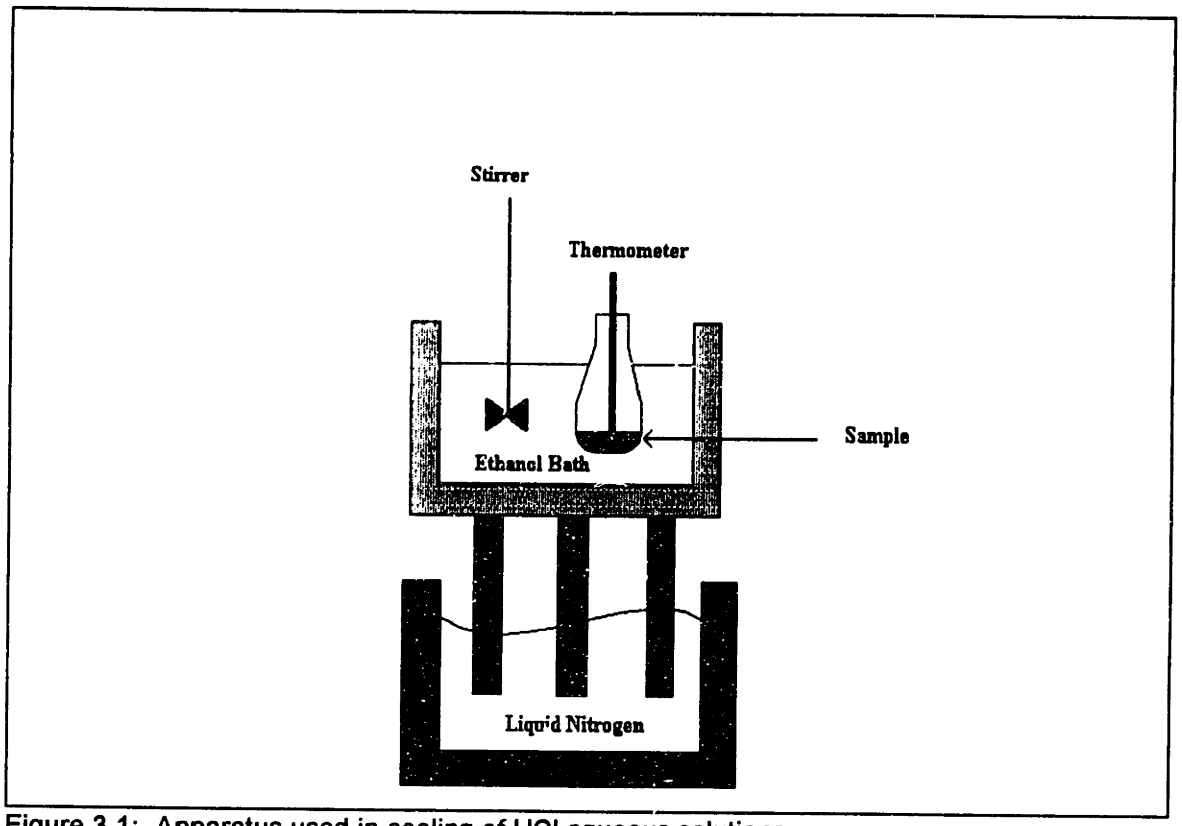

Figure 3.1: Apparatus used in cooling of HCl aqueous solutions.

temperature/concentration curve. This method was used to establish an equilibrium between the liquid and solid phases at some given temperature where the concentration of the liquid can be known. In experiments 9-14 the bath temperature was set at three degrees C below the initial freezing point in order to make ice that had a higher surface/volume ratio. This was done because our postulate was that HCl is incorporated only into the surface layers of ice. Therefore, the highest amount of HCl per volume would be observed if the ice particles had high surface/volume ratios. The solutions were then allowed to freeze slowly as mentioned above. In all of the experiments, the solutions were kept at the respective temperatures for about one hour Large changes in the solution concentration were avoided by allowing only a small fraction of the solution to freeze (this was confirmed by titrating some of the remaining liquid). The crystals were recovered by filtration and dried as best as possible by compressing the crystals while using suction filtration. The filtered ice was then melted, the resulting solution diluted, and the

Table 3.1

Data from HCl solution freezing experiments

Experiment # 1

Solution	Dye Conc	Fluorescence	Ratio (b)	Fluoresc #2	Ratio (r)	Molarity	Density	Mole Fraction
Ice		114	0.3891	121	0.3763	2.37	1.0391	0.04478294
Stock	0.04	117		128		5.45	1.089	0.11021543
1:50	0.02	62		69				
3:50	0.06	176		203				
						Ice/Stock mole fraction ratio		0.40632182
Partition			0.0281909		0.04813504			

Experiment #

Solution	Dye Conc	Fluorescence	Ratio (b)	Fluoresc #2	Ratio (r)	Molarity	Density	Mole Fraction
Ice		720	0.6509	783	0.6434	1.18	1.0191	0.02176163
Stock	0.04	462		491		1.76	1.0293	0.03282697
3:50	0.06	664		724				
4:50	0.08	884		996				
						Ice/Stock mole fraction ratio		0.66291903
Partition			0.03442862		0.05473649			

Experiment # 3

Solution	Dye Conc	Fluorescence	Ratio (b)	Fluoresc #2	Ratio (r)	Molarity	Density	Mole Fraction
Ice		1313	0.6233	1385	0.6288	1.78	1.0292	0.03322859
Stock	0.04	911		1012		3.02	1.0501	0.05783779
3:50	0.06	1271		1040				
4:50	0.08			1664				
						Ice/Stock mole fraction ratio		0.57451346
Partition			-0.1295103		-0.1462461			

Experiment # 4

Solution	Dye Conc	Fluorescence	Ratio (b)	Fluoresc #2	Ratio (r)	Molarity	Density	Mole Fraction
Ice		960	0.5439	993	0.5643	3.28	1.0544	0.063166
Stock	0.04	652		648		5.86	1.0956	0.11963117
3:50	0.06	1080		1068				
4:50	0.08	1291		1025				
						Ice/Stock mole fraction ratio		0.52800623
Partition			-0.0348471		-0.0832999			

Table 3.1 continued

Experiment # 5

Solution	Dye Conc	Fluorescence	Ratio (b)	Fluoresc #2	Ratio (r)	Molarity	Density	Mole Fraction
Ice		1219	0.4065	1137	0.3896	2.57	1.0426	0.04875658
Stock	0.04	1201		1162		5.97	1.0973	0.12219765
1:50	0.02	665		685				
3:50	0.06	1756		1684				
						Ice/Stock mole fraction ratio		0.3989977
Partition			-0.0126408		0.01539598			

Experiment # 6

Solution	Dye Conc	Fluorescence	Ratio (b)	Fluoresc #2	Ratio (r)	Molarity	Density	Mole Fraction
Ice		1117	0.3687	1070	0.3614	2.17	1.036	0.04082379
Stock	0.04	1201		1162		5.97	1.0973	0.12219765
1:50	0.02	665		685				
3:50	0.06	1756		1684				
						Ice/Stock mole fraction ratio		0.33408002
Partition			-0.0548392		-0.0427811			

Experiment # 7

Solution	Dye Conc	Fluorescence	Ratio (b)	Fluoresc #2	Ratio (r)	Molarity	Density	Mole Fraction
Ice		1128	0.3728	1251	0.4341	2.3	1.0436	0.04314073
Stock	0.04	1201		1162		5.97	1.0973	0.12219765
1:50	0.02	665		685				
3:50	0.06	1756		1684				
						Ice/Stock mole fraction ratio		0.35304058
Partition			-0.0315042		-0.1432398			

Experiment # 8

Solution	Dye Conc	Fluorescence	Ratio (b)	Fluoresc #2	Ratio (r)	Molarity	Density	Mole Fraction
Ice		1246	0.4168	1389	0.487	2.67	1.0442	0.05076341
Stock	0.04	1201		1162		5.97	1.0973	0.12219765
1:50	0.02	665		685				
3:50	0.06	1756		1684				
						Ice/Stock mole fraction ratio		0.41542048
Partition			-0.0023654		-0.1395312			

Table 3.1 continued

Experiment # 9

Solution	Dye Conc	Fluorescence	Ratio (b)	Fluoresc #2	Ratio (r)	Molarity	Density	Mole Fraction
Ice		1002	0.3257	980	0.3237	1.74	1.0286	0.03245293
Stock	0.04	1201		1162		5.97	1.0973	0.12219765
1:50	0.02	665		685				
3:50	0.06	1756		1684				
						Ice/Stock mole fraction ratio		0.26557739
Partition			-0.089163		-0.0859421			

Experiments from here down, the ice was made by cooling only to 2-3 degrees below the freezing point

Experiment # 10

Solution	Dye Conc	Fluorescence	Ratio (b)	Fluoresc #2	Ratio (r)	Molarity	Density	Mole Fraction
Ice		677	0.2049	627	0.1757	1.38	1.0223	0.0255574
Stock	0.04	1201		1162		5.97	1.0973	0.12219765
1:50	0.02	665		685				
3:50	0.06	1756		1684				
						Ice/Stock mole fraction ratio		0.20914802
Partition			0.00534275		0.04057749			

Experiment # 11

Solution	Dye Conc	Fluorescence	Ratio (b)	Fluoresc #2	Ratio (r)	Molarity	Density	Mole Fraction
Ice		116	0.2535	114	0.237	1.67	1.0275	0.03110047
Stock	0.04	307		312		5.85	1.0954	0.11940468
1:100	0.01	93		99				
2:100	0.02	179		180				
3:100	0.03	249		240				
6:100	0.06	410		397				
						Ice/Stock mole fraction ratio		0.26046271
Partition			0.00932714		0.03075061			

Table 3.1 continued

Experiment # 12

Solution	Dye Conc	Fluorescence	Ratio (b)	Fluoresc #2	Ratio (r)	Molarity	Density	Mole Fraction
Ice		78	0.2064	74	0.1728	1.31	1.0211	0.02422723
Stock	0.04	307		312		5.85	1.0954	0.11940468
1:100	0.01	93		99				
2:100	0.02	179		180				
3:100	0.03	249		240				
6:100	0.06	410		397				
						Ice/Stock mole fraction ratio		0.20290018
Partition			-0.0044101		0.03638803			

Experiment # 13

Solution	Dye Conc	Fluorescence	Ratio (b)	Fluoresc #2	Ratio (r)	Molarity	Density	Mole Fraction
Ice		312	0.4097	375	0.5482	2.65	1.0438	0.0503656
Stock	0.04	307		312		5.85	1.0954	0.11940468
1:100	0.01	93		99				
2:100	0.02	179		180				
3:100	0.03	249		240				
6:100	0.06	410		397				
						Ice/Stock mole fraction ratio		0.42180592
Partition			0.02050807		-0.2797567			

Experiment # 14

Solution	Dye Conc	Fluorescence	Ratio (b)	Fluoresc #2	Ratio (r)	Molarity	Density	Mole Fraction
Ice		210	0.2443	238	0.2259	1.636	1.0269	0.03044709
Stock	0.04	307		312		5.85	1.0954	0.11940468
1:100	0.01	93		99				
2:100	0.02	179		180				
3:100	0.03	249		240				
6:100	0.06	410		397				
						Ice/Stock mole fraction ratio		0.25499077
Partition			0.01414685		0.03758012			

Table 3.1 continued

Experiment # 15

Solution	Dye Conc	Fluorescence	Ratio (b)	Fluoresc #2	Ratio (r)	Molarity	Density	Mole Fraction
Ice		246	0.2019	262	0.1911	1.052	1.0168	0.01935401
Stock	0.04	456		523		4.857	1.0796	0.09689029
1:100	0.01	129		160				
2:100	0.02	244		272				
3:100	0.03	345		401				
6:100	0.06	664		770				
						Ice/Stock mole fraction ratio		0.19975178
Partition			-0.0026917		0.01069573			

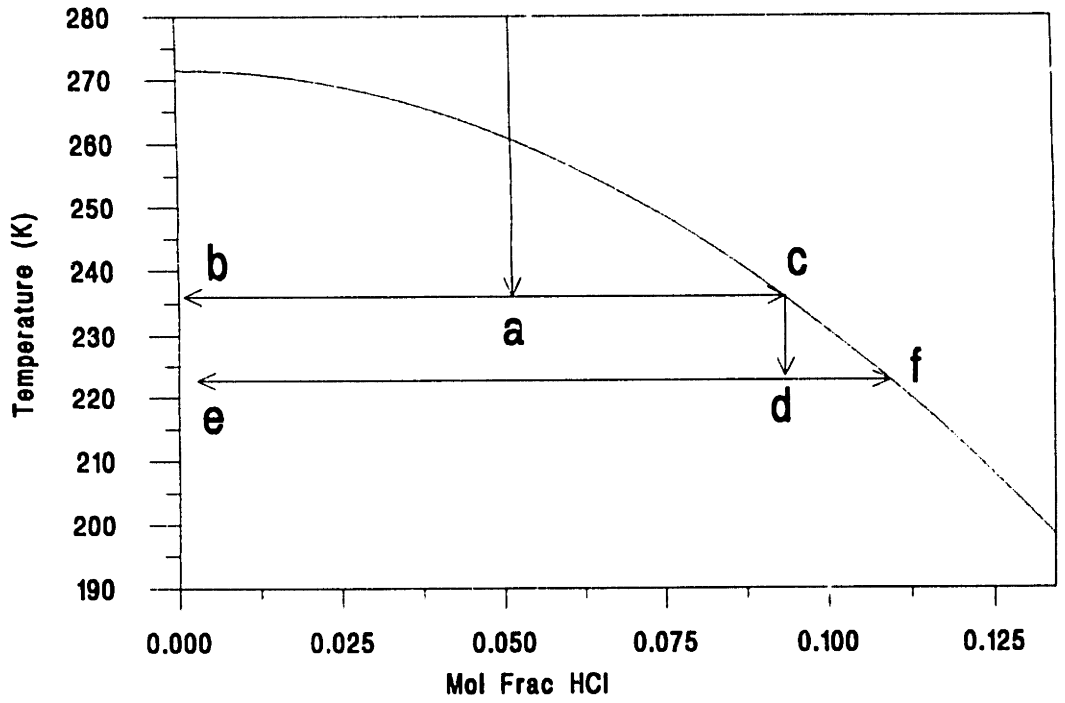

Figure 3.2: Illustration of the freezing of a typical solution of HCl: Upon cooling to point (a) the solution crosses the liquid/solid equilibrium line. At point (a) nucleation of the ice phase occurs. Ice forms with a concentration of HCl corresponding to point (b). The resulting solution has a concentration corresponding to point (c). Upon further cooling, more ice is formed at point (d). This ice has an HCl concentration corresponding to point (e) with the resulting solution having a concentration corresponding to point (f). This process continues with cooling in infinitesimally small steps.

concentration of HCl determined by titration with NaOH. The data for these experiments is recorded in Table 3.1.

Since it was impossible to remove all of the liquid from the filtered ice by any method, a correction needed to be used to take into account the HCl contribution to the melted ice by the liquid that remained "stuck" to the ice, yet still in liquid form. In the experiments performed by Wofsy et al., the filtered crystals were washed with an alcohol and a dye was added to the alcohol to check for contamination of the crystals. An alternative method was used in the experiments reported here. The dye Rhodamine B was added to the HCl solution initially, before it was frozen. The theory is that the dye is a

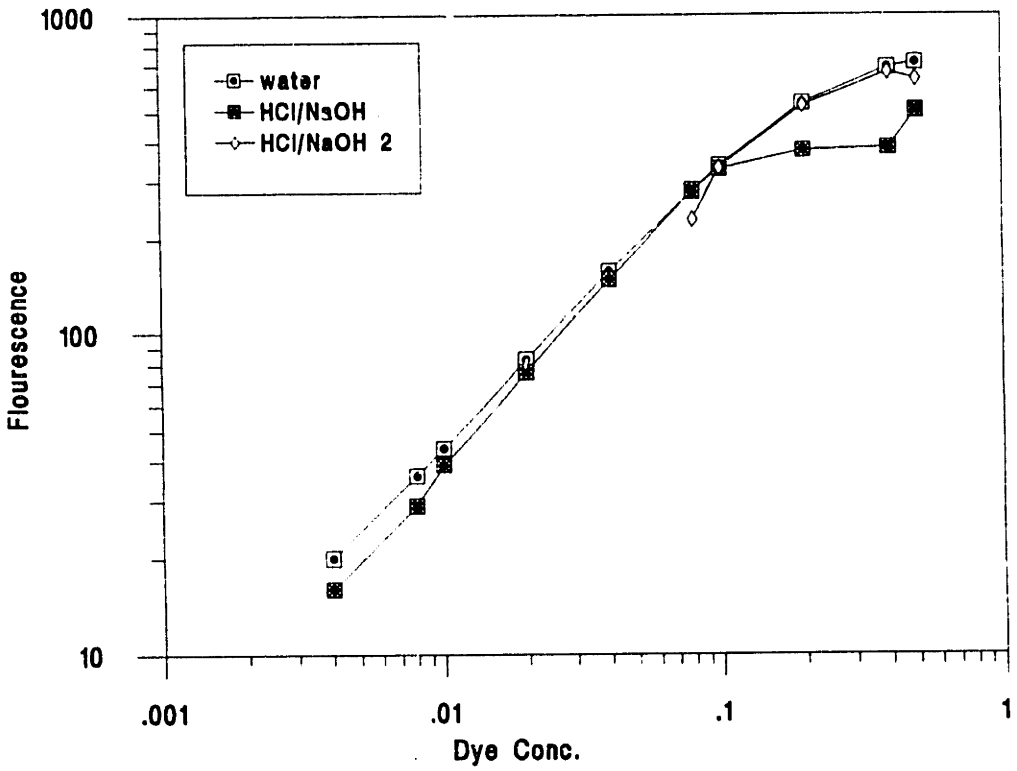

Figure 3.3: Plot of fluorescence of dye in water and in an HCl solution that was neutralized with NaOH.

sufficiently large molecule so that it will not be incorporated into the ice, but will only stay in the liquid phase for a sufficiently slow freezing process. Rhodamine B is a fluorescent dye, therefore the fluorescence of the melted ice solutions were determined, as well as the fluorescence of the starting solution that was frozen (which shall hereafter be referred to as the stock solution). Then, based on the fluorescence of the melted ice mixture and that of the stock solution, a correction can be made for the amount of stock liquid that remained on the ice even after filtration. Unfortunately the use of the dye as a tracer was not as simple as explained above. It was determined that the fluorescence of Rhodamine B is destroyed in concentrated acid. However, whatever reaction occurs, it is mostly reversible. Upon neutralization of the acid solution the fluorescent nature of Rhodamine B returns, although the intensity of fluorescence is diminished (Fig. 3.3). To remedy this problem, the HCl solutions (stock and ice melt) were neutralized and then buffered with a

pH 8.5 buffer before fluorescence readings were taken.

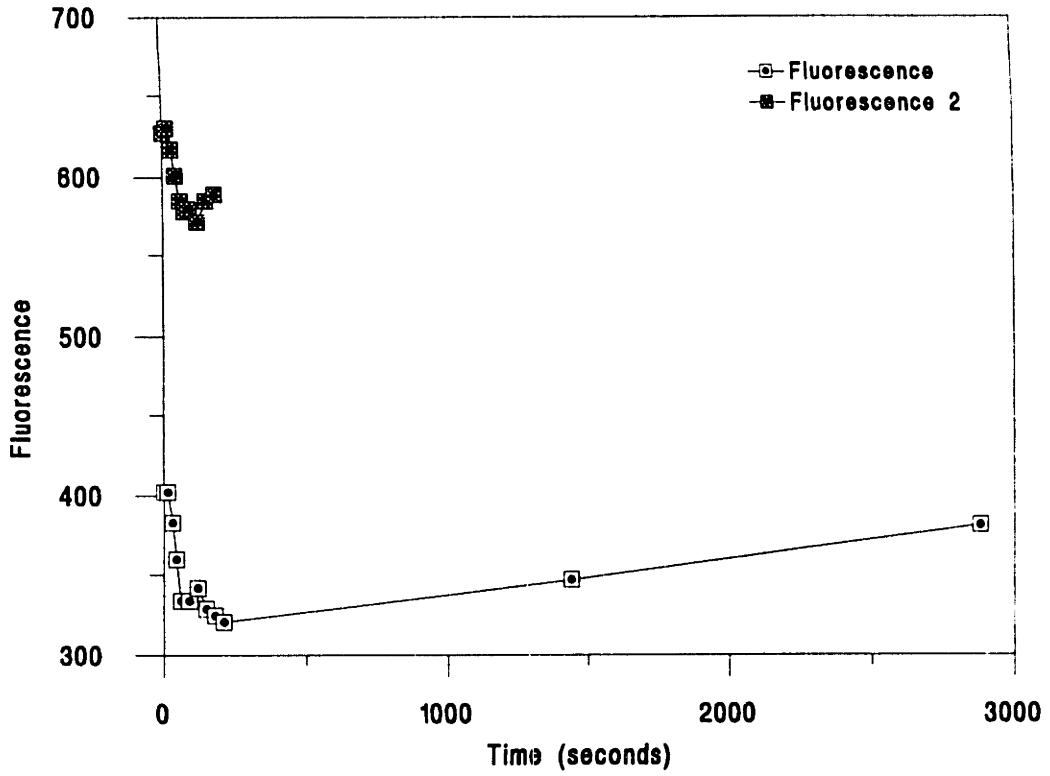

Figure 3.4: Plot of fluorescence of dye in a solution of HCl versus time. Note that the change in fluorescence was quite rapid in the first few hundred seconds, but became slower at longer times.

The fluorescence of Rhodamine B was found to be dependent on the amount of time the dye was in the concentrated HCl solutions (Fig. 3.4). In this case the first hour of dye contact with concentrated HCl seemed to be the most crucial. Fluorescence in this time region dropped about one fourth in an hour. The data plotted in Figure 3.4 resulted from an experiment where a solution of HCl and dye were made and the time noted. At specific time intervals an aliquot of the solution was removed, neutralized and diluted to a specific volume. The fluorescence was then measured with a Sequoia-Turner Series 450 Fluorometer. The problem of the dye fluorescence being time dependent was resolved by preparing the HCl solutions with dye the day pervious to using the solution in a freezing experiment. Therefore we would be in the relatively flat region of the time vs.

fluorescence plot, though the fluorescence was still changing with time thereby enhancing the experimental error.

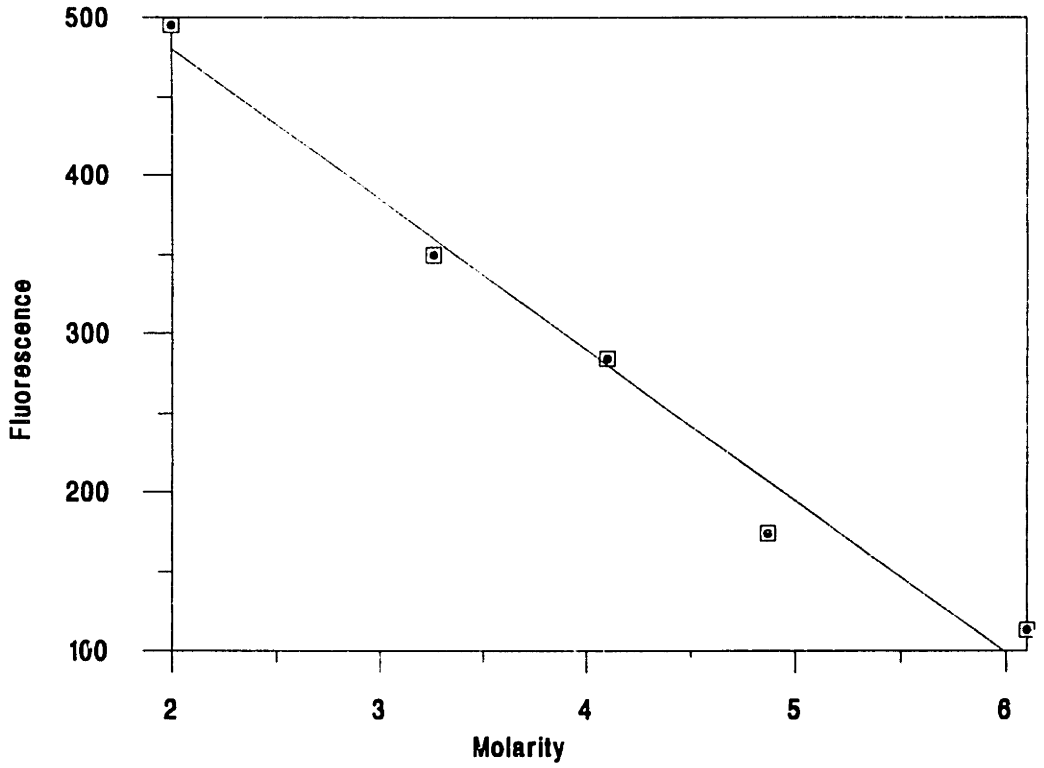

Figure 3.5: Plot of fluorescence of dye versus the molarity of HCl in solution (keeping the dye concentration constant). The line is a linear fit of the data.

It was also found that the fluorescence of a solution is dependent on the concentration of HCl (Fig. 3.5). The data for the plot in Figure 3.5 were obtained by keeping the concentration of dye the same, but varying the HCl concentration in various solutions. This problem was addressed by taking aliquots of the stock solution and diluting them to concentrations of dye that fall very near the dye concentrations of the ice melt solution. The ice melt solution was thereby "bracketed" on each side by a diluted stock solution (in regard to fluorescence readings). Linearity was assumed between the bracketing points, and then the dye concentration of the ice melt solution determined from this (see Figure 3.6 as an example, which uses the data from experiment #1). The dye concentration of the ice melt is directly related to the ratio of the ice/liquid in the ice melt

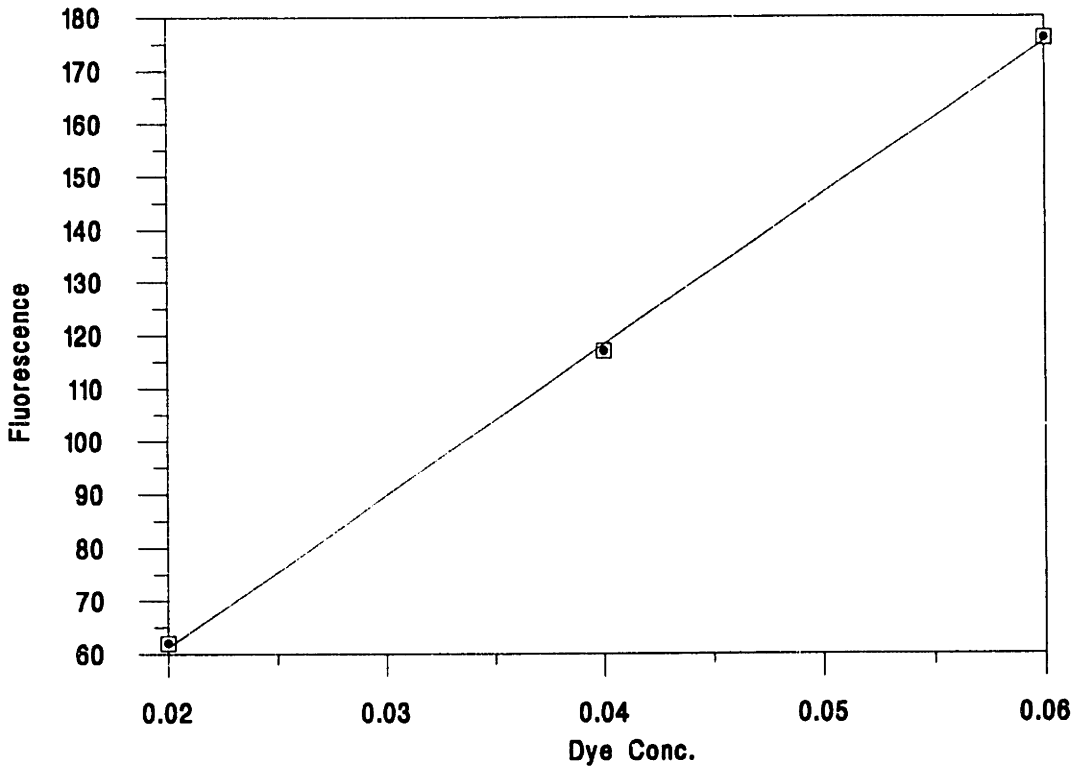

Figure 3.6: Illustration of the linear bracketing technique used to determine the amount of dye in the ice melt solutions. The line is a linear fit of the data.

given that the concentration of dye in the stock solution is set equal to one. In other words, the concentration of dye in the stock solution is conveniently set equal to one (in arbitrary units). Then the ice melt must logically contain some concentration of dye less than one since the dye is not incorporated into the ice. So the dye is only in the liquid portion of the ice melt. Therefore the fraction of the stock dye concentration that is in the ice melt is the fraction of liquid in the ice melt, as compared to the total volume of the ice melt. This ratio is then compared to the ratio of mole fractions of HCl in the ice melt and stock solutions via a derived formula: $z = \frac{B-b}{1-b}$ where: $B = \frac{\text{[HCl] in melt}}{\text{[HCl] in stock}}$ and $b = \frac{\text{fluorescence of stock}}{\text{fluorescence of melt}}$. The result of this equation gives the partitioning of the HCl from solution into the ice (z). The derivation of z is given in the Appendix (section 3.3).

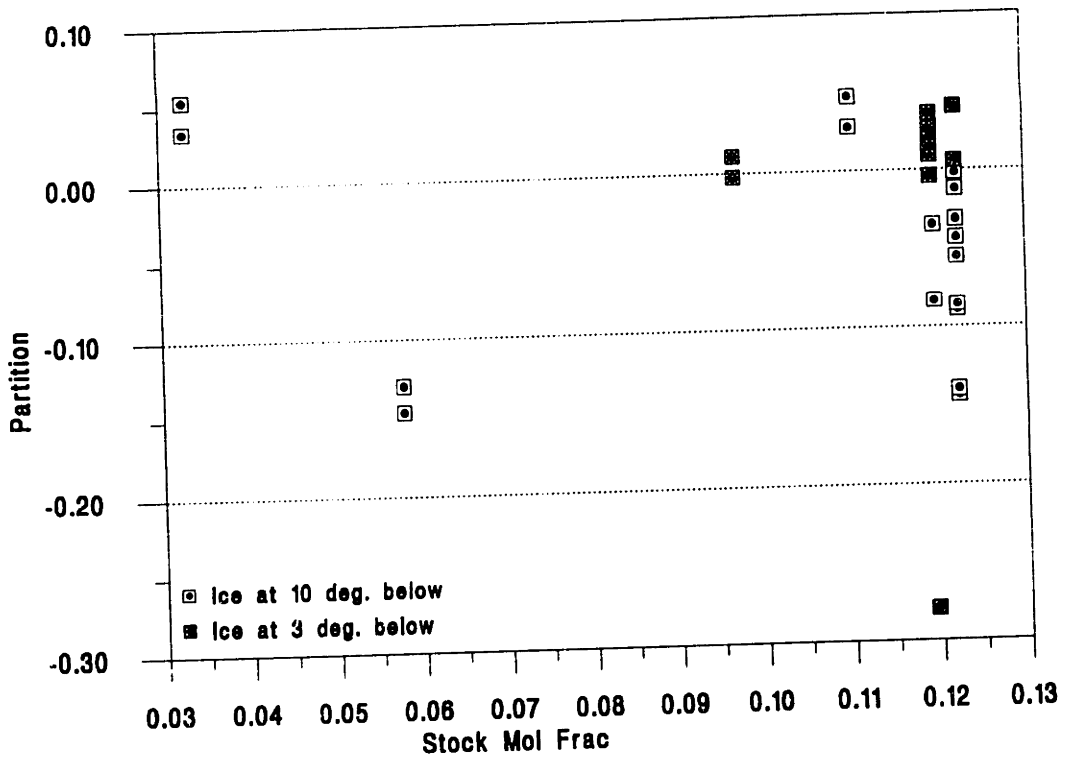

Figure 3.7: Plot of partition (z) versus the mole fraction of HCl in the stock solution used in the experiment.

One final change was made in experiment #14. The stock solution that was cooled was stirred vigorously in the cooling bath for approximately one hour. The purpose of this was to induce the growth of only small particles, specifically those of high surface area/low volume. The crystals appeared different visually, however the results were similar to the other experiments.

3.1.3 *Results:*

Figure 3.7 shows the calculated partition vs. the mole fraction of HCl in the stock solution. Figure 3.8 plots the calculated partition vs. the mole fraction ratio of the HCl in the ice melt over the HCl in the stock solution. Special note should be taken that the data are much better grouped for the experiments where the ice was formed three degrees below the initial freezing point. The results show that HCl is not incorporated into the bulk of the ice as had been previously reported [Wofsy et al., 1988]. Our conclusions are

in agreement with other laboratory studies [Wolff et al., 1989; Hanson and Mauersberger, 1988, 1990] and with a recent review of the earlier HCl-ice solubility literature [Elliot et al., 1990]. We found the concentration of HCl in the melted ice (with the correction from the fluorescence measurements) is much lower than that of the solution the ice was made from. Approximately 5% of the HCl in solution remained mixed with the ice; at most 1-2% cold have been incorporated into the ice matrix. The scatter of the results in Figure 3.8 is relatively small, hovering around +0.05/-0.1. To determine the partition with better accuracy will require a better technique.

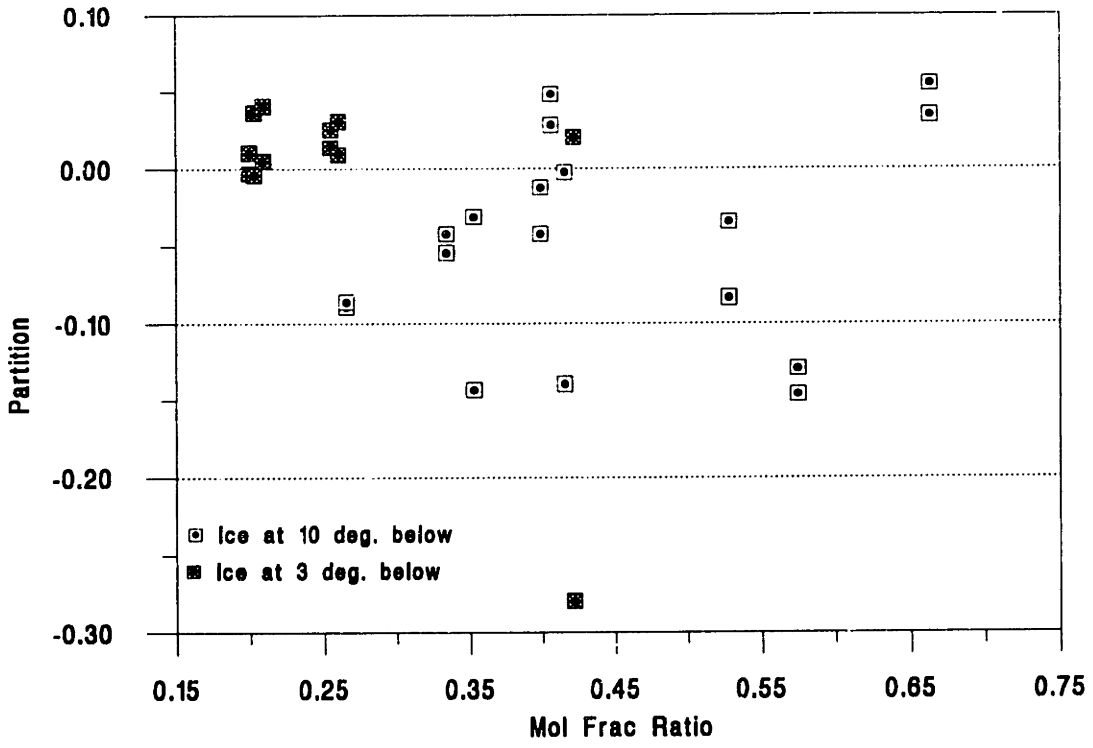

Figure 3.8: Plot of partition (z) versus the mole fraction ratio of HCl (*B*).

3.2 Uptake of Gas Phase HCl on Ice Films

3.2.1 *Introduction*

The goal of these experiments was to show that HCl uptake on ice occurs through forming a liquidous layer. We were also interested in disproving the theory that HCl

uptake on ice is simply physical adsorption (as proposed by Elliot, et al., [1991], and Tabazadeh and Turco, [1992], among others.)

3.2.2 *Experimental*

The apparatus for this experiment is shown in Figure 3.9. Ice films were made at four temperatures, 195 K, 178 K, 143 K and 113 K, and a plot of each run (two runs at 113K) is shown in Figures 3.10 - 3.14. In each case a sample of deionized water was measured out and then deposited by vapor deposition onto the walls of a small, cooled glass cell. An amount of HCl was measured out to correspond to a 1% by weight concentration of HCl in the ice film. The HCl gas was then expanded over the ice film and the total pressure of the system monitored. In each case a "background" experiment was

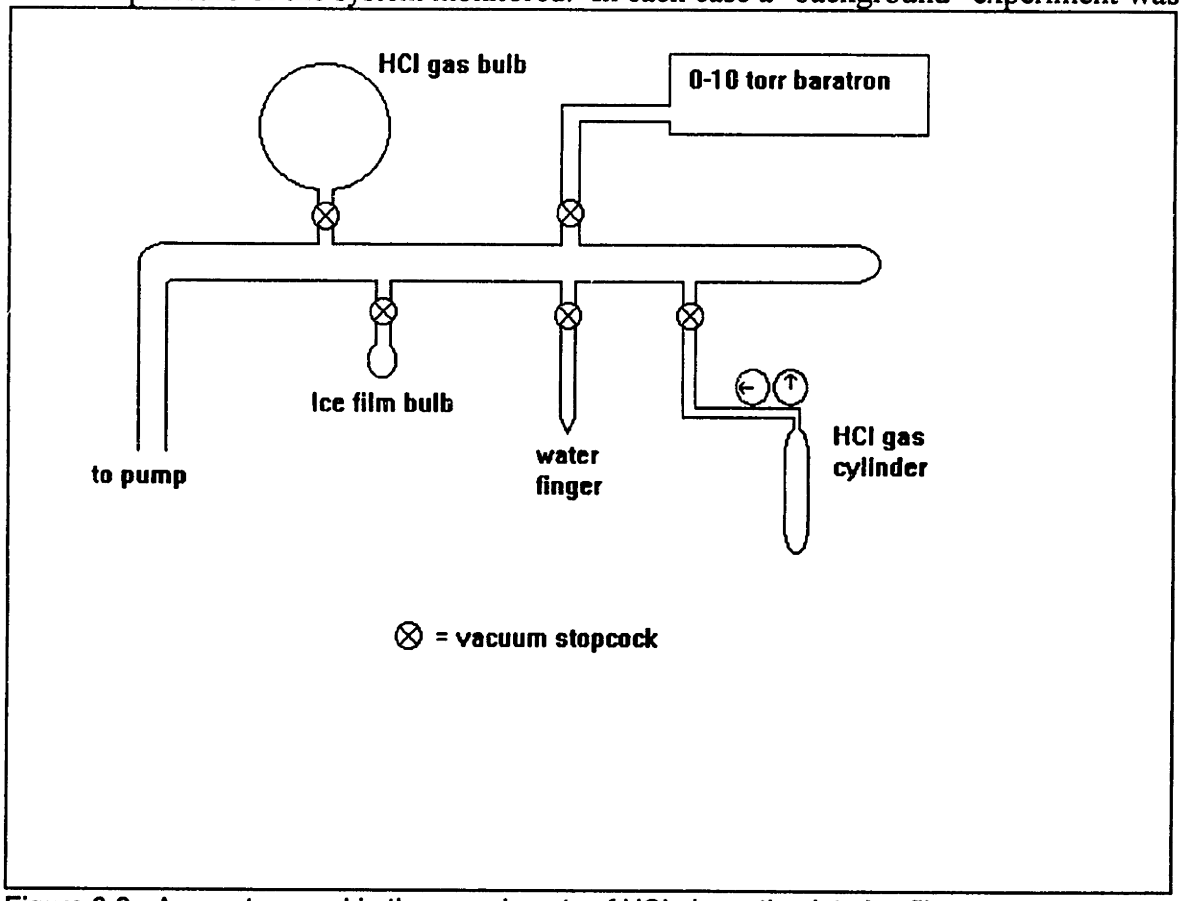

Figure 3.9: Apparatus used in the experiments of HCl absorption into ice films.

performed using identical conditions for the runs with ice in the cell, except no ice was deposited. This was to check that I was not seeing any condensation of the HCl, or that I was not getting a significant loss due to HCl adsorption onto the glass. The runs at 113K

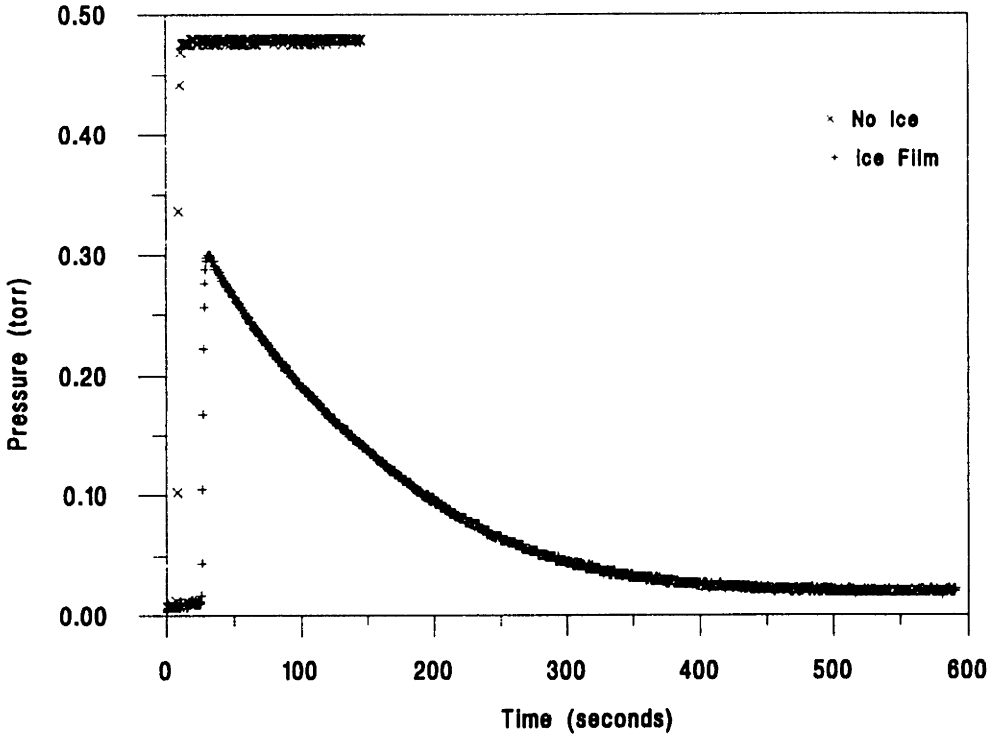

Figure 3.10: Plot of HCl uptake versus time for a temperature of 195 K.

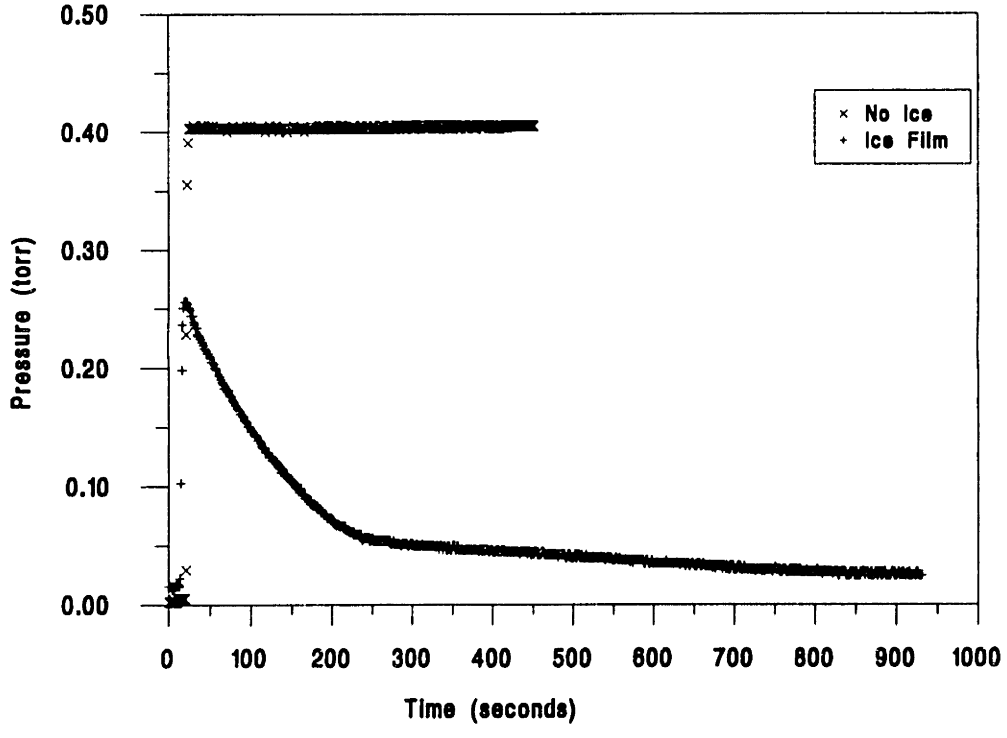

Figure 3.11: Plot of HCl uptake versus time for a temperature of 178 K.

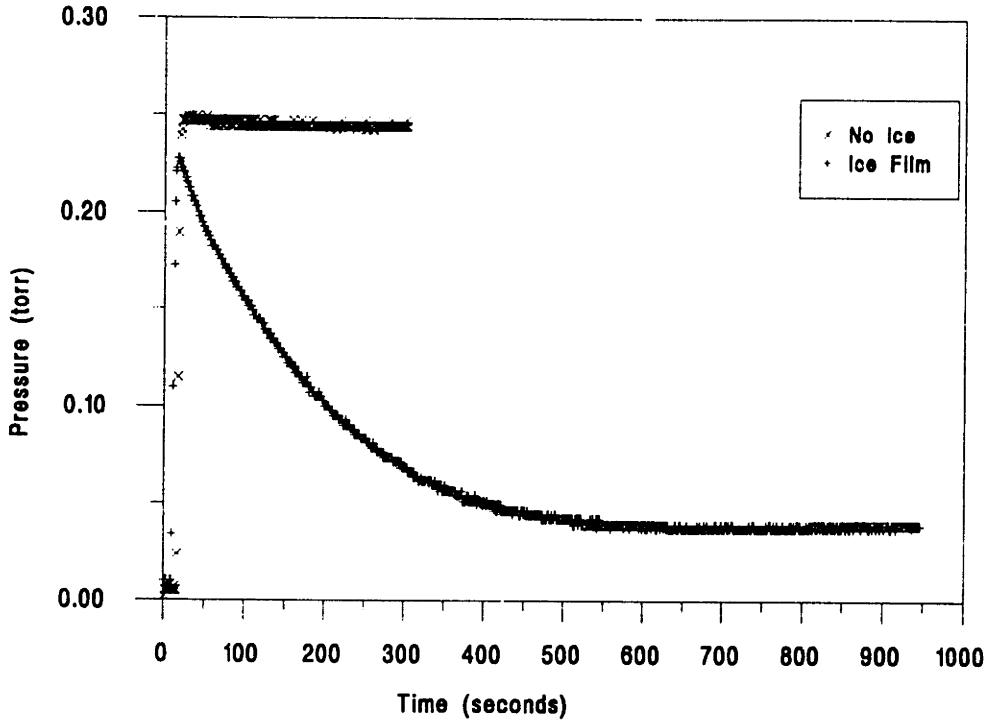

Figure 3.12: Plot of HCl uptake versus time for a temperature of 143 K.

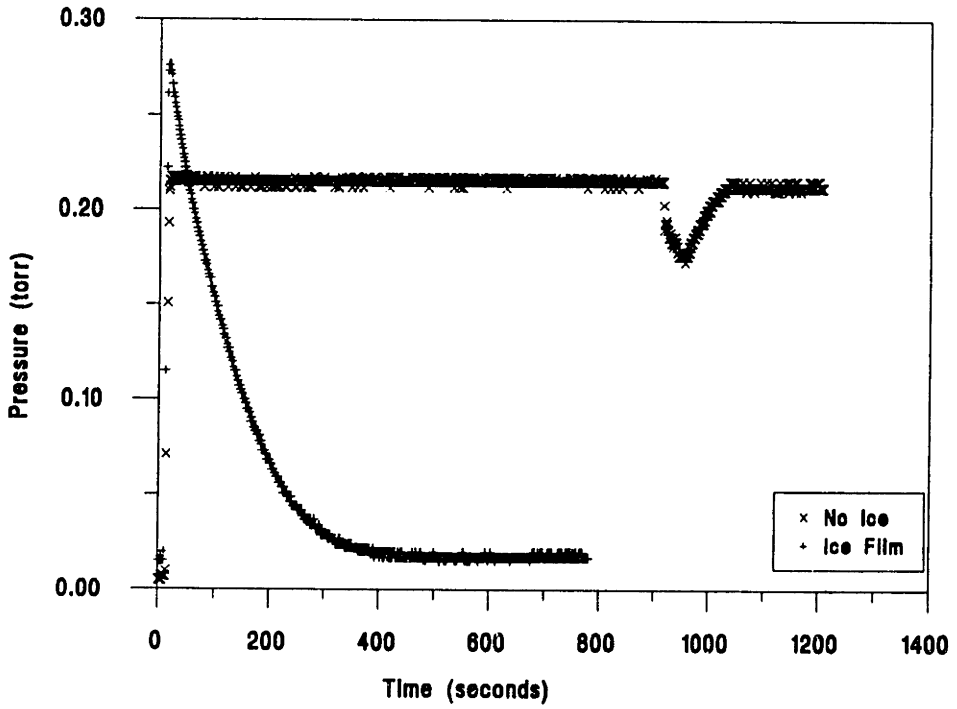

Figure 3.13: Plot of HCl uptake versus time for a temperature of 113 K. (The dip in the data for the run with no ice corresponds to liquid nitrogen being added to the cooling bath.)

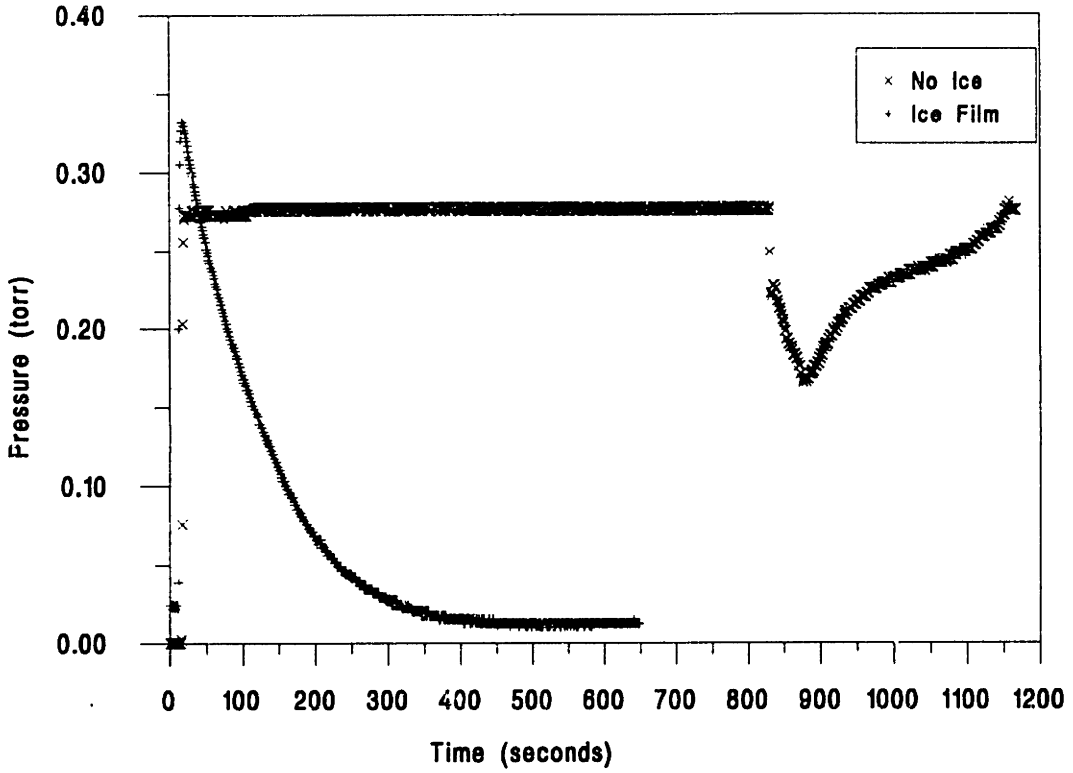

Figure 3.14: Plot of HCl uptake versus time for a temperature of 113 K (run 2). (The dip in the data for the run with no ice corresponds to liquid nitrogen being added to the cooling bath.)

were very close to the condensation point for HCl at the pressure used. The dip in the data for the cell with no ice film was caused by adding liquid nitrogen to the bath (liquid nitrogen / isopentane).

3.2.3 *Results*

As, expected, in each case with no ice film, no drop in pressure was observed. In the runs performed with an ice film, a systematic trend was seen for the three highest temperatures. As the temperature decreased, less total uptake was seen, and the time to asymptotically reach an equilibrium temperature increased. This is best illustrated in Figure 3.15 where -log(slope) vs. 1/T is plotted (an Arrhenius plot, where the slope is the initial rate of decrease in pressure over time for each run). For an uptake of HCl on ice explained by kinetic effects, we expect an Arrhenius behavior; however, for physical

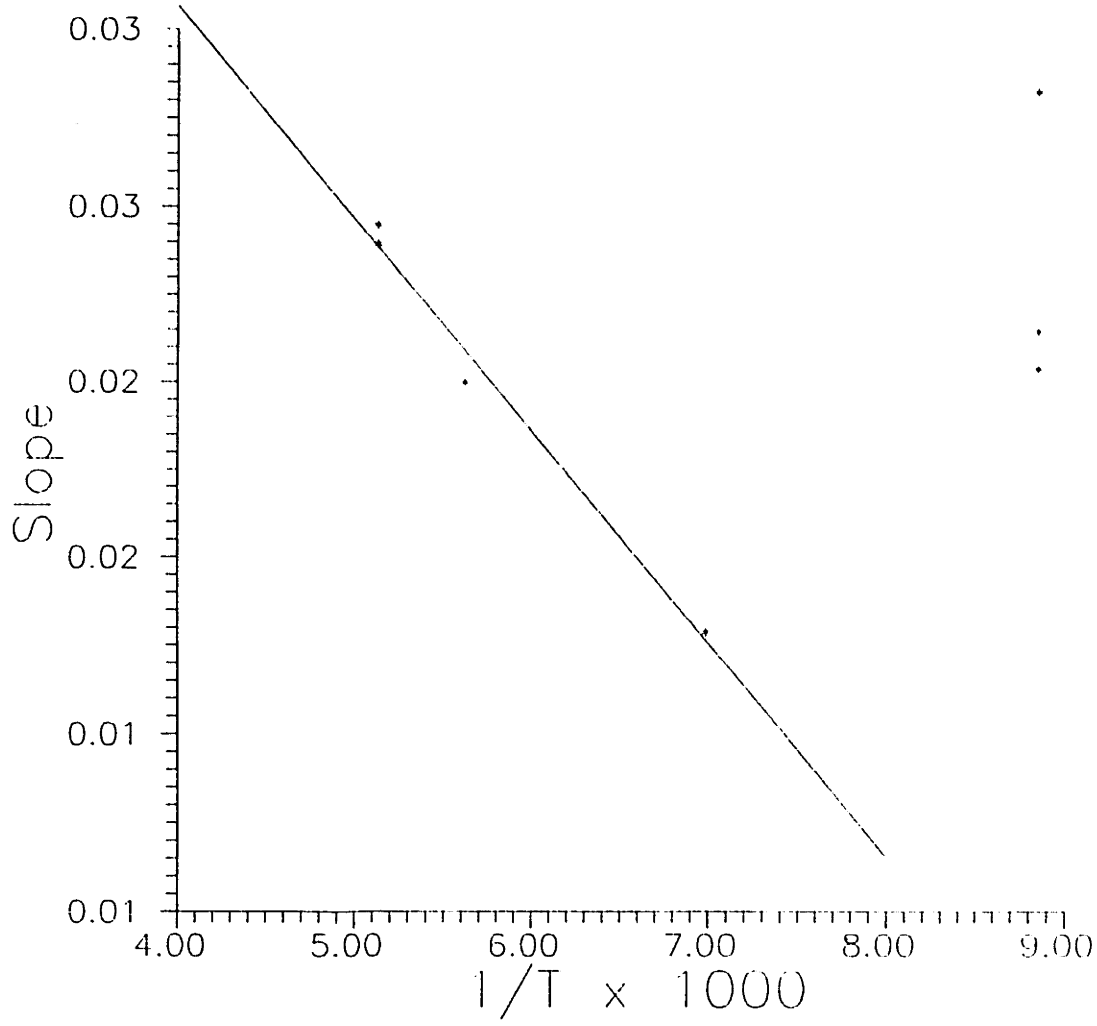

Figure 3.15: Plot of -log(slope) (of initial HCl uptake rate) vs. 1/T. The line is a linear fit of the data at the three highest temperatures.

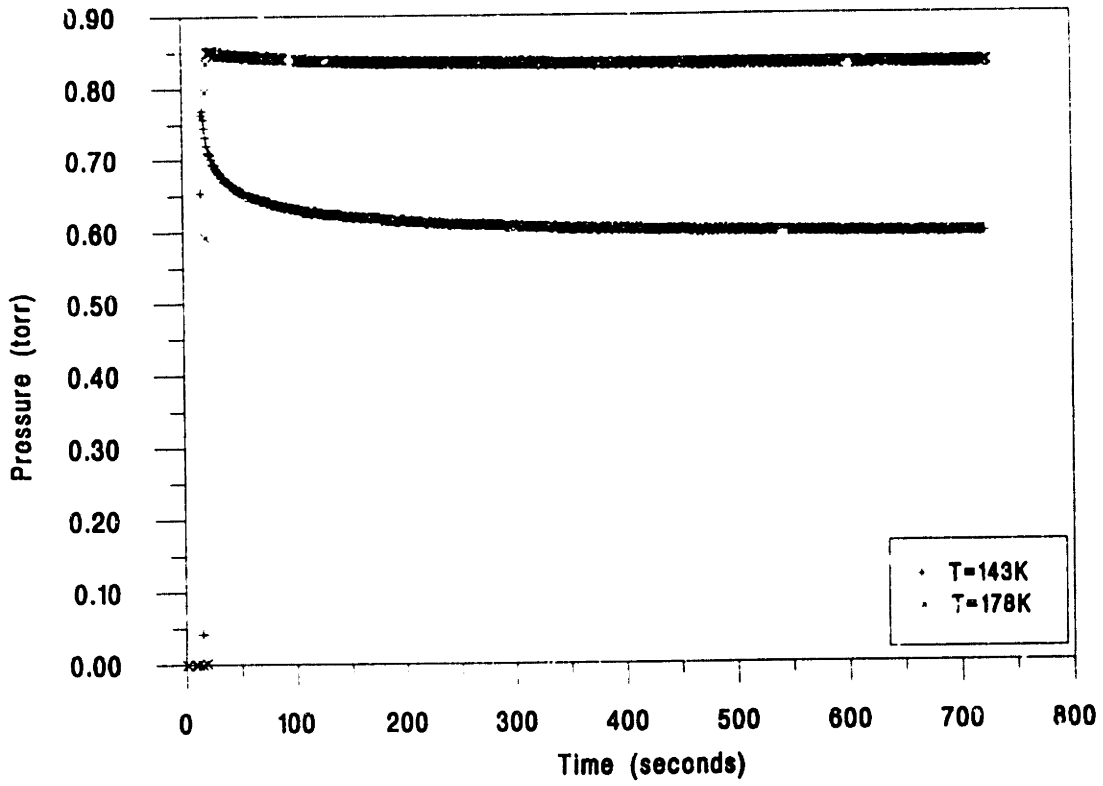

Figure 3.16: Plot of HCl uptake versus time for cell with glass beads (details in Table 2) for temperatures of 143 and 178 K.

adsorption, one would not expect Arrhenius behavior. From Figure 3.15, one can see that the three highest temperatures follow Arrhenius behavior very well. However, the run at 113K does not. It is possible that at the three higher temperatures, the uptake of HCl by the ice films is due to the formation of a liquidous layer, while at 113K the process is due to physical adsorption. The explanation why the three higher temperatures can not be due to adsorption is that if adsorption were the process, then one would see an increase in the rate and amount of uptake with a decrease in temperature. In fact, the opposite is seen (excepting the experiment at 113K where the rate of uptake increases). Why there is a threshold change into a new process at this low temperature is not immediately clear. A temperature of 113K may be so low (below the glass transition) that no liquidous layer can thermodynamically form. If one assumes that both physical adsorption and the formation of a liquidous layer are competing processes at all temperatures, then the

Table 3.2

Summary of data for HCl adsorption onto glass beads experiment.

10 ml of glass beads weighs: 14.9330 g	Density of glass: 1.4933 g/ml
Weight of glass beads used: 37.8776 g	Volume of glass beads used: 25.3650 ml
Average radius of glass beads: 0.0143 cm	Volume of glass bead: 1.231×10^{-5} cm
Number of beads used: 2061018.8	Total surface area of beads: 5312.034 cm^2
Monolayer coverage of glass beads by HCl: 1×10^{15} molec/cm^2	Total number of molecules needed for a monolayer coverage of the glass beads: 5.31×10^{18}
Volume of bulb and system: 1.3188 liters	

T = 143 K	T = 178 K
HCl molecules before expansion: 4.01×10^{19}	HCl molecules before expansion: 3.87×10^{19}
HCl molecules after expansion: 2.60×10^{19}	HCl molecules after expansion: 3.62×10^{19}
HCl molecules adsorbed: 1.41×10^{19}	HCl molecules adsorbed: 2.54×10^{18}
Number of monolayers on glass beads: 2.65	Number of monolayers on glass beads: 0.478

liquidous layer dominates at higher temperatures while physical adsorption takes over at the very lowest temperatures. Such a process would show a smooth transition between the two regimes. One would need more data at low temperatures to discern this. Also of note, the pressure of HCl used at 113 K was very close to the condensation pressure, therefore, condensation of some of the HCl may have also taken place.

To see the extent of adsorption that would occur at various temperatures, identical experiments to the ice films were performed, except glass beads were used in place of ice. The data for these experiments are given in Figure 3.16, and in Table 3.2. Clearly, as indicated from the data, more adsorption occurs at the lower temperature. Therefore, adding the glass beads increases the adsorption (above that which occurred without ice or glass beads, having, then just the glass wall of the container), however, this is due to a massive increase in the surface area. Of course, this assumes that adsorption onto glass is similar to adsorption onto ice.

3.3 Appendix

The following is the derivation of the equation used to calculate the partition of HCl between the liquid and the solid.

Symbols	Subscripts
V: volume of liquid	s: stock HCl solution (solution that was frozen)
D: dye concentration	i: ice
A: HCl concentration	l: liquid sticking to ice
F: fluorescence signal (from the dye)	m: mixture solution (ice + liquid)
B: HCl concentration ratio $= \frac{A_m}{A_s}$	
b: dye concentration ratio $= \frac{D_m}{D_s}$	
z: partition coefficient $= \frac{A_i}{A_l} \approx \frac{A_i}{A_s}$	

Assumptions:

$D_l=D_S$: (when freezing, dye does not incorporate into ice, it remains in liquid); $D_i = 0$

$A_i=A_S$: HCl concentration of liquid around ice changes negligibly from stock concentration.

$V_m = V_i + V_l$: (after melting); not strictly true, but good to first order.

$F \propto D$: fluorescence is proportional to dye concentration.

Equations:

(3.1) $A_m V_m = A_l V_l + A_i V_i$ (HCl mass conservation)

(3.2) $V_m = V_l + V_i$ (volume is additive)

(3.3) $D_m V_m = D_l V_l + D_i V_i$ (dye mass conservation)

$= D_l V_l$ (if $D_i = 0$)

(3.4) $F_s = \kappa D_s$

(3.5) $F_m = \kappa D_m$

Derivation:

Use 3.4 and 3.5 to set up a proportionality:

$$\frac{F_s}{F_m} = \frac{D_s}{D_m} = \frac{1}{b} \quad \Rightarrow \quad D_s = \frac{F_s}{F_m} D_m = D_l \text{ then, use 3.3 to get: } V_m = \frac{F_s}{F_m} V_l = \frac{D_s}{D_m} V_l = \frac{V_l}{b}$$

therefore:

$$V_m = \frac{V_l}{b} \tag{3.6}$$

Use (3.1) with (3.2) to eliminate V_i:

$$V_i = V_m - V_l \tag{3.2}$$

then, with $A_l = A_s$, (3.1) becomes: $A_m V_m = A_s V_l + A_i (V_m - V_l)$.

Using (3.6): $V_m = \frac{V_l}{b}$ with the above, eliminate V_m: $A_m \frac{V_l}{b} = A_s V_l + A_i \left(\frac{V_l}{b} - V_l \right)$ then

divide by V_l: $\frac{A_m}{b} = A_s + A_i \left(\frac{1}{b} - 1 \right)$, multiply by b: $A_m = A_s b + A_i (1 - b)$, then solve for A:

$$A_i = \frac{A_m - A_s b}{1 - b}$$

Now, $z = \frac{A_i}{A_l} = \frac{A_i}{A_s}$, so:

$$z = \frac{A_m - A_s b}{(1-b) A_s} = \frac{\left(A_m / A_s \right) - b}{1 - b} = \frac{B - b}{1 - b}$$

What was measured in the experiment:

$$B = \frac{A_m}{A_s} = \frac{\text{concentration of HCl in mixture}}{\text{concentration of HCl in stock solution}} \Bigg\rangle \text{ titration}$$

$$b = \frac{D_s}{D_m} = \frac{F_s}{F_m} = \frac{\text{fluorescence of dye in stock soution}}{\text{fluorescence of dye in mixture}} \Bigg\rangle \text{ Fluorometer measurement}$$

Chapter IV

Study of the Reaction $ClONO_2 + HCl \rightarrow Cl_2 + HNO_3$ on Ice Particles in a Turbulent Flow

4.1 Introduction

An experiment has been designed to study heterogeneous reactions of gas molecules on particle surfaces. A schematic diagram of the complete apparatus is shown in Figure 4.1. The process of studying these types of reactions has many steps. Many heterogeneous reactions can be studied using this process; however, we focus here on one key reaction:

$$ClONO_{2(abs)} + HCl_{(abs)} \xrightarrow{ice} Cl_{2(g)} + HNO_{3(s)} \qquad (4.i)$$

Each section below will describe one unique step in studying this reaction while giving additional information that would be relevant for other reactions (for example, reaction 4.i on a NAT surface.) Several key goals need to be met in this experiment:

1. Generate solid aerosols (simulated PSCs).
2. Determine size distribution and number density of aerosols, and be able to control these parameters.
3. Use FTIR spectroscopy to characterize aerosols of: water/ice and nitric acid solution/solid hydrate.
4. Perform the chemical reactions in a 'wall-less', high pressure, low temperature flow tube.
5. Separate gas phase products from particles.
6. Detect products at very low concentrations, i.e. sub parts per billion (ppb), at one atmosphere total pressure in real time.

The following sections in this chapter describe each of these points.

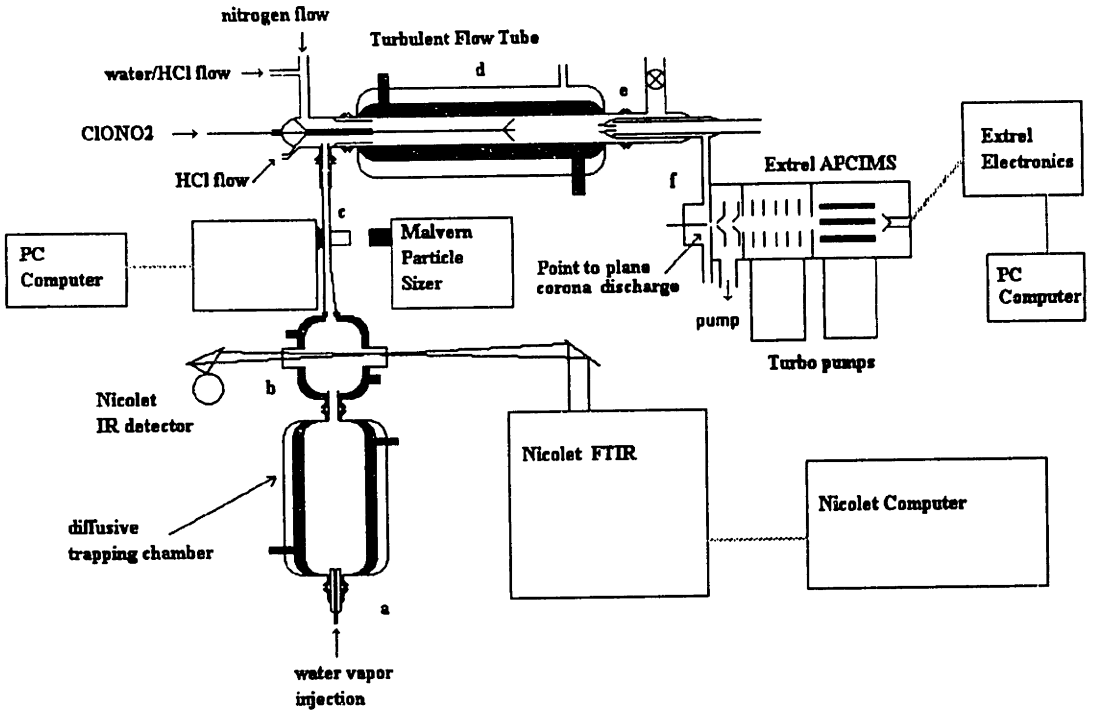

Figure 4.1: Schematic of apparatus used in kinetics experiment. Lower case letters denote different areas of the experiment which are described separately in the text.

In the previous laboratory studies [Molina et al., 1987; Tolbert et al., 1987; Leu, 1988; Hanson and Ravishankara, 1991], the reactions that were studied were carried out on ice and on NAT films coated on the inside of a flow tube, and at low total pressures (~ millitorr). In each case the sticking coefficient of HCl and $ClONO_2$ on the respective substrate was measured. The present study attempts to more closely approach stratospheric conditions by using higher total pressures than those before, and by determining the sticking coefficient of $ClONO_2$ on ice particles flowing with the gasses, rather than on an ice film coated on the walls. Molina et al. [1987] performed experiments that qualitatively showed reaction (4.i) does occur on ice, and that it occurs on a time scale of at most a few milliseconds for the concentration of reactants they were using. However, those experiments were not carried out at stratospheric concentrations of HCl or $ClONO_2$. Similar experiments were performed by Tolbert et al. [1987] and Leu [1988]. More recent studies have been performed at stratospheric pressures of reactants

by Hanson and Ravishankara [1991] which gave results comparable to that of the previous studies. However, recently questions have arisen regarding the porosity of the films that have been used previously [Keyser and Leu, 1993a,b], and whether the surface area of the films has been correctly determined. This experiment does not have such questions since we are using an ensemble of particles rather than depositing a film. The experiment described in this chapter will allow us to better mimic the actual conditions that exist in the stratosphere when heterogeneous reactions occur.

4.2 Production of PSC Particles

4.2.1 *Thermodynamics of ice nucleation*

The thermodynamics of nucleation of an ice particle from a liquid drop of water that is supercooled with respect to the equilibrium freezing point of ice is described below. We have chosen *homogeneous* nucleation to describe the experiments we carried out rather than *heterogeneous* nucleation because it is unlikely that we have heterogeneous nucleation occurring in our system. Though we make no *a priori* effort to eliminate condensation nuclei in the system, we have a continuous flow of condensable vapors (which will be described in the next section) which, if any nuclei are present, will deplete all the nuclei at most within a few minutes. We are also continuously flowing gas from a liquid nitrogen gas pack which we expect to be practically nuclei free.

Turnbull and Fisher [1949] first applied the work of Becker and Doring [1935] and Becker [1938] for nucleation of liquids from the mother vapor to the case of solids nucleating from the mother liquid. For a single component system, Turnbull and Fisher give the equation for the free energy change as:

$$\Delta G = Ai^{2/3} - Bi \qquad (4.1)$$

where i is the number of molecules in the germ. Oxtoby [1988] states that the first term represents the surface free energy and is proportional to the surface area, while the second

term represents the free energy of the bulk solid and is proportional to the volume. Assuming the germs are spherical, Oxtoby lists the A and B terms as:

$$A = (36\pi)^{1/3} v^{2/3} \sigma_{ls} \tag{4.2}$$

$$B = \frac{|\Delta G_m|}{N^0} \tag{4.3}$$

where v is the volume per molecule, σ_{ls} is the surface energy between the liquid and solid interface, ΔG_m is the free energy change per mole between solid and liquid and N^0 is Avagadro's number. Instead of this approach to the description of free energy changes, we prefer to write the free energy equations in terms of moles and partial molar volumes (this is the approach that is universally used when describing nucleation of liquids from the vapor mother phase, and would seem to be more recognizable to physical chemists!) In this case equation 4.1 for the free energy becomes:

$$\Delta G = n\Delta\mu + 4\pi r^2 \sigma_{ls} \tag{4.4}$$

where $\Delta\mu = \mu^c - \mu^l$, is the change per mole in the chemical potential between the liquid and crystalline phases, n is the number of moles in the crystallite and r is the radius of the crystallite with the assumption that it is spherical. For ease of calculation, it is necessary to write equation 4.4 in terms of only one variable: n. To do this, we use the equation of the volume: $V = \frac{4}{3}\pi r^3 = nV_m$ where V_m is the molar volume. Then, the equation for the crystallite radius is: $r = \left(\frac{3nV_m}{4\pi}\right)^{1/3}$. Substituting this into equation 4.4 gives:

$$\Delta G = n\Delta\mu + 4\pi\left(\frac{3nV_m}{4\pi}\right)^{2/3}\sigma \tag{4.5}$$

Figure 4.2 shows a plot of n versus ΔG ($\Delta\mu$ is negative, since the formation of the more stable phase lowers the free energy, while the surface energy term is positive since the new interface is of higher energy.) We can see that at some value of n the free energy function reaches a maxima, and then decreases without bound for larger values of n. This is called the critical point: n^*, with a crystallite radius, r^*. This is the point where:

$$\left(\frac{d\Delta G}{dn}\right) = 0 \tag{4.6}$$

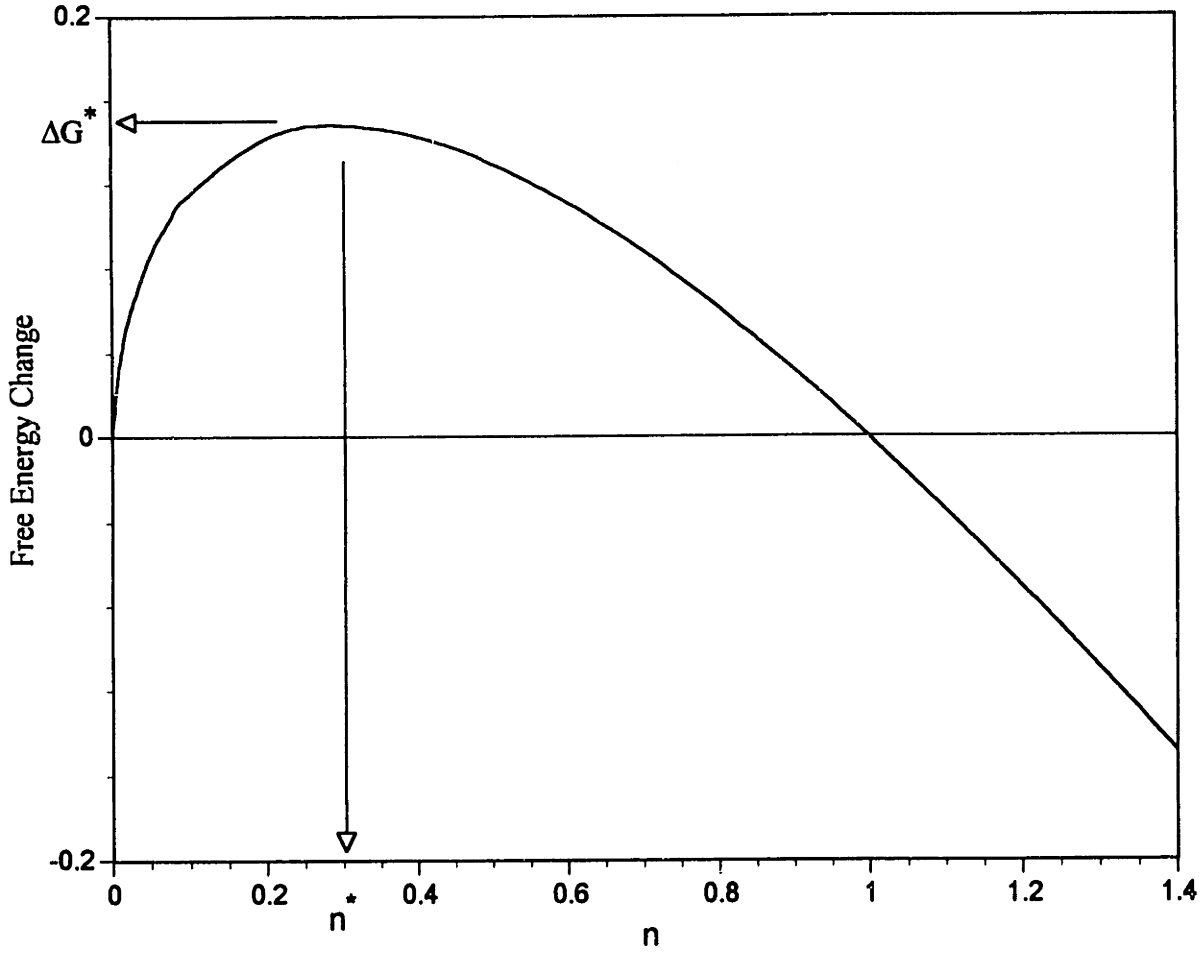

Figure 4.2: Plot of the free energy change for nucleation of ice from the liquid as a function of the number of molecules, n. ΔG^* denotes the critical free energy and n* denotes the critical number of molecules in the crystallite.

Applying equation 4.6 to equation 4.5 we have:

$$\Delta\mu + \frac{2V_m^*\sigma_{ls}}{r^*} = 0 \tag{4.7}$$

which is the well known Gibbs-Thomson (Kelvin) equation. Solving this equation for the critical radius, we have:

$$r^* = \frac{-2V_m^*\sigma_{ls}}{\Delta\mu} \tag{4.8}$$

Now, we substitute equation 4.8 into equation 4.5, and remembering that $n = \frac{4\pi r^3}{3V_m}$, we get the critical free energy:

$$\Delta G^* = \frac{16\pi V_m^{*2}\sigma_{ls}^3}{3(\Delta\mu)^2} \tag{4.9}$$

Finally, we are left to determine the analytic expression for $\Delta\mu$. Oxtoby [1988] notes that close to the melting point we can write:

$$\Delta\mu = \Delta H - T\Delta S = \Delta S(T_m - T) \tag{4.10}$$

where ΔH is the enthalpy change and ΔS is the entropy change, and T_m is the melting temperature. Substituting equation 4.10 into 4.9 gives:

$$\Delta G^* = \frac{16\pi V_m^{*2}\sigma_{ls}^3}{3\left(\Delta S[T_m - T]\right)^2} \tag{4.11}$$

The difficulty in this equation will be the determination of the change in entropy. We can use a more convenient form for the chemical potential [Noggle, 1989]:

$$\mu = \mu^0 + RT\ln\left(\frac{P}{P^0}\right) \tag{4.12}$$

where μ^0 is the standard state chemical potential and P and P^0 are the equilibrium and standard state equilibrium pressures, respectively. Then for the change in chemical potential from solid to liquid we have:

$$\mu_s - \mu_l = \mu_s^0 - \mu_l^0 + RT\left[\ln\left(\frac{P_s}{P_s^0}\right) - \ln\left(\frac{P_l}{P_l^0}\right)\right] \tag{4.13}$$

Now, the liquid and solid are in equilibrium with the vapor over them, therefore the chemical potentials are equal:

$$\mu_s = \mu_v = \mu_v^0 + RT\ln\left(\frac{P_s}{P^0}\right) \tag{4.14}$$

$$\mu_l = \mu_v = \mu_v^0 + RT\ln\left(\frac{P_l}{P^0}\right) \tag{4.15}$$

Using these equations, equation 4.13 becomes:

$$\Delta\mu = -RT\ln\left(\frac{P_l}{P_s}\right) \tag{4.16}$$

Now, we can substitute equation 4.16 into equation 4.9 to give:

$$\Delta G^* = \frac{16\pi V_m^{*2}\sigma_{ls}^3}{3\left(-RT\ln\frac{P_l}{P_s}\right)^2} \tag{4.17}$$

Equation 4.17 will be easier to use since the vapor pressures of the solid and the liquid can easily be measured for the systems of interest. However, we are still left with a surface

tension term to the third power. Fortunately measurements have been made of the surface energy of the water liquid/solid interface (see Hobbs [1974] for a detailed account of the experimental methods and a tabulation of results.)

It must be noted that in the case of the experiments outlined below, water vapor is rapidly being cooled. From Ostwald's phase rule [Hobbs, 1974] at temperatures above -100 C, the vapors will condense to first form a liquid water drop. Then, if the chamber is below -40 C, the drops will instantaneously freeze [Schaeffer, 1952]. However, when ice freezes it does not form a sphere, but rather other geometric shapes such as hexagonal plates or prisms, cubes, dendrites, etc. [Hobbs, 1974] There is other evidence that ice particles in the atmosphere are trigonal plates [Yamashita, 1973]. In any case, assuming the frozen particles are spheres is only an approximation to the actual shapes. This will be discussed further in section 4.4 regarding the sizing of the particles.

4.2.2 *Rate of Nucleation*

This theory was given in Chapter 2 for the case of binary nucleation. Here we have the simpler case of homomolecular nucleation. Walton [1969] has given the equation for the rate of nucleation of solids from the liquid mother phase as (equation 2.29 of Chapter 2):

$$J = R_i A^* N^* \tag{4.18}$$

where R_i is the rate of arrival of the post-critical molecule at the crystallite, A^* is the surface area of the crystallite, and N^* is the number of critical clusters per unit volume of the solution. R_i and N^* are discussed in Chapter 2. The resulting nucleation equation is repeated here (equation 2.32):

$$J = \frac{k_B T}{h} A^* \exp\left(\frac{-\Delta G_a}{k_B T}\right) N_1 \exp\left(\frac{-\Delta G^*}{k_B T}\right) \tag{4.19}$$

where ΔG_a is the activation energy for a "jump" across the solid/liquid interface and ΔG^* is as given in equation 4.17. This equation for the nucleation rate is based on the assumption that equilibrium thermodynamics can be validly applied to a kinetic situation.

The difficulty of this situation is circumvented by introduction of the so-called Zeldovich factor [Zeldovich, 1943] which takes into account the difference between an equilibrium and a steady-state distribution of crystallite sizes. The Zeldovich factor is discussed in Chapter 2 and the final rate equation is repeated here (equation 2.35):

$$J = \frac{2V_m^{*3}(\sigma_{lc}k_BT)^{1/2}}{h}\exp\left(\frac{-\Delta G_a}{k_BT}\right)N_1\exp\left(\frac{-\Delta G^*}{k_BT}\right) \qquad (4.20)$$

When we discussed the binary case we noted that values of the surface energy and ΔG_a were essentially non-existent for binary systems. However, the formation of ice has been a subject of great interest in the past 60 years and much work has been done on these problems. The solid/liquid free energy was determined by Hobbs [1974] and is approximately 20 erg/cm^2. The pre exponential factor for the reduced equation: $J = A\exp\left(\frac{-\Delta G}{k_BT}\right)$ is approximately 10^{30} [Houghton, 1985]. Table 4.1 shows the temperature and supersaturation for ice in our experiments. Since S is a parameter in ΔG^* (which is in an exponential) in equation 4.20, it is easy to see that the ice nucleation rate will be very large in our experiments.

4.2.3 *Experimental Technique*

We have found two different methods of making particles that simulate PSCs; however, one method appears to be preferable over the other. Region (a) of Figure 4.1 is expanded in Figure 4.3. This figure illustrates one of our methods of particle production. The cooling chamber is made out of glass and has an inner diameter of approximately 70 mm with an overall volume of about 2.35 liters. It is a double walled chamber with the outer space containing the circulating cooling liquid. The chamber is wrapped with Armaflex insulation. To make ice particles, nitrogen gas from a liquid nitrogen dewar is passed through a gas bubbler containing deionized water. The amount of water vapor in the resulting flow can be regulated by changing the temperature of the bubbler or by mixing the flow with more dry nitrogen from the dewar in a known ratio; we favor the

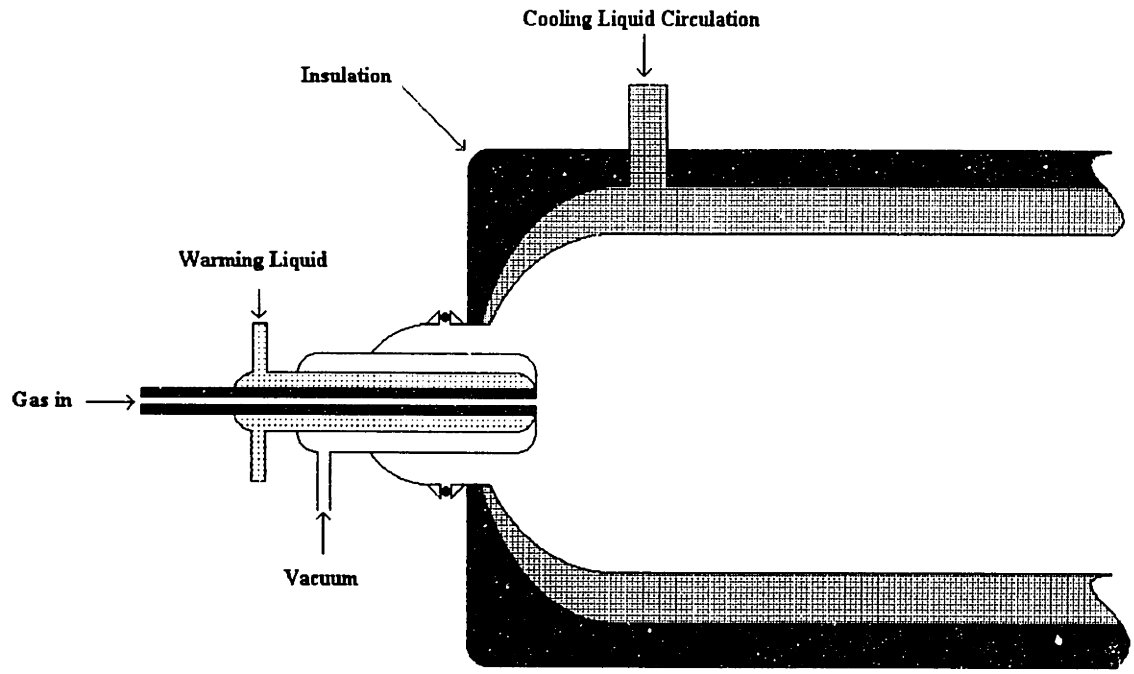

Figure 4.3: Blow up of region a in Figure 4.1: gas injection region. Water vapor in a nitrogen carrier gas flows through the center of the injector which is kept warm by room temperature circulating water and insulated by a vacuum jacket. The gas enters the chamber which is cooled by circulating liquid pentane.

Table 4.1

Temperature	Equilibrium ice vapor pressure	Supersaturation ratio
221	0.023	1033
211	0.00614	3869
201	0.00143	16,613
195	0.00056	42,421
191	0.00029	81,917
185	0.00010	237,560
181	0.000048	494,917

latter method. At 25 C the equilibrium vapor pressure of water is 23.756 torr [Weast, 1984]. A flow of nitrogen through the water bubbler at 25 C will then contain that partial pressure of water. The flow of gas then enters the chamber through the injector. The injector is made of glass in a triple wall configuration. The inner tube is where the water/nitrogen mix passes to the cooling chamber and has an inner diameter of 1 mm. The second jacket carries warm liquid to keep the water vapor from condensing in the inner jacket, and the outer jacket is vacuum pumped for insulation. The temperature of the cooling chamber can be varied and is usually 221 to 190 K.

The water vapor that enters the chamber is highly supersaturated with respect to the equilibrium vapor pressure of ice at these temperatures, thereby facilitating rapid condensation of the water. Table 4.1 shows the equilibrium vapor pressure of ice at various temperatures, and the respective supersaturation ratio: $S = \frac{P}{P^0}$, where P is the vapor pressure of the water entering the chamber, and P^0 is the equilibrium vapor pressure of water at that temperature. The same case can be made for NAT, except using the vapor pressures of nitric acid, water and NAT. We can control the size and number density of the particles. It must be noted that for a fixed mass of water the size and number density of the particles are strongly interdependent. This is shown clearly by Figure 4.4 where both average particle diameter and the number density of particles are plotted as a function of temperature. Clearly there is a strong relationship between these three parameters: as the temperature increases the average size increases and the total number density decreases. However, the parameter of interested for heterogeneous kinetics is the total surface area of particles per unit volume of air: Θ (units: cm^2/cm^3):

$$\Theta = \sum_i 4\pi(\bar{r}_i)^2 (N_p)_i \qquad (4.21)$$

Observing this equation, we see the total surface area increases with the square of the size parameter (radius), but increases only linearly with the particle number density. Therefore, since particle size and number density are dependent, smaller total surface areas should

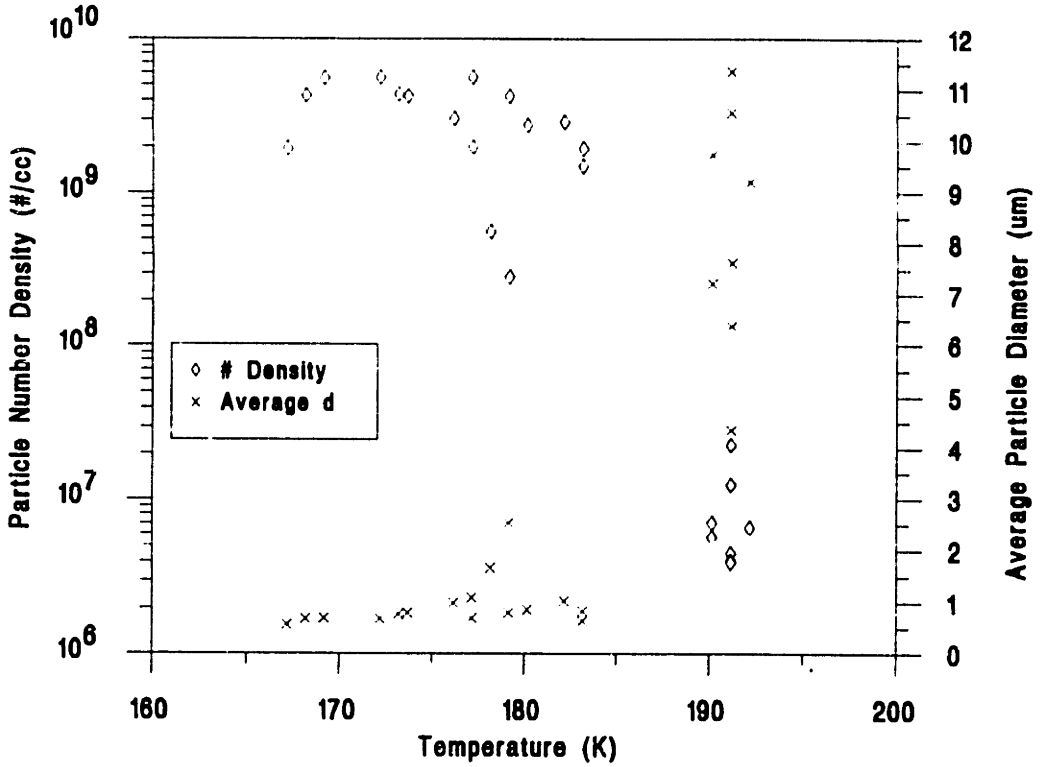

Figure 4.4: Plot of particle number density and average diameter vs. temperature for ice particles. Data are from the Malvern Mastersizer. See text for details.

result from small particles (there will be many of them, but the radius will be small). Again, this is not observed to be the case because the relationship between the particle size and the number density is not linear. We found that an average particle radius of ~$5x10^{-5}$ cm (0.5 μm) resulted in ~$5x10^{9}$ particles per cm^3, while an average particle radius of ~$5x10^{-4}$ cm (5 μm) resulted in ~$5x10^{6}$ particles per cm^3. In the first case theta is 31.4 and in the second case theta is 15.7; therefore, smaller total surface areas are obtained by making larger (and fewer) particles at higher temperatures. Figure 4.5 illustrates this phenomenon by plotting particle number density and average diameter vs. theta (Θ). Interestingly, for very high values of theta, the particle number density and average diameter do not change.

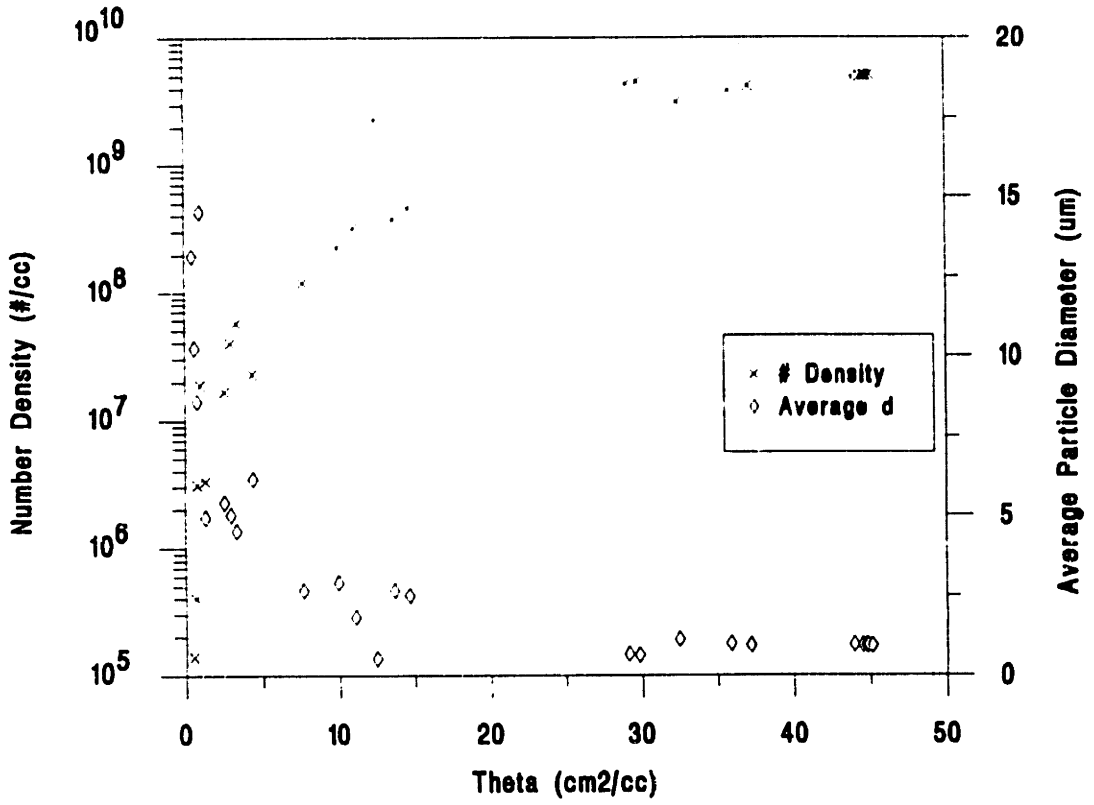

Figure 4.5: Plot of particle number density and average diameter vs. total surface area per cm^3 (Θ). Data are from the Malvern Mastersizer. See text for details.

The second method of particle generation is shown in Figure 4.6. Here the crystal from an ultrasonic humidifier is used to generate aerosols. Dry air was used as a carrier gas to transport the aerosols to the cooling chamber. In general, the particles produced by this method were rather large. The flow rate of the carrier gas appeared to not have any effect on the size distribution. Also, since the aerosols are well developed before reaching the cooling chamber, the temperature of the cooling chamber had no effect on the size distribution. Besides the problem of not having control over the size distribution of the aerosols, the major problem with this method is that the particles build up on the wall of the cooling chamber very rapidly. After only ~15 minutes of flowing aerosols, the outlet of the cooling chamber (which has a 22 mm diameter) was clogged with ice particles. This method seemed to be impractical for generating PSC particles.

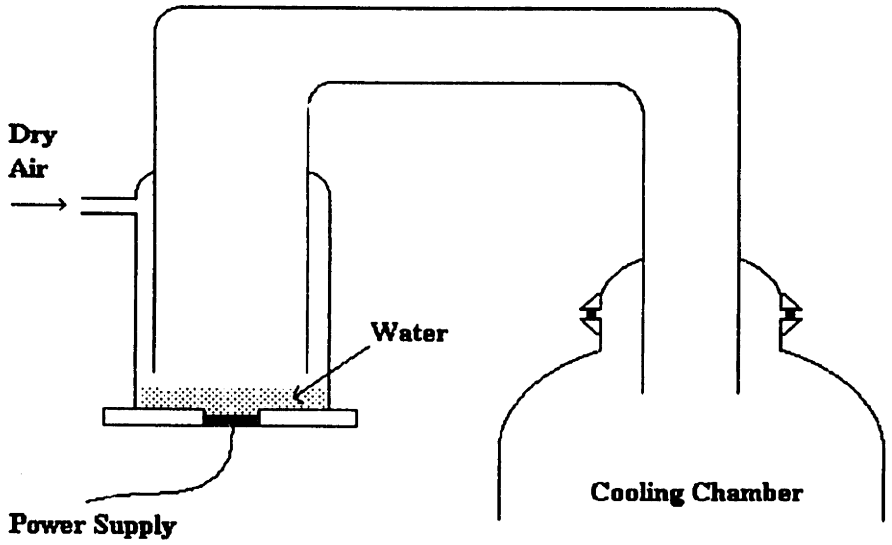

Figure 4.6: Alternative particle generation apparatus. The ultrasonic vibrator from a commercial humidifier was attached to a Teflon plate with water over it. Aerosols were generated with this device and dry carrier gas carried the particles to the cooling chamber.

4.3 Characterization of Particles by FTIR

Section (b) of Figure 4.1 shows the design of the single pass IR cell used to characterize the particles. The number density of particles that is produced in this experiment is sufficiently high to enable a single pass of the IR beam to produce quality spectra. Figure 4.7 shows the IR spectrum of ice particles in the apparatus. IR spectra of ice have been shown in the literature [Molina et al., 1987; Tolbert and Middlebrook, 1990]. The critical freezing point of 1 μm water drops has been shown to be -40 C [Schaeffer, 1952]. In our experiments, we will work at polar stratospheric temperatures which are -70 C or below, therefore, it actually is not necessary to characterize our particles by FTIR. Figure 4.8 is a plot of the IR spectrum of NAT particles. IR spectra of NAT have been published several times in the literature [Tolbert and Middlebrook,

Figure 4.7: FTIR spectrum of ice particles. Average size of the particles is approximately 5 micrometers, as derived from the Malvern Mastersizer.

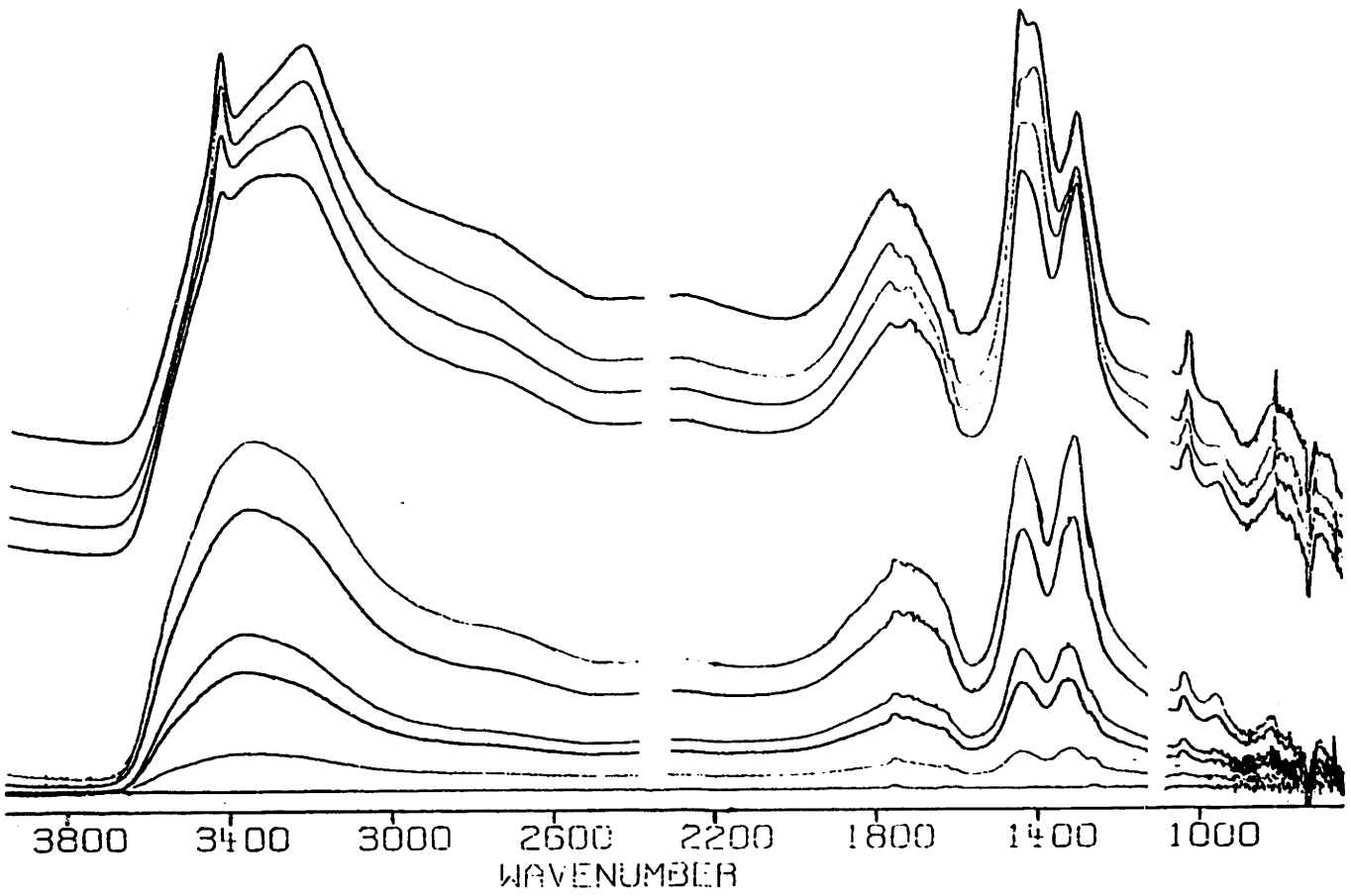

Figure 4.8: FTIR spectrum of NAT particles.

1990; Ritzhaupt and Devlin, 1991; Smith et al., 1991], and our spectra are in agreement with these previous reports. Our studies did not involve using NAT particles as the reaction substrate; however, we demonstrate here that NAT particles can be made by our method as evidenced by the IR spectrum for use in studies of heterogeneous chemistry on particles.

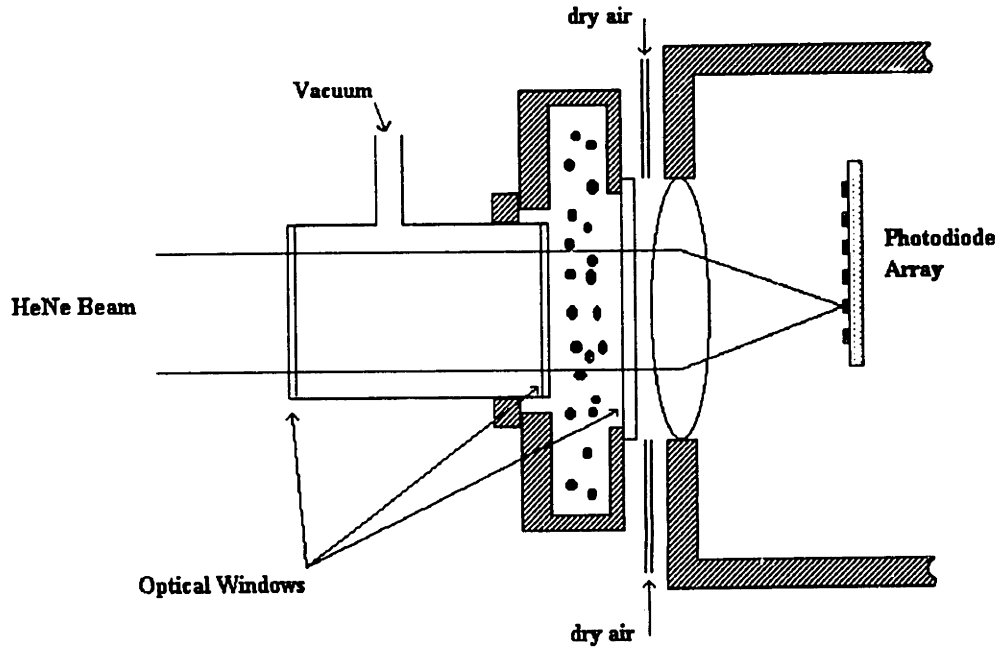

Figure 4.9: Cross section of apparatus in area c of Figure 4.1. The HeNe laser beam of the Malvern Mastersizer crosses the flow of particles and is focused on the photodiode array (see Figure 4.10 for detail of the array). The particles are constrained in a Teflon coated stainless steel flow box which has two ports for passing the laser beam. The front side shows two optical windows which are separated by an evacuated tube, and the rear side has a single optical window which is kept clear of condensing room water by flowing dry air over it.

4.4 Characterization of Particles Using Laser Scattering

A Malvern Mastersizer particle sizing instrument was used to characterize the particles with respect to size distribution, obscuration and relative volume concentration. From these measured values the total particle number density and total particle surface area per volume of air are calculated.

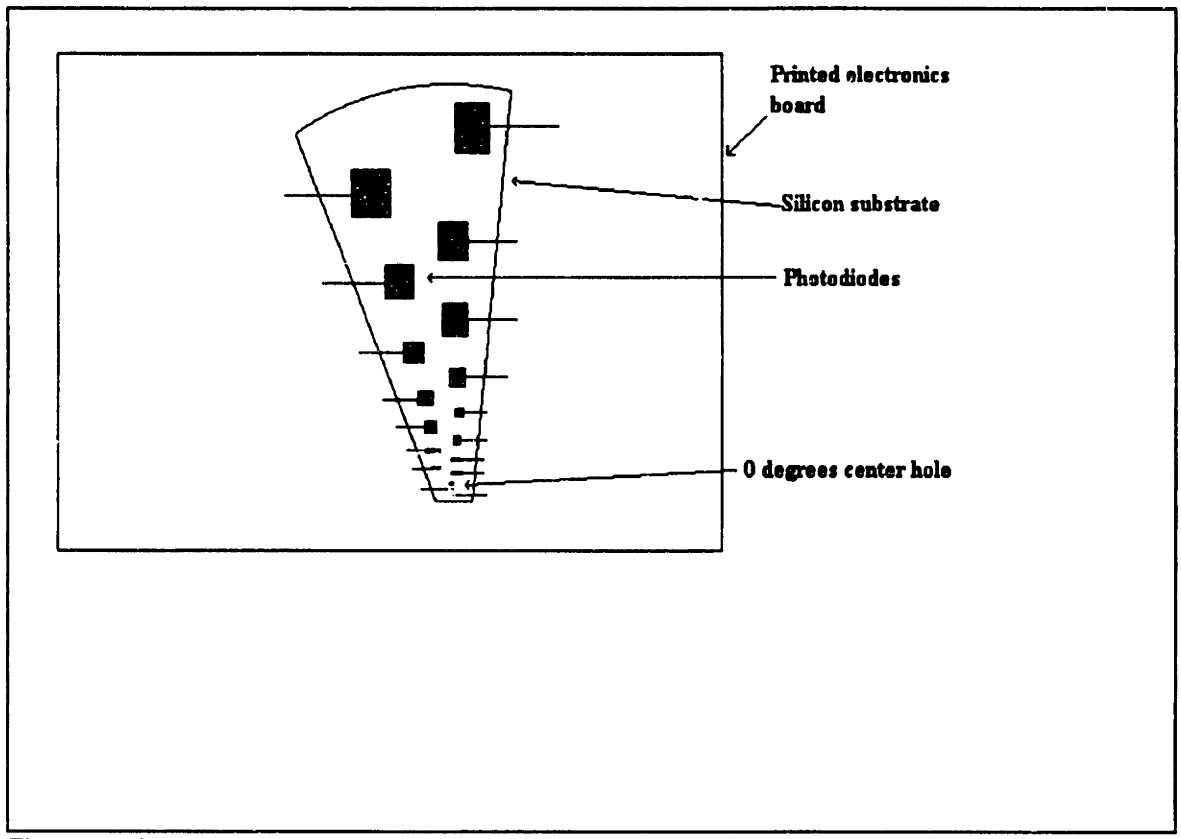

Figure 4.10: Schematic of the photodiode array detector in the Malvern Mastersizer.

4.4.1 *Instrument Operation*

The instrument consists of shining a collimated HeNe laser beam (λ= 632 nm) across a flow of particles as is shown in Figure 4.9. The flow of particles will scatter light at varying intensities at all angles; however, only light scattered in the range of 0 to 50 degrees (forward scattering) is captured by the focusing lens situated on the opposite side of the particle flow. This lens focuses the scattered light on a photodiode array pattern as shown in Figure 4.10. Light scattered to a high angle by the particles will be focused on a photodiode that is further from the center, and low angle scattered light will focus on the photodiodes closer to the center. In total there are 32 photodiodes that are arranged from the center of the beam upwards to a position that corresponds to light scattered at 50 degrees from center. The light impinging on the photodiodes is then converted into a signal which is passed to proprietary control boards in a standard IBM compatible PC. This signal is read by proprietary software developed by Malvern Instruments.

MALVERN MasterSizer SB.0A Master Mode Thu 14 Oct 1993 8:53 am

Source Sample 128

Ring Data Focus 100

Ring	Data	Ring	Data
0	0.32	16	7.17
1	-21.41	17	9.03
2	-56.93	18	25.02
3	-49.76	19	39.24
4	-56.56	20	53.87
5	-59.06	21	68.70
6	-65.43	22	84.02
7	-65.97	23	100.75
8	-85.76	24	114.59
9	-58.19	25	121.06
10	-128.02	26	125.67
11	-47.58	27	127.72
12	-42.60	28	122.44
13	-28.42	29	112.15
14	-15.28	30	99.48
15	-15.40	31	53.39

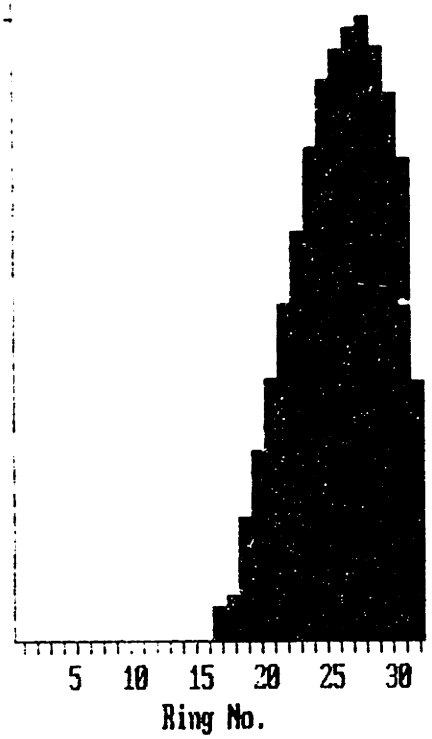

3860 1400 lbv474m

Figure 4.11: Table and plot of light signal at the photodiode array. Ring 0 corresponds to no scattering, and thus is the bulk of the light impinging on the array. Ring numbers indicate distance from the center (ring 0). Higher ring numbers correspond to larger scattering angles. Scattered light can be detected up to 50 degrees from center.

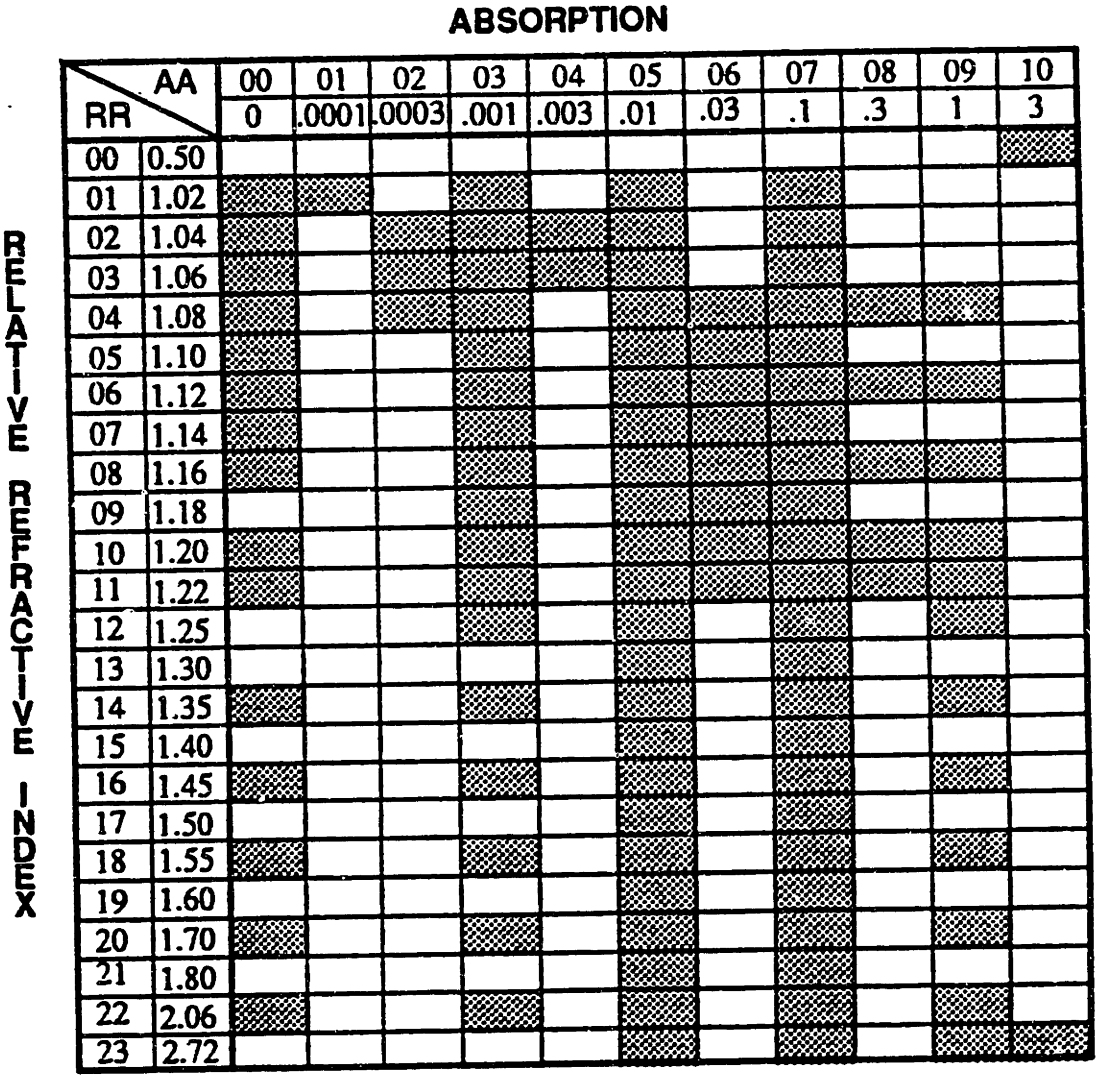

Figure 4.12: Table of light scattering matrices available in the Malvern software (from Malvern manual).

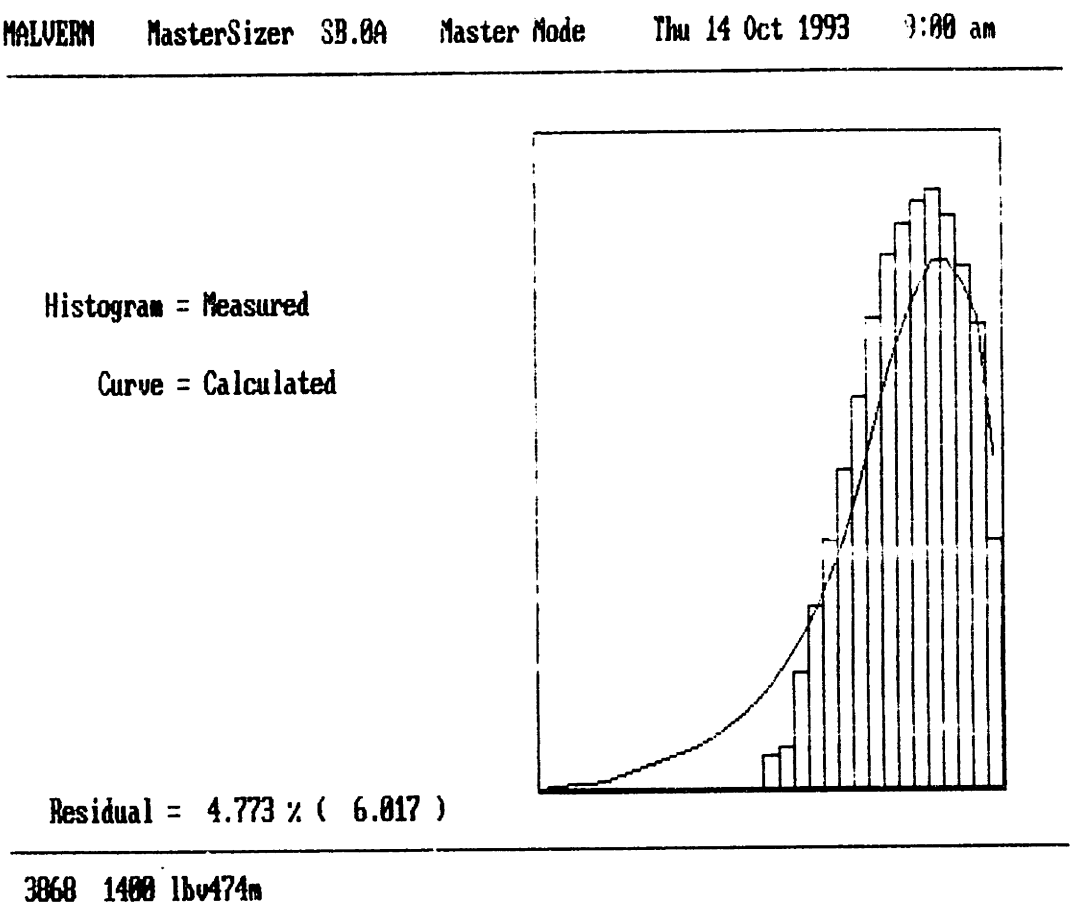

Figure 4.13: Plot of the light scattering data (histogram) with the calculated fit to the data (line) from the Malvern software.

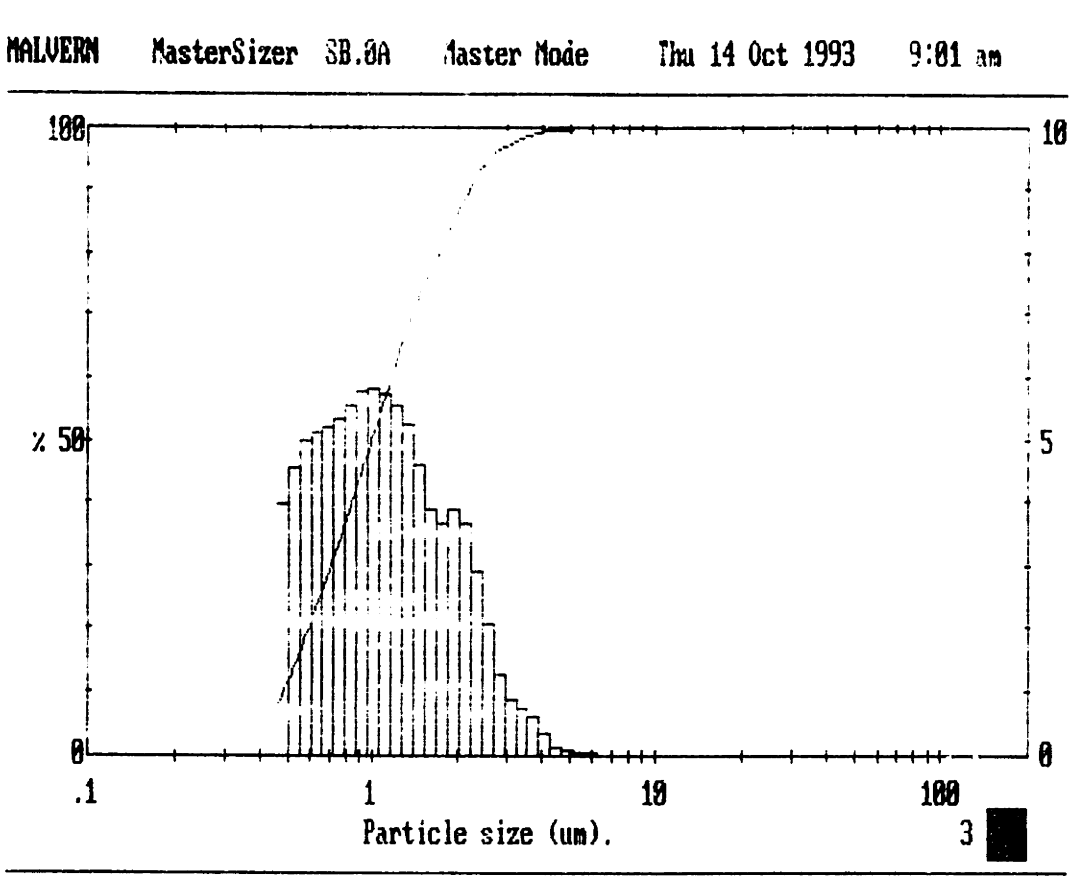

Figure 4.14: Plot of the calculated particle size distribution (histogram) with the calculated fit to the data (line) from the Malvern software.

MALVERN MasterSizer 3B.0A Master Mode Thu 14 Oct 1993 9:03 am

Upper	in	Lower	Under	Upper	in	Lower	Under	Upper	in	Lower	Under	Span 1.73
				39.1	0.0	32.3	100	3.95	1.4	3.27	98.0	
				32.3	0.0	26.7	100	3.27	2.2	2.70	96.5	D[4,3] 1.18µm
				26.7	0.0	22.0	100	2.70	5.1	2.23	90.8	
				22.0	0.0	18.2	100	2.23	7.8	1.84	83.1	
180	0.0	149	100	18.2	0.0	15.1	100	1.84	7.8	1.52	75.3	D[3,2] 0.81µm
149	0.0	123	100	15.1	0.0	12.4	100	1.52	10.1	1.26	65.2	
123	0.0	102	100	12.4	0.0	10.3	100	1.26	11.7	1.04	53.5	
102	0.0	83.9	100	10.3	0.0	8.48	100	1.04	11.8	0.86	41.7	D[v,0.9] 2.18µm
83.9	0.0	69.3	100	8.48	0.0	7.01	100	0.86	11.2	0.71	30.5	
69.3	0.0	57.3	100	7.01	0.0	5.79	100	0.71	10.2	0.59	20.3	
57.3	0.0	47.3	100	5.79	0.1	4.79	99.8	0.59	10.2	0.48	10.1	D[v,0.1] 0.48µm
47.3	0.0	39.1	100	4.79	0.4	3.95	99.4	0.48	10.1	0.20	0.0	

Source = Res.:i5oct1	Beam length = 15.0 mm	Model indp	D[v,0.5] 0.98µm
Record No. = 3	Residual = 4.773 %		
Focal length = 100 mm	Obscuration = 0.3373	Volume Conc. = 0.0006%	
Presentation = 1400	Volume distribution	Sp.S.A 7.4221 m²/cc.	

3868 1400 lbv474a

Figure 4 .15: Table of results from the Malvern software. Shown are the 32 size categories and the per cent of particles in each size range. Other parameters are given as indicated.

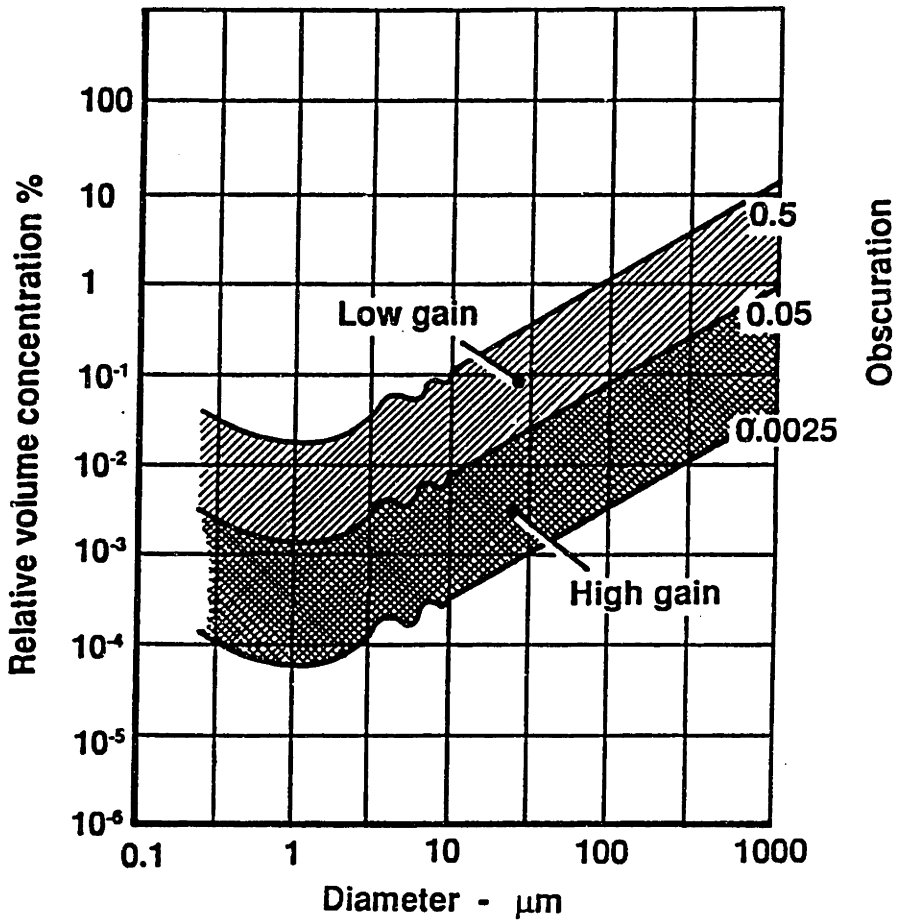

Figure 4 .16: Plot of the Malvern detection limits (from the Malvern software manual) as a function of the particle diameter. Shown are the limits for settings of high and low gain.

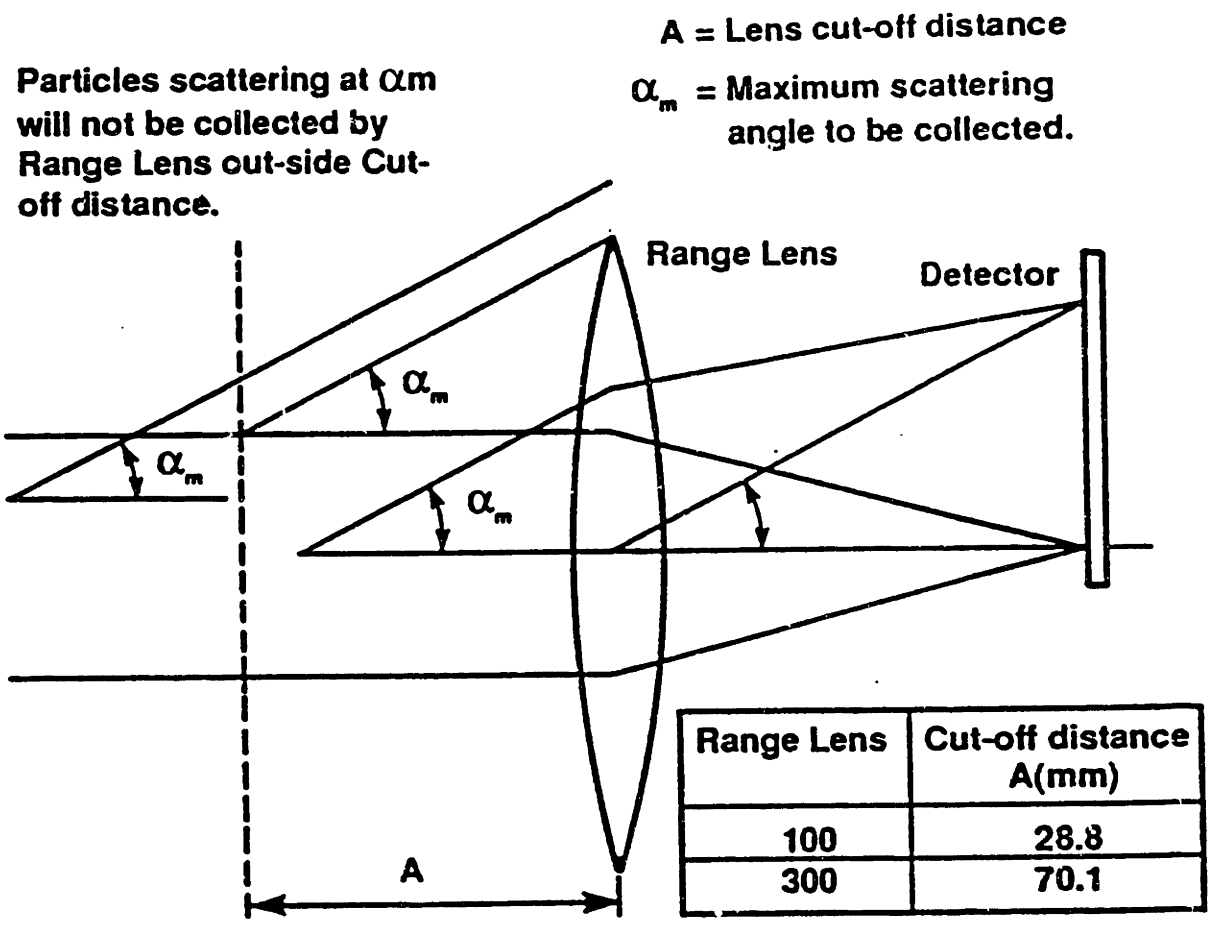

Range Lens	Cut-off distance A(mm)
100	28.8
300	70.1

Figure 4.17: Schematic illustration of the range limits of the Malvern optics. Distance A is the furthest particles can be from the lens in order for them to be sized properly. In the experiments presented here the 100 range lens was used, thus A=28.8 mm. See text for details. Figure taken from the Malvern software manual.

4.4.2 *Malvern Software Calculations*

When making measurements with the Mastersizer, the data is reported as a difference from the background measurement; therefore, a background measurement must first be made with all conditions identical to the data measurements except without a flow of particles. Then, a scattering spectrum is acquired from the instrument by the software; a sample is displayed in Figure 4.11. A graphical display is given as well as a table of the actual values for each photodiode detector. Also listed in the Table is the measurement of ring number 0. This is the measurement of the total obscuration since the majority of the laser intensity is not scattered, and thus is focused by the lens on the detector at 0 degrees from center.

The Malvern software uses Mie theory to calculate the particle size distribution based on the light scattering pattern that the instrument measures. Mie theory uses the solution of the electromagnetic wave equations for a spherical particle of arbitrary optical properties. The optical properties of the particle and surrounding medium are set in the Malvern software by the user. Malvern uses two parameters to determine the appropriate Mie theory matrices to use in the calculations: *DRI* and U_a where: $DRI = \frac{U_s}{U_m}$ (U_S is the real refractive index of the sample material and U_m is the real refractive index of the supporting medium) and U_a is the sample absorption of 632 nm light. For a flow of ice particles in nitrogen: U_S=1.33, U_m=1 and U_a=0. Malvern, however, has not provided matrices for all possible configurations of optical constants. The shaded areas in Figure 4.12 show the combinations that Malvern has calculated matrices for. The nearest matrix for *DRI*=1.33 and U_a=0, is that for *DRI*=1.35 and U_a=0. The Malvern has a 'standard' matrix corresponding to *DRI*=1.16 and U_a=0.1 (for glass beads in air). We used this matrix for a few experiments to compare the results with experiments using a matrix corresponding to ice in air. The differences in the calculated distributions were not great,

thus using the matrix corresponding to DRI=1.35 seems reasonable for ice, as it is much closer to the actual value of 1.33.

Besides the raw data and an optical properties matrix, a third component is needed to calculate the particle size distribution. This third component is the analysis model which is a mathematical description of the form of the result. Three different models are available in the software, but for the purposes of this experiment the 'model independent' model is used. This model assumes that there is no mathematical description relating the volume in one sizeband to the volume in any other sizeband. Using the model, the data and the optical constants for ice, the size distribution can be calculated. The basic equation is of the form:

$$D_k = U_{i,k}\, V_i \tag{4.22}$$

where the subscript i is the index of size bands, the subscript k is the index of detector elements, D_k is the data from detector k, V_i is the relative volume in sizeband i, and $U_{i,k}$ describes how particles in size band i scatter light to detector element k. This is a matrix equation and describes how a known distribution of particle sizes will scatter light. We need to determine the size distribution matrix V. Normally we would invert the matrix U; however, for a light scattering matrix this is not possible. Thus, the equation is solved using successive approximations. To begin the process the software estimates a size distribution based on the measured data. Then the difference between the estimate and the actual data is calculated using the equation:

$$Rs = 100\frac{\sqrt{\sum (D_k - L_k)^2}}{\sum D_k} \tag{4.23}$$

where Rs is the residual described as a percentage, L_k is the calculated data value for detector element k. This result is used to calculate a new distribution, and the process is repeated until the residual reaches a minimum. A plot of a typical measured data set and the calculated set is shown in Figure 4.13. The calculated size distribution can then be displayed in graphical form (Figure 4.14) or tabular form (Figure 4.15). The table in

Figure 4.15 shows the size range for each of the 32 size bands, and the relative volume (as a fraction of the total volume of particles) in each size band is given. Other parameters reported are: the residual (calculated from equation 4.23), the obscuration (the light intensity at 0.00 degrees), the median diameter and volume concentration which are described below. The median diameter is simply the diameter at which half the particles are larger and half smaller. The volume concentration is calculated using the Beer-Lambert law and expressed as a percentage:

$$C = \frac{100\ln(1-Ob)}{\frac{-3}{2}b\sum\frac{V_iQ_i}{d_i}} \tag{4.24}$$

where C is the concentration per cent, Ob is the obscuration, b is the beam length (15 mm in our case), V_i is the relative volume in size band i, Q_i is the extinction coefficient of size band i, and d_i is the mean diameter of size band i.

4.4.3 *Limitations of the Malvern Particle Sizer*

The Malvern instrument is actually quite versatile in the range of the total number of particles that it can detect. However, we are generally interested in the lower limit for the purposes of this experiment. Figure 4.16 is reproduced from the Malvern Mastersizer manual and shows the limits of the instrument detection in terms of the obscuration. For a setting of high gain the lower limit is an obscuration of 0.0025 (upper limit of 0.05), and the corresponding volume concentration is given by the graph as a function of particle diameter. If we have an ensemble of 1 μm (diameter) particles which is monodisperse, the minimum number of particles needed to get an obscuration of 0.0025 is approximately 10^6 particles/cm^3, hence this is the minimum number of particles needed to retrieve reliable sizer data.

A second limitation of the Malvern is shown in Figure 4.17. This Figure shows the problem of the lens cutoff distance. As shown in the figure, any particles outside of the lens cutoff distance (A) that scatter light at the maximum angle ($\alpha_m = 50^o$) will not be properly sized by the instrument because the high angle scattered light will miss the lens.

In these experiments, the 100 Range Lens is used for which, as shown in the figure, the cut off distance is 28.8 mm. To address this limitation, a special flow box was designed to constrain the particle flow to within 28.8 mm of the Range Lens. The flow box is represented by area c in Figure 4.1. A cross section of the flow box is shown in Figure 4.7. The flow box allows the particles to flow past the sizer without constricting the flow. As can be seen from the figure, only a portion of the total flow is sampled; however, at our flow rates (~2 slpm) and particle sizes (~1 μm), we don't expect significant settling of the particles in the flow. The actual cross sectional dimensions of the flow box are: 15 mm width, 73.1 mm height. The thickness of the flow box wall nearest to the Range Lens and the thickness of the optical window near the Range Lens add 9.5 mm to the total distance from the Range Lens to the farthest particle. So, all of the particles are constrained to a distance of 24.5 mm from the Range Lens.

4.4.4 *External Calculations*

The Malvern software does not calculate two parameters that are of interest for this experiment: total number of particles per unit volume (Np) and total particle surface area per unit volume (Θ). These parameters are calculated externally by a C program using the calculated results of the Malvern software. The total number of particles is given by:

$$N_p = \sum \frac{\frac{C}{100} V_i}{\frac{4}{3}\pi\left(\bar{r}_i\right)^3} \tag{4.25}$$

where C is the volume concentration as defined above, V_i is the calculated relative volume fraction in the size class i from the data, $\bar{r}_i$ is the mean radius of size class i. The total surface area was given above and is repeated here::

$$\Theta = \sum_i 4\pi\left(\bar{r}_i\right)^2 \left(N_p\right)_i \tag{4.21}$$

where $(Np)_i$ is the number of particles in size class i. As will be shown is section 4.5, Θ is the parameter of interest to characterize the particles for these kinetic studies.

4.5 Turbulent Flow Kinetics

Determining the sticking coefficient of $ClONO_2$ on ice particles doped with HCl is of fundamental importance to understanding the processes that occur on Polar Stratospheric Clouds (PSCs) in the polar winter. This section describes a detailed method for determining such sticking coefficient on an ensemble of ice particles in a turbulent flow at polar stratospheric conditions. The turbulent flow kinetics method has been developed by other workers in our lab [Seeley, 1993a] and is applied here.

4.5.1 *Diffusion of Gas Molecules to the Particles*

The reaction under study is as follows:

$$ClONO_2 + HCl \xrightarrow{ice} Cl_2 + HNO_3 \qquad (4.i)$$

We have three critical steps here illustrated as:

$$ClONO_{2(g)} \xrightarrow{k_2} ClONO_{2(abs)} \qquad (4.ii)$$

$$HCl_{(g)} \xrightarrow{k_1} HCl_{(abs)} \qquad (4.iii)$$

$$ClONO_{2(abs)} + HCl_{(abs)} \xrightarrow{ice} Cl_{2(g)} + HNO_{3(s)} \qquad (4.iv)$$

In the experiment we will measure the total rate of the reaction (R_T) which incorporates all of the above steps. To get an idea under what conditions to perform the experiment, it will be useful to calculate the flux of gas-phase molecules to the particles. To a first approximation we will consider only molecular diffusion; turbulent diffusion will be discussed later.

4.5.1.1 *Molecular Diffusion*

Schwartz [1981; 1983] has developed much of the theory of gas phase diffusion to particles. First, we start with a gas phase diffusion (continuity) equation:

$$\frac{dC}{dt} = D_g \nabla^2 C \qquad (r \geq a) \qquad (4.26)$$

where a is the particle radius, D_g is the molecular diffusion coefficient for the species in a given medium (N_2 in our case), C is the concentration of the species of interest and r is

the distance from the center of the particle. We then have the boundary condition for $C(r,t)$: $C(\infty,t)=C_\infty$; and using a steady state approximation: $\frac{dC}{dt}=0$ then:

$$D_g\frac{1}{r^2}\frac{d}{dr}\left(r^2\frac{dC_{ss}}{dr}\right)=0 \qquad \Rightarrow \qquad \frac{d}{dr}\left(r^2\frac{dC_{ss}}{dr}\right)=0 \tag{4.27}$$

integrating this:

$$\int d\left(r^2\frac{dC_{ss}}{dr}\right) \quad \Rightarrow \quad r^2\frac{dC_{ss}}{dr}+B=0 \quad \Rightarrow \quad \frac{dC_{ss}}{dr}+\frac{B}{r^2}=0$$

where B is a constant of the integration. We also have the condition where the flux at the particle surface is:

$$\overline{F}=D_g\left(\frac{dC_{ss}}{dr}\right)_{r=a} \tag{4.28}$$

Then we have:

$$\frac{\overline{F}}{D_g}+\frac{B}{a^2}=0 \qquad \Rightarrow \quad B=-\frac{a^2\overline{F}}{D_g}$$

then integrating:

$$dC_{ss}+\frac{B}{r^2}dr=0 \qquad \Rightarrow \quad \int_{C(a)}^{C_\infty} dC_{ss}=-\int_a^\infty \frac{B}{r^2}dr$$

$$C_{ss}(a)=C_\infty-\frac{a\overline{F}}{D_g} \tag{4.29}$$

From the kinetic theory of gasses [Atkins, 1986] we have for the flux to a surface: $\overline{F}=\frac{1}{4}\bar{\nu}\,C(a)$ where $\bar{\nu}$ is the mean speed and $C(a)$ is the number density of the gas phase species of interest at the surface. Now, since not all collisions result in accommodation into the particle, we introduce a "sticking" coefficient: γ which ranges between zero and one. Then our equation becomes:

$$\overline{F}=\frac{1}{4}\bar{\nu}\,C(a)\gamma \tag{4.30}$$

Now, to get $C_{SS}(a)$, we substitute equation (4.30) into equation (4.29) and then solve for $C_{SS}(a)$:

$$C_{ss}(a)=C(\infty)-\frac{C(a)\bar{\nu}\gamma a}{4D_g}$$

$$C_{ss}(a) = \left(\frac{C(\infty)}{1 + \frac{\bar{v}\gamma a}{4D_g}} \right) \tag{4.31}$$

Now, to calculate $\bar{F}$ we need to calculate D_g and $\bar{v}$. The gas phase diffusion coefficient for $ClONO_2$ in N_2 has not been experimentally determined. Therefore we will use the method of Fuller et al. [1966] to theoretically determine D_g:

$$D_g = \frac{10^{-3} T^{1.75} \left[\frac{M_A + M_B}{M_A M_B} \right]^{0.5}}{P\left[\left(\sum v\right)_A^{1/3} + \left(\sum v\right)_B^{1/3} \right]^2} \tag{4.32}$$

where M_X is the molecular weight in grams/mole; T is temperature in Kelvin; P is pressure in atmospheres; and v is the empirical atomic diffusion volume for each atom in the respective molecule. Fuller et al. list the following relevant values for v: N_2: 17.9; Cl: 19.5; O: 5.48; N: 5.69. Using these values, we get for v_{ClONO2}: 41.63 and v_{N2}: 17.9. With the other parameters: M_{ClONO2}: 97.5; M_{N2}: 28; T: 200K; P: 1 atm, then D_g = 0.062 cm^2/s.

Now for the mean speed:

$$\bar{v} = \left(\frac{8RT}{\pi\mu} \right)^{\frac{1}{2}} \quad \text{with R=8.3143 J/K, T=200 K, } \mu = \left(\frac{M_A M_B}{M_A + M_B} \right)$$

then $\bar{v} = 4.41x10^4\ cm/s$. Now, with the following conditions:

$$C(\infty) = 3.6x10^8 \text{ molecules/cm}^3$$

$$a = 0.5\mu m = 5x10^{-5}\ cm$$

$$\gamma = 0.3 \text{ (from Ravishankara and Hanson [1991])}$$

we find $C(a)$ = 9.82x10^7 molecules/cm^3. We see that there is a small decrease in the concentration of the gas phase species at r = a from the background level; therefore, we can assume that the gas concentration at the particle surface is equal to the background level.

Using equation (4.30), we get: $\overline{F} = 3.25\text{x}10^{11}$ molecules/cm^{2}s. The rate of the process described by 4.i-iv is: $R_T = \overline{F}\Theta$, where Θ is the total surface area of particles per unit volume of air (cm^2/cm^3). For simplicity, we can write R_T in terms of a rate constant and concentrations:

$$R_T = \frac{d[ClONO_2]}{dt} = k_T C(a)\Theta \qquad (4.33)$$

where,

$$k_T = \frac{(0.25)\bar{\nu}\gamma}{1 + \frac{\bar{\nu}\alpha\gamma}{4D_g}} \qquad (4.34)$$

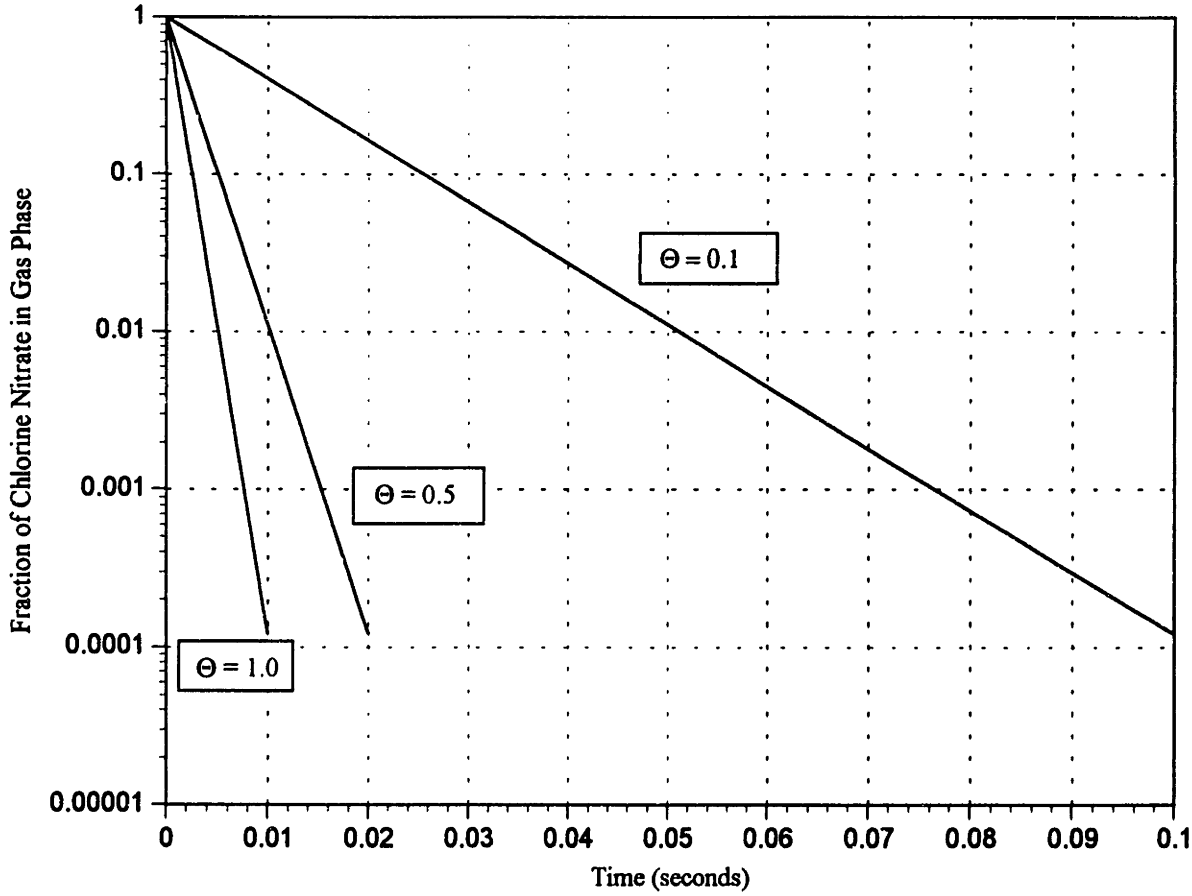

Figure 4.18: Plot of the decrease in chlorine nitrate concentration as a function of time for different values of theta for the following conditions: $\alpha = 0.3$, $\bar{\nu} = 4.41\text{x}10^4$ cm/s, $D_g = 0.062$ cm^2/s.

Now, we can get an equation for the concentration of $ClONO_2$ at a given time t:

$$\frac{d[ClONO_2]}{[ClONO_2]} = -k_T\Theta dt. \quad \Rightarrow \quad [ClONO_2] = [ClONO_2]_\infty e^{-k_T\Theta t} \qquad (4.35)$$

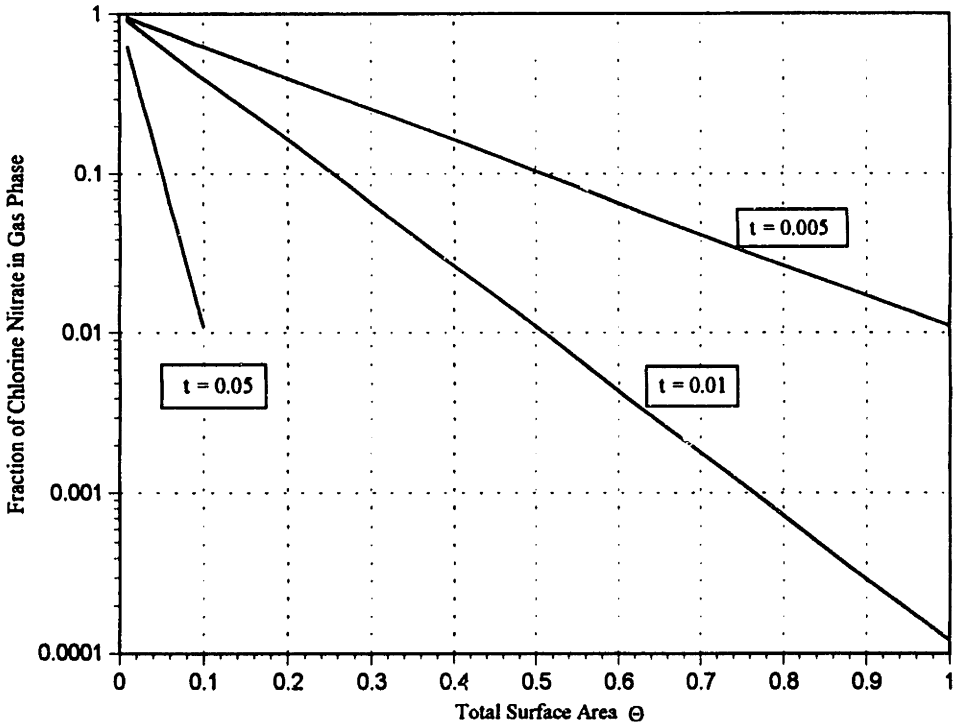

Figure 4.19: Plot of the decrease in chlorine nitrate concentration as a function of total surface area of particles (cm^2/cm^3) for various times. Conditions are the same as in Figure 4.18.

Assuming that γ is in the range of the previously reported value of 0.3, we can perform some calculations varying theta and time to determine the appropriate conditions to run the experiment under. Figure 4.18 shows a plot of the fraction of chlorine nitrate in the gas phase as a function of time for different values of theta. One can see that the time scales are very short for theta values of 1 and 0.5 cm^2/cm^3. A theta value of 0.1 cm^2/cm^3 is more reasonable, giving an order of magnitude decrease in the $ClONO_2$ in about 25 milliseconds. For a flow velocity of 500 cm/s a tube distance of 12.5 cm would be needed to see this decrease. Alternatively we can focus on changing particle surface area for different time values as shown in Figure 4.19. We can easily produce particles characterized by a theta of 0.5 cm^2/cm^3. If we had a time constant of 0.005 seconds at 500 cm/s velocity, the tube length would be 2.5 cm. This is fairly short, but could be workable. The various parameters will need to be adjusted in the actual experiment to optimize the data collection.

Using conventional mass spectrometry it is not possible to measure $ClONO_2$ in the presence of HNO_3, which is a product of the reaction. We can, however, measure Cl_2 which will give us a unique signal in the mass spectrum. By mass balance we can write the concentration of chlorine nitrate in terms of the measured quantity, Cl_2 and the background concentration of chlorine nitrate: $[ClONO_2] = [ClONO_2]_\infty - [Cl_2]$. Then our final equation becomes:

$$[Cl_2] = [ClONO_2]_\infty \left(1 - \exp(-k_{ii}\Theta t)\right) \tag{4.36}$$

Now, solving equation 4.34 for gamma:

$$\gamma = \frac{k_{ii}}{(0.25)\bar{v} - \frac{k_{ii}\bar{v}a}{4D_g}} \tag{4.37}$$

and we rearrange 4.36 to get the value of k_{ii}:

$$k_{ii} = \frac{\ln[ClONO_2]_\infty - \ln\left([ClONO_2]_\infty - [Cl_2]\right)}{\Theta t} \tag{4.38}$$

Once all the experimental parameters are measured, we can substitute equation 4.38 into equation 4.37 to determine gamma.

4.5.1.2 *Turbulent Diffusion*

The significance to mass transport of turbulent diffusion is that it enhances diffusion to the particle surface above that of molecular diffusion alone. Friedlander [1977] shows that particles 1 μm and larger do not flow with the turbulent eddies because of inertial effects. This effect would give us a new diffusion constant for gas transport to the particles: $D_{eff} = D_g + D_t$ where D_t is the diffusion coefficient due to turbulence. Figure 4.20 is a plot of the flux versus the value of the diffusion coefficient with particle size as a parameter. For a one micron particle, $C(a) \sim C_\infty$ when $D \geq 1$. Since our D_g's are on the order of 0.1 (at atmospheric pressure), and generally D_t's are on the order of 5 (see Figure 4.20), the resulting D_{eff} will place us in the region where $C(a) \sim C_\infty$.

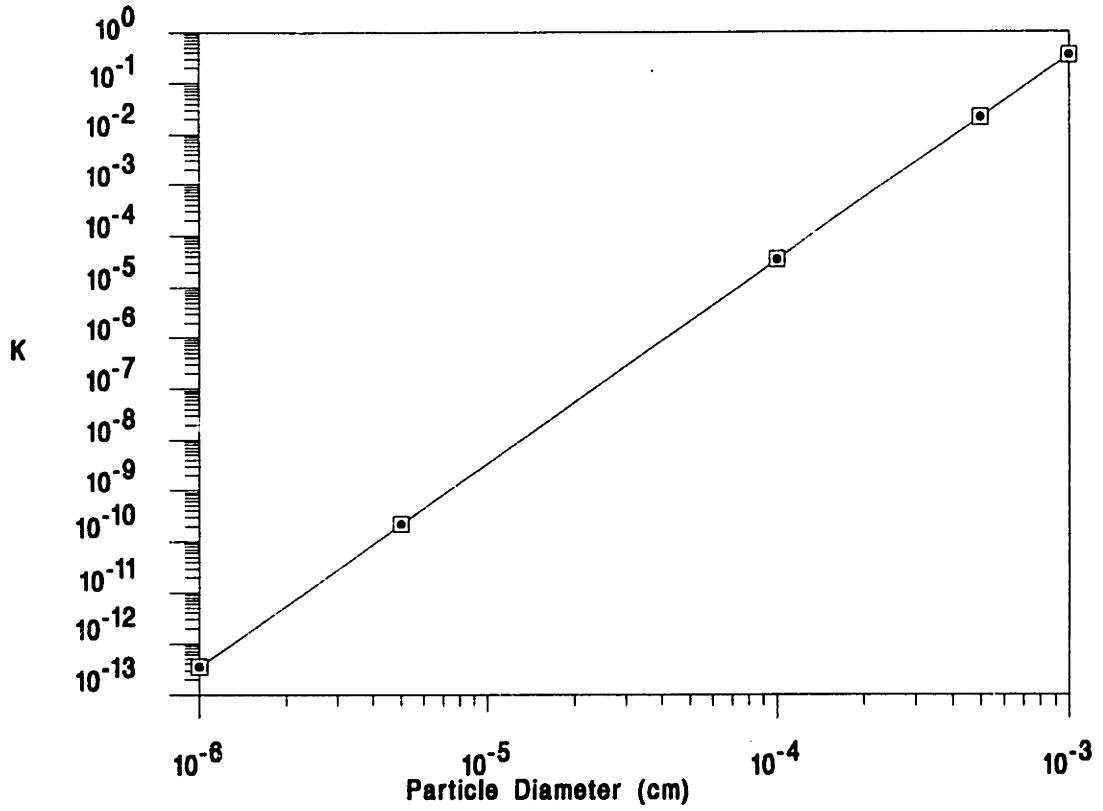

Figure 4.20: Plot of the flux coefficient (K) of particles to the flow tube walls vs. particle diameter.

4.5.2 *Diffusion of Particles to the Tube Walls*

Friedlander and Johnstone [1957] have done extensive studies on the phenomena of particle deposition on tube walls in a turbulent flow. Friedlander further expands the topic in the book Smoke, Dust and Haze [Friedlander, 1977]. Friedlander and Johnstone report an empirical equation using a new parameter: particle transfer coefficient:

$$K = \frac{d_p^4 \rho_p^2 \left(\bar{v}\right)^5 \rho^2 \varphi^{2.5}}{6.1 x 10^5 \eta^4} \qquad (4.39)$$

where:

d_p: particle diameter

ρ_p: density of particle substance

= 1 for ice

$\bar{v}$: average velocity of flow in tube

ρ: density of carrier gas

φ: friction factor, for a smooth surface: $3.5 x 10^{-3}$

η: viscosity

and K equal to the average particle flux per wall surface area per second over the average particle number density: $K = \frac{\bar{J}}{n}$. Obviously the particle wall flux will be linearly proportional to the particle number density in the flow. Figure 4.20 is a plot of the flux of the particle transfer coefficient as a function of particle diameter.

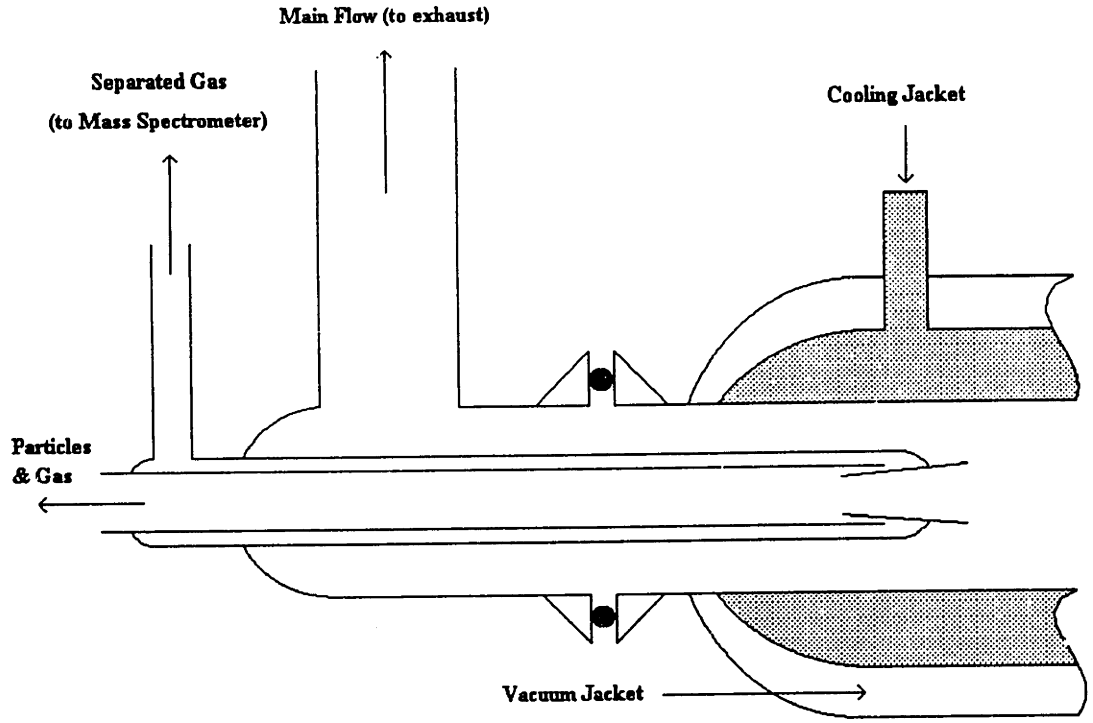

Figure 4.21: Schematic of the momentum separator (area e in Figure 4.1). Most of the flow of the flow tube exits to the main flow exhaust. The scoop on the separator samples the center of the main flow. Most of the particles in this flow pass straight down the center tube and exit to the left. Some gas passes the two corners and flows to the mass spectrometer.

4.6 Particle/Gas Separation

Region e in Figure 4.1 is detailed in Figure 4.21. This is the momentum separator. It separates a fraction of the gas flow from the particles by taking advantage of the fact that the particles have a much larger momentum than gas molecules. Thus they can less readily negotiate sharp corners in a fast flow. In the figure, the main flow tube is partially shown to the right. The center probe samples only the center of the flow with the scoop opening being about 1 cm in diameter. Some of the gas will then turn the two corners to

flow down the outside of the center tube and exit to the mass spectrometer. The flow to the mass spectrometer is a function of the main tube flow and was calibrated using a bublometer. A plot of this ratio is shown in Figure 4.22. Most of the flow (particles and gas) passes around the momentum separator and exits to the exhaust.

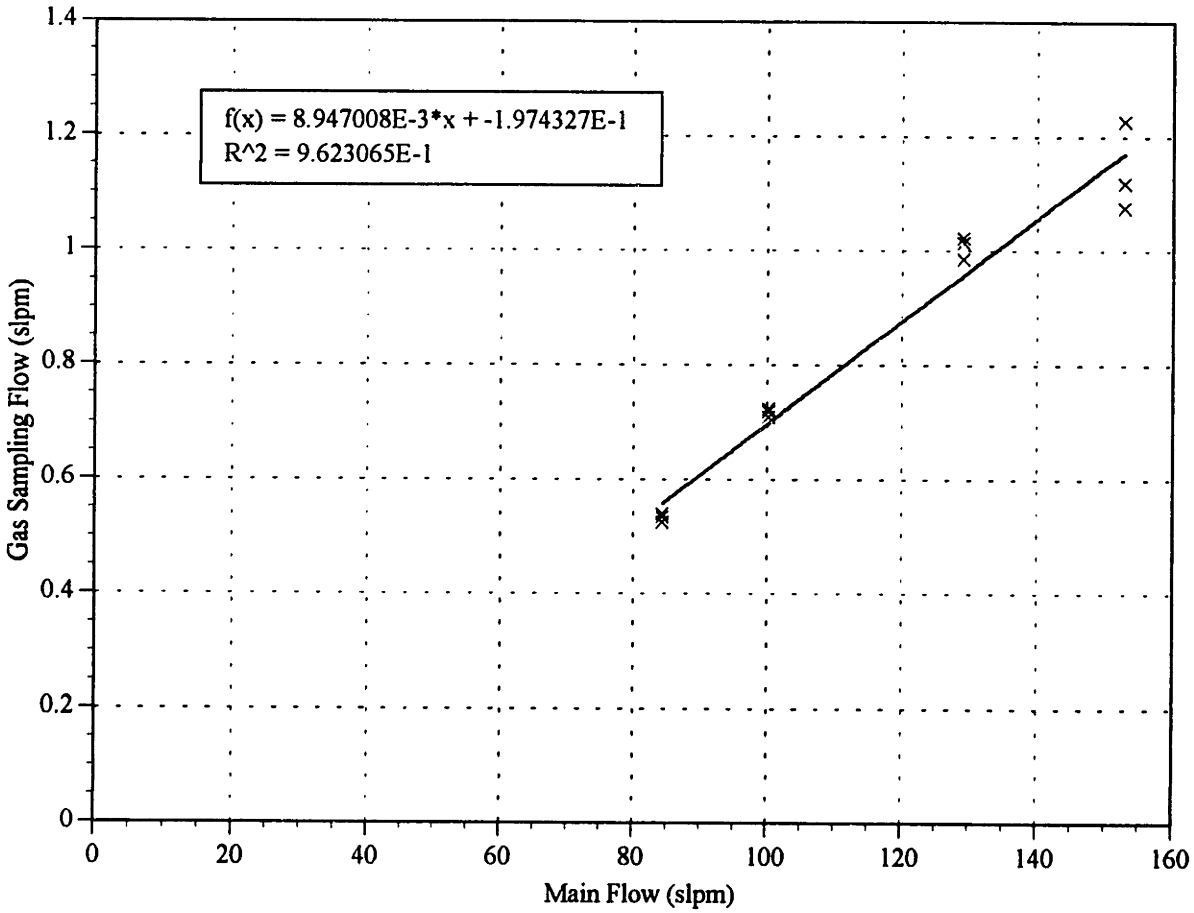

Figure 4.22: Plot of the ratio of the main flow in the kinetics tube to the flow of sampled gas from the momentum separator. Measurements of the sampled gas were made using a bublometer. The equation is the fit through the data.

Few particles negotiate these two corners as has been checked using polystyrene microspheres with an average diameter of 0.247 μm and a standard deviation of 0.0014 μm. A solution of spheres was made to have a concentration of approximately 4×10^9 spheres per cm^3. This solution was placed over an ultrasonic vibrator to make liquid particles carrying the spheres. These particles were carried by dry air so that the liquid (water) would evaporate. The spheres were then introduced into the flow tube in the

normal manner at a flow rate of 2 slpm, with a main flow down the reaction tube of 150 slpm. At the sample gas exit, a HeNe laser was placed across the flow, and a photomultiplier placed perpendicular to the flow and the laser beam. The response of the photomultiplier was monitored with an oscilloscope. When a particle crossed the beam the signal from the photomultiplier could readily be seen with the oscilloscope. The tubing i.d. is ~9 mm, and the width of the beam is ~2 mm. Therefore the fraction of the tube flow that crosses the beam is 0.28. With a typical flow rate out the gas sampling tube around 1 slpm, we observed 1 signal from the photomultiplier every 2 - 3 seconds, which is approximately 1 particle per second in the total sample gas flow.

A second check on the efficiency of the particle separator was performed with the mass spectrometer connected to the apparatus. Tests had been performed with the mass spectrometer to determine what effect a large amount of water vapor would have on the chlorine signal (the high water vapor concentration would correspond to all the particles passing through the gas sampling tube and vaporizing.) For water concentrations around 300 ppm a the chlorine signal corresponding to several hundred parts per trillion (ppt) vanished. The signal recovered progressively for lower concentrations of water vapor (down to 5 ppm which is the vapor pressure over ice for our flow tube conditions). When we performed experiments for particles, no significant decrease was seen in the chlorine signal compared to conditions without ice particles. This is strong indication that we are efficiently separating the bulk of the particles from the main flow.

4.7 Atmospheric Pressure Chemical Ionization Mass Spectrometer

4.7.1 *Description of Apparatus*

This experiment requires the detection of chlorine in the presence of HCl, chlorine nitrate, nitric acid and water at atmospheric pressures (~760 torr). To perform this task we have employed an Extrel Atmospheric Pressure Chemical Ionization Mass Spectrometer (APCIMS), which is shown in region f of Figure 4.1 and given in greater

detail in Figure 4.23. In this spectrometer ionization occurs at atmospheric pressure via a corona discharge. In our experiments nitrogen gas with about 4 ppm of SF_6 was flowed over the needle to create the discharge. The discharge needle was typically held at a potential of -3 to -4 kilovolts. Discharge currents were typically around 25 microamps. The discharge occurred between the needle and the metal tube which was typically held at -200 volts. The ionization scheme is described below.

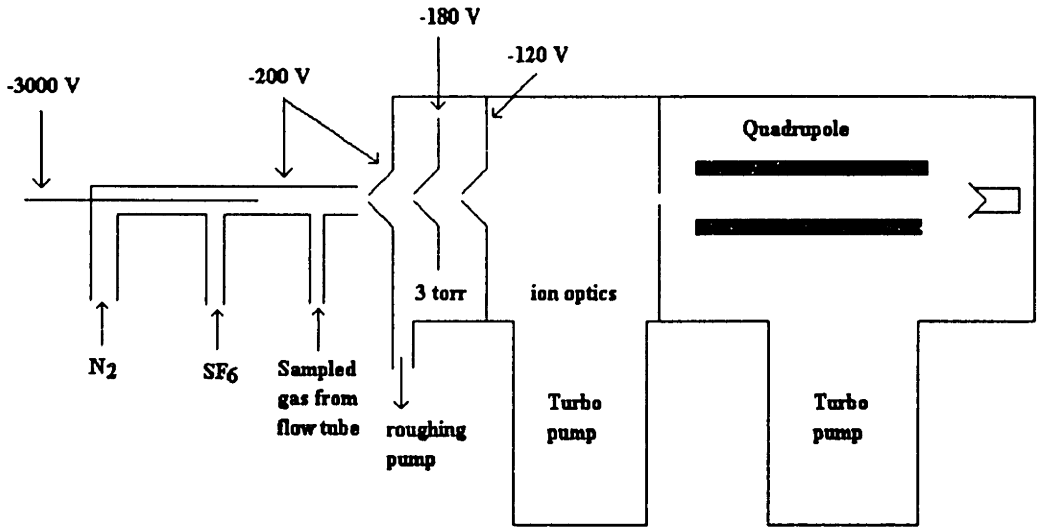

Figure 4.23: Schematic of Extrel Atmospheric Pressure Chemical Ionization Mass Spectrometer (APCIMS, region f in Figure 4.1). Shown in the diagram are the voltages on the lenses and ionization apparatus. The discharge occurs from the needle at -3000 volts to the metal tube at -200 volts.

4.7.2 *Ionization/Detection Scheme*

Chlorine molecules can readily be detected in the negative ion mode [Hanson and Ravishankara, 1991], and can be ionized via a secondary process involving SF_6 [Ikezoe et al., 1987; Seeley, 1993b]. The ionization reaction scheme involves the following steps (rate constants are from Ikezoe et al., [1987]):

$$SF_6 + e^- \rightarrow SF_6^- \qquad (4.v)$$

$$SF_6^- + Cl_2 \rightarrow Cl_2^- + SF_6 \qquad k = 6.1 \pm 1.8 \times 10^{-11} \qquad (4.vi)$$

However, we also have competing reactions from HCl:

$$SF_6^- + HCl \rightarrow SF_5^-, ClFH^-, ClSF_5^- \quad k = 4.2 \pm 1.3x10^{-10} \qquad (4.vii)$$

$$ClFH^- + HCl \rightarrow Cl_2H^- + HF \qquad k = 1.4x10^{-10} \qquad (4.viii)$$

which are faster than the reaction of SF_6 with Cl_2. This could be a large problem if HCl significantly depletes the SF_6^- to the detriment of reaction 4.vi. We believe this was the case under conditions where we had high concentrations of HCl (5 ppb) and low concentrations of Cl_2 (~300 ppt). These results will be discussed in the next section. One alternate scheme is to use NO_2^- as the reagent ion. However, in this case also, HCl has a faster reaction rate than Cl_2. It would seem that finding a workable ionization scheme for Cl_2 in the presence of HCl is a difficult task, and the research is ongoing in our laboratory.

4.8 Preliminary Results

4.8.1 *Chlorine Calibration*

We have performed preliminary experiments using the above mentioned instruments, apparatus and techniques. We first attempted to calibrate the mass spectrometer signal for chlorine in the presence of ice particles. Figure 4.24 shows the results of the first calibration where Cl_2 concentration is plotted vs. the ion counts per second of the mass spectrometer detector. In all cases we determine the signal due to chlorine by monitoring mass 70. Ice particles were made flowing 720 sccm of dry N_2 through the water bubbler at room temperature and mixing in 2 slpm of dry N_2. The number density of particles down the flow tube was calculated to range from $7.6x10^7$ and $2.2x10^7$ particles/cm^3, and the surface area of particles per cm^3 of air (Θ) ranged from 0.82 to 0.47 cm^2/cm^3. The median diameter ranged between 1.02 and 1.46 μm, and the flow tube temperature fell between -82 and -79 C. After this first calibration, the particle

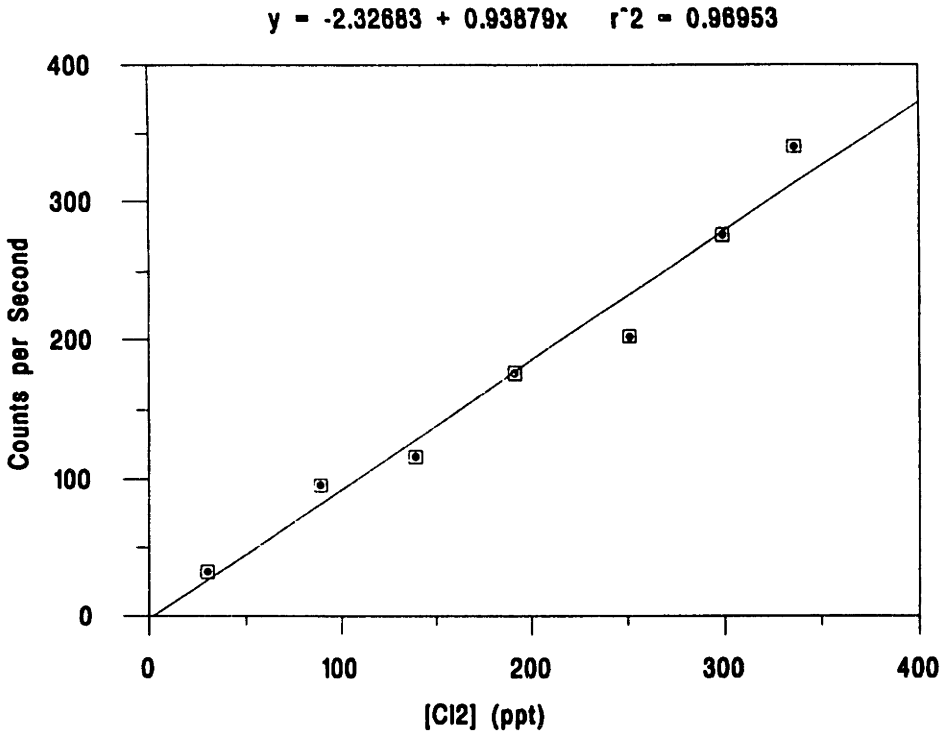

Figure 4.24: Plot of the signal at mass 70 (chlorine) vs. concentration of chlorine. Experimental conditions are with ice particles flowing in the kinetics tube at -80 C with a carrier gas flow rate of 100 slpm.

production was shut off and until the particle flow went back to zero. A second run was initiated using the same conditions as that of the first calibration, and the results are shown in Figure 4.25. The respective particle parameters are: number density: 7.0×10^7 - 8.8×10^7; Θ: 0.54 - 0.77; median diameter: 0.75 - 1.01; temperature: -83 to -87 C. It is apparent that there is some difference in the two calibrations. Since we do not expect chlorine to interact with the ice particles, differences in the size distribution and number density should not change the chlorine signal from the mass spectrometer. However, what will affect the signal is the partial pressure of water in the region of the ion chemistry. Higher partial pressures of water lowers the chlorine signal [Seeley, 1993]. However, the calibration experiments showed the opposite trend: when the temperature was lower (hence higher partial pressure of water over ice) the chlorine signal was higher. This

discrepancy is most likely due to our lack of complete understanding of the ion chemistry occurring with the corona discharge.

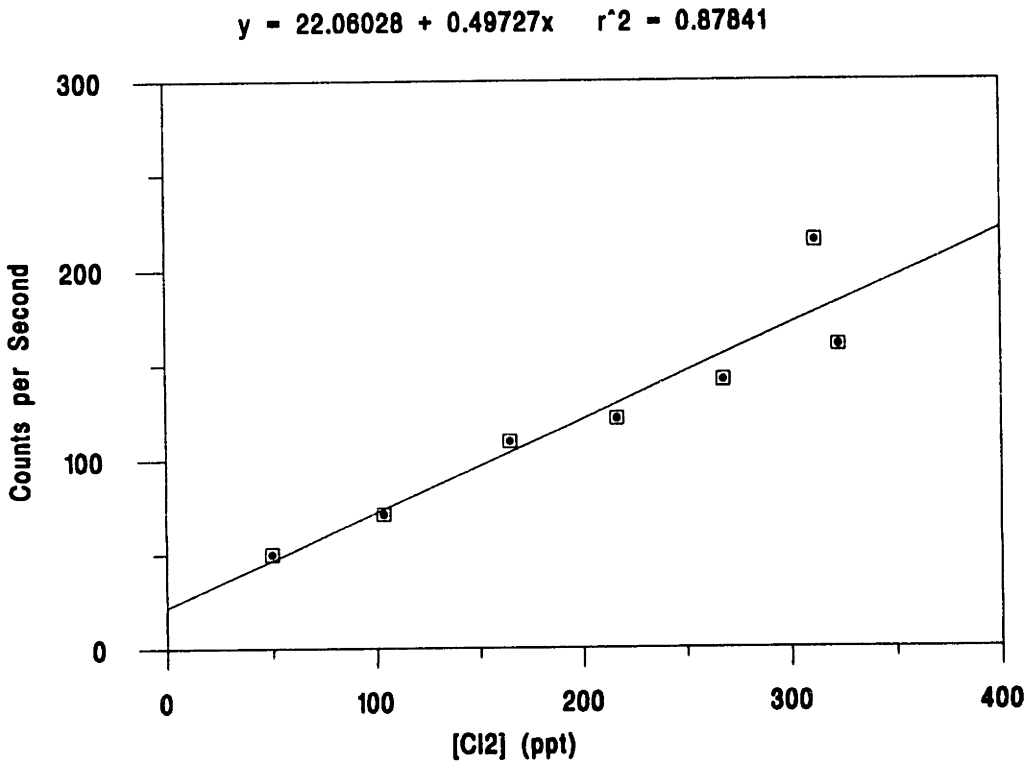

Figure 4.25: Same as Figure 4.24 except flow tube temperature was -84 C.

4.8.2 *Room Temperature Control Experiment*

Next we performed a room temperature control experiment where HCl and $ClONO_2$ were introduced into the flow tube at room temperature as shown in Figure 4.1. The reaction tube flow was 102 slpm, the temperature was 26 degrees, concentration of HCl was ~500 ppt and that of $ClONO_2$ was ~5 ppb. The chlorine signal was 50 counts per second (cps) and remained constant with injector distance. Water was then introduced into the flow at ~2 ppm. The chlorine signal was 30 cps and did not change with injector distance. These control experiments indicated the following: first, there is no detectable chlorine impurity in the $ClONO_2$, second, in the absence of ice, any reaction in our system of HCl with $ClONO_2$ gives negligible amounts of Cl_2. However, one point to note, the

HCl was mistakenly an order of magnitude less than the $ClONO_2$. This ended up being important for the ion chemistry as will be discussed later.

4.8.3 *Low Temperature Control Experiment*

We then proceeded to perform the same control experiment at cold temperatures (~ -70 C). Table 4.2 summarizes the results of this experiment where "Re" is the Reynold's number defined as: $Re = \frac{2r\bar{v}\rho}{\eta}$, with r the radius of the flow tube, $\bar{v}$ the average flow velocity, ρ the gas density and η the gas viscosity. We need Reynold's numbers of a few thousand and

Table 4.2

Summary of data from background experiment under the following conditions: [HCl]=~2ppb, [$ClONO_2$]=~1.5ppb, [H_2O]=~2.5ppm, Flow=101slpm, Re=13,000

Injector Distance (cm)	Flow Temperature (C)	Cl_2 cps
0	-57	400
5	-65	400
10	-67	600
15	-67	700
20	-67	800
0	-67	1000

above to insure being in turbulent flow. The results of this experiment indicate that we likely were having significant wall reactions. This should require having ice on the walls. We add water to the reaction tube flow so that the particles will not evaporate (the main flow is dry, coming from a liquid nitrogen gas pack). However, if we are above the saturation point of ice, the water vapor may condense on the tube walls. Taking this possibility into account, we performed experiments without the turbulizer, which enhances interaction with the walls. However, similar results were obtained without the turbulizer.

We then went back to the configuration where we flowed chlorine with ice particles, and found that our previous results were reproducible. We then added HCl in varying amounts from 5 ppb to 500 ppt. The concentration of HCl affected the ion chemistry dramatically as evidenced by a peak at mass 71 due to $HClCl^-$ and a decrease in the SF_6 concentration with increasing HCl. At this point it became apparent that the ion chemistry was not under control, nor well understood.

4.9 Conclusions and Future Work

We have demonstrated a controlled experiment for the production of model PSC ice particles, characterizing their size, number density and phase. We have also been able to control these parameters using the variables of temperature and vapor concentrations. We have implemented the turbulent flow technique [Seeley et al., 1993a] in the study of heterogeneous reactions on particles, and we have developed a momentum separator which efficiently separates particles from gas for sampling purposes. What remains is to refine and understand the interface of this experiment with a detection technique for chlorine in the presence of other reactants. The main conclusion from our preliminary work on the reaction of HCl with $ClONO_2$ on ice particles is that with the APCIMS we have no difficulty detecting Cl_2 down to less than 100 ppt in the presence of ice particles. However, there appears to be interference from other reactants in the ion chemistry of the ionization and sampling technique. Much work needs to be done in this area if this APCIMS detection technique is to be used.

References

Abbatt, J. P. D., K. D. Beyer, A. F. Fucaloro, J. R. McMahon, P. J. Wooldridge, R. Zhang, M. J. Molina, "Interaction of HCl vapor with water-ice: implications for the stratosphere", *J. Geophys. Res.*, **97** (D14), 15,819-15,826, 1992.

Abbatt, J. P. D, and M. J. Molina, "The heterogeneous reaction of HOCl + HCl $\rightarrow$ Cl_2 + H_2O on ice and nitric acid trihydrate: reaction probabilities and stratospheric implications", *Geophys. Res. Lett.*, **19**, 561-464, 1992a.

Abbatt, J. P. D., and M. J. Molina, "Heterogeneous interactions of $ClONO_2$ and HCl on nitric acid trihydrate at 202 K", *J. Phys. Chem.*, **96**, 7674-7679, 1992b.

Anderson, J. G., D. W. Toohey, W. H. Brune, "Free radicals within the Antarctic vortex: the role of CFCs in Antarctic ozone loss", *Science*, **251**, 39-46, 1991.

Atkins, P. W., Physical Chemistry, 3rd ed., p 653, Freeman, New York, 1986.

Becker, R., *Ann. Physik*, **32**, 128, 1938.

Becker, R., and W. Doring, *Ann. Physik*, **24**, 719, 1935.

Beyer, K. D., S. W. Seago, M. J. Molina, "Supercooling of stratospheric aerosols: implications for the formation of Polar Stratospheric Clouds" *manuscript in preparation.*, 1993.

Bigg, E. K., "The Supercooling of Water", *Proc. Phys. Soc.*, **B66**, 688-703, 1953.

Bluth, G. J. S., S. D. Doiron, C. C. Schnetzler, A. J. Krueger, L. S. Walter, "Global tracking of the SO_2 clouds from the June, 1991 Mount Pinatubo eruptions", *Geophys. Res. Lett.*, **19**, 151-154, 1992.

Carpenter, C. D. and A. Lehrman, "The solid-liquid temperature relation in the ternary system H_2SO_4-HNO_3-H_2O and its relation to the ternary system N_2O_5-H_2O-SO_3", *Trans. Am. Inst. Chem. Eng. (Trans. AIChE)*, **17**, 35-73, 1925.

Chiang, P. and M. D. Donohue, "A kinetic approach to crystallization from ionic solution I. Crystal growth", *J. Colloid Interf. Sci.*, **122**, 230, 1988.

Chiang, P. M. D. Donohue, J. L. Katz, "A kinetic approach to crystallization from ionic solution II. Crystal nucleation" *J. Colloid Interf. Sci.*, **122**, 251, 1988.

Crutzen, P. J., and F. Arnold, "Nitric acid cloud formatoin in the cold Antarctic stratosphere: A major cause for the springtime 'ozone hole'", *Nature*, **324**, 651-655, 1986.

Denbigh, K. The Principles of Chemical Equilibrium 4th ed., Cambridge: New York, 1981.

Doyle, G. J., "Self-nucleation in the sulfuric acid-water system" *J. Chem. Phys.*, **35** (3), 795-799, 1961.

Doyle, G. J. "Response to the comment on 'Self-nucleation in the sulfuric acid-water system' " *J. Chem. Phys.*, **75** (3), 1585-6, 1981.

Dye, J. E., D. Baumgardner, B. W. Gandrud, S. R. Kawa, K. K. Kelly, M. Loewenstein, G. V. Ferry, K. R. Chan, B. L. Gary, "Particle Size Distributions in Arctic Polar Stratospheric Clouds, Growth and Freezing of Sulfuric Acid Droplets and Implications for Cloud Formation", *J. Geophys. Res.*, **97**, 8015-8034, 1992.

Elliot, S., R. P. Turco, O. B. Toon, P. Hamill, "Incorporation of stratospheric acids into water ice", *Geophys. Res. Lett.*, **17**, 425-428, 1990.

Elliot, S., R. P. Turco, O. B. Toon, P. Hamill, "Application of Physical Adsorption Thermodynamics to Heterogeneous Chemistry on Polar Stratospheric Clouds", *J. Atmos. Chem.*, **13**, 211-224, 1991.

Farman, J. C., B. G. Gardiner, J. D. Shanklin, "Large losses of total ozone in Antarctic reveal seasonal ClO_X/NO_X interaction", *Nature*, **315**, 207-210, 1985.

Flood, H., "Tropfenbildung in Ubersattigten Athylalkohol-Wasserdampfgemischen" *Z. Phys. Chem.*, **A170**, 286-294, 1934.

Friedlander, S. K., Smoke, Dust and Haze, Wiley, New York, pp. 317, 1977.

Friedlander, S. K., and H. F. Johnstone, "Deposition of suspended particles from turbulent gas streams", *Ind. Eng. Chem.*, **49**, 1151, 1957.

Fua, D., Cacciani, M., Di Girolamo, P., Fiocco, G., Di Sarra, A., "Stratospheric Clouds at South Pole During 1988 2. Their Evolution in Relation to Atmospheric Structure and Composition", *J. Geophys. Res.*, **97**, 5947-5952, 1992.

Fuller, E., P. Schettler, J. Giddings, "A new method for prediction of binary gas-phase diffusion coefficients", *Ind. Eng. Chem.*, **58**, 19, 1966.

Gable, C. M., Betz, H. F., Maron, S. H., "Phase equilibria of the system sulfur trioxide-water", *J. Amer. Chem. Soc.*, **72**, 1445-1448, 1950.

Hallet, J. and Lewis, R. E. J., "Mother-of Pearl Clouds", *Weather*, **22**, 56-65, 1967.

Hallet, J., "Nucleation and Growth of Ice Crystals in Water and Biological Systems", in Low Temperature Biology of Foodstuffs, Permagon Press, Oxford, 1968, pp 23-52.

Hamill, P. and O. B. Toon, "Polar Stratospheric Clouds and the Ozone Hole", *Physics Today*, **44**, 34-42, 1991.

Hanson, D. R., and K. Mauersberger, "Solubility and equilibrium vapor pressurs of HCl dissolved in polar stratospheric cloud materials: ice and the trihydrate of nitric acid", *Geophys. Res. Lett.*, **15**, 1507, 1988.

Hanson, D. R., and K. Mauersberger, "HCl/H_2O solid phase vapor pressures and HCl solubility in ice", *J. Phys. Chem.*, **94**, 4700-4705, 1990.

Hanson, D. R., and A. R. Ravishankara, "The reaction probabilities of $ClONO_2$ and N_2O_5 on polar stratospheric cloud materials", *J. Geophys. Res.*, **96** (D3), 5081-5090, 1991.

Heist, R. H. and H. Reiss. "Hydrates in supersaturated binary sulfuric acid-water vapor" *J. Chem. Phys.*, **61**, 573-581, 1974.

Hobbs, P., Ice Physics, Oxford U. Press: New York, 1974.

Hofmann, D. J., Oltmans, S. J., Solomon, S., Deshler, T., Johnson, B. J., "New Antarctic Ozone Depletion Provides Evidence for Volcanic Effects", *Nature*, **359**, 283-287, 1992.

Holmes, W. C., "The Freezing Points of Mixtures of Sulfuric and Nitric Acids", *J. Ind. Eng. Chem.*, **12**, 781-783, 1920.

Houghton, H. G., Physical Meteorology, MIT Press, Cambridge, Mass, 1985.

Ikezoe, Y., S. Matsuoka, M. Takebe, A. Viggiano, Gas Phase Ion-Molecule Reaction Rate Constants Through 1986, Maruzen Co., Tokyo, Japan, 1987.

Jensen, E., Toon, O. B., Hamill, P., "Homogeneous Freezing Nucleation of Stratospheric Solution Droplets", *Geophys. Res. Lett.*, **18**, 1857-1860, 1991.

Ji, K. and J. C. Petit, "The HNO3-H2O phase diagram revisited in the temperature and concentration ranges of PSC formation" CEC/EUROTRAC Discussion meeting on Multiphase Processes of Atmospheric Interest, The Royal Society of Chemistry, September 1991.

Junge, C. E., "Verticle profiles of condensation nuclei in the stratosphere", *J. Met.*, **18**, 501, 1961

Kanno, H., "Complete ionization of concentrated sulfuric acid at low temperatures", *Chem. Phys. Lett.*, **170**, 382-384, 1990.

Keyser, L. F. and M.-T. Leu, "Surface areas and porosities of ices used to simulate stratospheric clouds", *J. Coll. Interf. Sci.*, **155**, 137-145, 1993a.

Keyser, L. F. and M.-T. Leu, "Morphology of nitric acid and water ice films", *Microscopy Res. and Technique*, **25**, 434-438, 1993b.

Leu, M. T., "Laboratory studies of sticking coefficients and heterogeneous reactions important in the Antarctic stratosphere", *Geophys. Res. Lett.*, **15**, 17-20, 1988.

Levy, P. W. and P. J. Herley in *Materials Science research*, Plenum Press: New York, Vol 4, pp. 23-52, 1969.

Luo, B. P., Th. Peter, P. J. Crutzen, "Maximum supercooling of H_2SO_4 acid aerosol droplets", *Ber. Bunsenges. Phys. Chem.*, **96**, 334-338, 1992.

Luo, B. P., Th. Peter, P. J. Crutzen, "Freezing of stratospheric aerosol droplets" *in press Geophys. Res. Lett.*, 1993.

Mason, B. J., The Physics of Clouds, Oxford U. Press, New York, 1957.

McCormick, M. P., H. M. Steele, P. Hamill, W. P. Chu, T. J. Swissler, "Polar stratospheric cloud sightings by SAM II", *J. Atmos. Sci.*, **39**, 1387-1397, 1982.

McCormick, M. P. and R. E. Veiga, "SAGE II measurements of early Pinatubo aerosols", *Geophys. Res. Lett.*, **19**, 155-159, 1992.

McElroy, M. B., R. J. Salawitch, S. C. Wofsy, J. A. Logan, *Nature*, **321**, 759, 1986.

Mirabel, P. and J. L. Katz, "Binary homogeneous nucleation as a mechanism for the formation of aerosols", *J. Chem. Phys.*, **60**, 1138-1144, 1974.

Molina, L. T., and M. J. Molina, "Production of Cl_2O_2 from the self-reaction of the ClO radical", *J. Phys. Chem.*, **91**, 433-436, 1987.

Molina, L. T., M. J. Molina, R. A. Stachnik, R. D. Tom, "An upper limit to the rate of the HCl + $ClONO_2$ reaction", *J. Phys. Chem.*, **89**, 3779, 1985.

Molina, M. J., and F. S. Rowland, "Stratospheric sink for chlorofluoromethanes: chlorine atom-catalysed destruction of ozone", *Nature*, **249**, 810, 1974.

Molina, M. J., T. Tso, L. T. Molina, F. C. Wang, "Antarctic stratospheric chemistry of chlorine nitrate, hydrogen chloride, and ice: release of active chlorine", *Science*, **238**, 1253-1257, 1987.

Molina, M. J., R. Zhang, P. J. Wooldridge, J. McMahon, J. E. Kim, H.Y.A. Chang, K. D. Beyer, "Physical Chemistry of the $H_2SO_4/HNO_3/H_2O$ system: implications for Polar Stratospheric Clouds", *Science*, **261**, 1418-1423, 1993.

Noggle, J. H., Physical Chemistry, 2nd ed., Harper Collins, New York, pp 1093, 1989.

Ohtake, T., "Freezing points of H2SO4 aqueous solutions and formation of stratospheric ice clouds" *Tellus*, **44B**, 1992.

Oxtoby, D. W., "Nucleation of crystals from the melt" *Adv. Chem. Phys.*, **70**(2), 263-297, 1988.

Pruppacher, H. R. and J. D. Klett, Microphysics of Clouds and Precipitation, Reidel, Boston, 1980.

Reiss, H. "The kinetics of phase transitions in binary systems", *J. Chem. Phys.*, **18**, 840-848, 1950.

Renninger, R. G., F. C. Hiller, R. C. Bone, "Comment on 'Self-nucleation in the sulfruic acid-water system' " *J. Chem. Phys.*, **75** (3), 1584-5, 1981.

Ritzhaupt, G. and J. P. Devlin, "Infrared spectra of nitric and hydrochloric acid-hydrate thin films", *J. Phys. Chem.*, **95**, 90-95, 1991.

Rogers, R. R. and M. K. Yau, A Short Course in Cloud Physics, 3rd ed., Pergamon Press, New York, 1989.

Schaeffer, V. J., "Formation of Ice Crystals in Ordinary and Nuclei-Free Air", *Ind. Eng. Chem.*, **44**, 1300 - 1304, 1952.

Schwartz, S. E., and J. E. Freiberg, "Mass-transport limitation to the rate of reaction of gasses in liquid droplets: application to oxidation of SO_2 in aqueous solutions", *Atmos. Env.*, **15**, 1129, 1981.

Schwartz, S. E., "Mass-transport considerations pertinent to aqueous phase reactions of gases in liquid-water clouds", *in* Chemistry of Multiphase Atmospheric Systems, W. Jaeschke, Ed., pp 415-471, Springer-Verlag, New York, 1983.

Seeley, J. S., J. T. Jayne, M. J. Molina, "High pressure fast-flow technique for gas phase kinetics studies" *Int. J. Chem. Kin.*, **25**, 571-594, 1993a.

Seeley, J. S., Work performed in our lab., 1993b.

Smith, R. H., M. T. Leu, L. F. Keyser, "Infrared spectra of solid films formed from vapors containing water and nitric acid", *J. Phys. Chem.*, **95**, 5924-5930, 1991.

Tabazadeh, A., and R. Turco, "A model for heterogeneous processes on the surfaces of ice and nitric acid trihydrate particles", *J. Geophys. Res.*, **98**, 12,727-12,740, 1992.

Thompson, C. V. and F. Spaepen, "Homogeneous crystal nucleation in binary metallic melts", *Acta Metall.*, **31**, 2021-2027, 1983.

Tolbert, M. A., M. J. Rossi, R. Malhotra, D. M. Golden, "Reaction of chlorine nitrate with hydrogen chloride and water at Antarctic stratospheric temperatures", *Science*, **238**, 1258-1260, 1987.

Tolbert, M. A., and A. M. Middlebrook, "Fourier transform infrared studies of model polar stratospheric cloud surfaces: growth and evaporation of ice and nitric acid/ice", *J. Geophys. Res.*, **95** (D13), 22,423-22,431, 1990.

Toon, O. B., P. Hamill, R. P. Turco, J. Pinto, "Condensation of HNO_3 and HCl in the winter polar stratosphere", *Geophys. Res. Lett.*, **13**, 1284-1287, 1986.

Trinkaus, H. "Theory of the nucleation of multicomponent precipitates" *Phys. Rev. B*, **27**, 7372-7378, 1983.

Turco, R. P., O. B. Toon, P. Hamill, "Heterogeneous physicochemistry of the polar ozone hole", *J. Geophys. Res.*, **94** (D14), 16,493-16,510, 1989.

Turnbull, D. and J. C. Fisher, "Rate of nucleation in condensed systems", *J. Chem. Phys.*, **17**, 71-73, 1949.

Vuillard, G., "A l'etude de l'etat vitreaux et de la cristallisatioin des solutions aqueuses", *Ann. de Chim.*, **13**, 233-297, 1957.

Wang, M. K. and B. Vonnegut, "Repeated nucleation of supercooled water sample", *J. Rech. Atmos.*, **18**, 23-29, 1984.

Walton, A. G., "Nucleation in liquids and solutions" in Nucleation, A. C. Zettlemoyer, Ed., Marcel Decker, New York, 1969.

Warneck, P., Chemistry of the Natural Atmosphere, Academic Press: New York, 1988.

Wilemski, G., "Composition of the critical nucleus in multicomponent vapor nucleation" *J. Chem. Phys.*, **80** (3), 1370-1372, 1984.

Wofsy, S. C., M. J. Molina, R. J. Salawitch, L. E. Fox, M. B. McElroy, "Interactions between HCl, NO_x, and H_2O ice in the Antarctic stratosphere: implications for ozone", *J. Geophys. Res.*, **93**, 2442-2450, 1988.

Wolff, E. W., R. Mulvaney, K. Oates, "Diffusion and location of hydrochloric acid in ice: Implications for polar stratospheric clouds and ozone depletion", *Geophys. Res. Lett.*, **16**, 487-490, 1989.

Worsnop, D. R., L. E. Fox, M. S. Zahniser, S. C. Wofsy, "Vapor pressures of solid hydrates of nitric acid: implications for Polar Stratospheric Clouds", *Science*, **259**, 71-74, 1993.

Wu, D. T, "General approach to barrier crossing in multicomponent nucleation" *J. Chem. Phys.*, **99**, 1990-2000, 1993.

Yamashita, A., "On the trigonal growth of ice crystals", *J. Met. Soc. Jap.*, **51**, 307-316, 1973.

Yue, G. K., "A quick method for estimating the equilibrium size and composition of aqueous sufuric acid droplets" *J. Aerosol Sci.*, **10**, 75-76, 1979.

Zeldovich, J. B., *Acta Physiocochem. URSS*, **18**, 17, 1943.

Zeng, X. C. and D. W. Oxtoby, "Binary homogeneous nucleation theory for the gas-liquid transition: A nonclassical approach", *J. Chem. Phys.*, **95**, 1991.

Zhang, R., P. J. Wooldridge, J. P. D. Abbatt, M. J. Molina, "Physical chemistry of the H_2SO_4/H_20 binary system at low temperatures: stratospheric implications" *J. Phys. Chem.*, **97**, 7351-7358, 1993a.

Zhang, R., P. J. Wooldridge, M. J. Molina, "Vapor pressure measurements for the $H_2SO_4/HNO_3/H_2O$ and $H_2SO_4/HCl/H_2O$ systems: incorporation of stratospheric acids into background sulfate aerosols", *J. Phys. Chem.*, **97**, 8541-8548, 1993b.

Postlogue

I kept this passage on my desk for those moments (and there were many) when I thought I would never see the light at the end of the tunnel.

Therefore we do not lose heart.
Even though our outward man is perishing,
yet the inward man is being renewed day by day.
For our light affliction, which is but for a moment,
is working for us a far more exceeding and eternal weight of glory,
while we do not look at the things which are seen,
but at the things which are not seen.
For the things which are seen are temporary,
but the things which are not seen are eternal.

2 Corinthians 4:16-18 (NKJV)